Australian Government
Department of Defence
Science and Technology

Copolymer Toughening of Epoxy Resin Systems for Low Temperature Cure Bonded Composite Repair

Andrew D. M. Charles and Andrew Rider

Aerospace Division
Defence Science and Technology Group

DST-Group-TR-3344

ABSTRACT

Epoxies are the most widely used resins for bonded composite repair; however they possess low fracture toughness, impact strength and peel strength due to high cross linking densities. Toughening agents can be added to epoxy resins to improve these qualities; however these typically lead to an increase in resin viscosity and undesirable changes in mechanical performance, which can in turn make the resin unsuitable for use in certain bonded composite repair applications. In this work, the impact of two commercially available tri-block copolymers on the mechanical performance of two different low temperature cure epoxy resin systems was evaluated. It was found that with the addition of the copolymers to these resins in a wet lay-up scenario (typical of bonded composite repair applications), the resin fracture toughness could be improved by as much as 125%, with negligible impact to resin interlaminar shear strength, flexural strength and glass transition temperature. Use of these resins will improve standard bonded composite repairs and support development of indigenous composite multi-functional structures for aerospace applications.

Produced by

Aerospace Division
Defence Science and Technology Group
506 Lorimer St
Fishermans Bend, Victoria 3207 Australia

Telephone: 1300 333 362
Fax: (03) 9626 7999

February 2017
AR-016-808

APPROVED FOR PUBLIC RELEASE

Copolymer Toughening of Epoxy Resin Systems for Low Temperature Cure Bonded Composite Repair

Executive Summary

Epoxies are the most widely used polymer resin used in aircraft structures and for bonded composite repairs because of their high strength, low shrinkage and good compatibility with a range of different reinforcing fibres. Unfortunately, these resins exhibit poor fracture toughness, resistance to crack propagation, impact strength and peel strength. Toughening agents can be added to epoxies to improve these qualities; however this typically leads to an increase in resin viscosity and undesirable changes in mechanical performance. The use of copolymer additives has shown promise in this area, improving fracture toughness without impacting upon other properties desirable for bonded composite repair applications.

The aim of the research reported herein was to identify two toughened low temperature cure epoxy resin systems suitable for bonded composite repair applications within the Australian Defence Force; one resin for room temperature cure wet lay-up repairs; and the other for low temperature cure pre-preg repairs. The effect of two commercially available tri-block copolymers on the mechanical performance of these two different epoxy resin systems was evaluated. Mechanical performance was quantified by Short Beam Shear (SBS), four point bend flexural and Double Cantilever Beam (DCB) testing. This destructive analysis was complimented by thermal degradation studies, Dynamic Mechanical Thermal Analysis (DMTA) and Field Emission Scanning Electron Microscopy (FESEM).

It was found that the copolymer additives provided considerable fracture toughness improvements, as much as 125%, for both the wet lay-up and pre-preg epoxy resins considered, with a negligible impact on interlaminar shear, flexural strength or glass transition temperature. This improvement in fracture toughness is a highly desirable quality both for bonded composite repair, but also for new multifunctional composite structure applications.

This page is intentionally blank

Authors

A. D. M. Charles
Aerospace Division

Andrew D.M. Charles completed his Bachelor of Science in Physics and Bachelor Engineering (Hons.) in Aeronautical (Space) engineering at the University of Sydney in 2006. He joined DST Group in 2007 as part of the Aerospace Composite Technologies Group, where he has been involved in a range of work programs focused on the design of new composite repair technologies and structures to support all Arms of the ADF. Through this work, he has received a number of awards, including a Silver Navy commendation, Gold Chief Defence Scientist commendation, and best client support awards. His current interests are in the areas of bonded and composite repair, and design of multifunctional composite structures.

Dr Andrew Rider
Aerospace Division

Andrew Rider has been employed by Aerospace Division (formerly Air Vehicles Division) since 1989 and has been involved in research examining surface treatments for bonded repairs to composite and metallic substrates. He is currently involved in the development of materials and processes for repairs to current and new generation aircraft.

This page is intentionally blank

Contents

Glossary

BCR	Bonded Composite Repair
CNC	Computer Numerically Controlled
DCB	Double Cantilever Beam
DGEBA	Diglycidyl ether of bisphenol-A
DMTA	Dynamic Mechanical Thermal Analysis
FESEM	Field Emission Scanning Electron Microscope
FRPC	Fibre Reinforced Polymer Composite
MAM	polymethylmethacrylate-block-polybutylacrylate-block-polymethylmethacrylate
PB	Polybutadiene
PBuA	Poly (butyl acrylate)
PBW	Parts-By-Weight
PMMA	Poly (methyl methacrylate)
RTM	Resin Transfer Molding
SBM	polystyrene-block-polybutadiene-block-poly-(methyl methacrylate)
SBS	Short Beam Shear
SEM	Scanning Electron Microscope
SEN	Single Edge Notch
SBSS	Short Beam Shear Strength
TALS	Thick Adherend Lap Shear

This page is intentionally blank

1. Introduction

Fibre Reinforced Polymer Composite (FRPC) materials offer a number of benefits over conventional metal alloys for aircraft structures. These include better corrosion and fatigue performance, higher specific strength (particularly for carbon fibre reinforced polymers) and the ability to tailor directional structural stiffness for improved aeroelastic behaviour (increased flutter speeds, lift effectiveness and control effectiveness). Manufacturing processes for FRPC's are also relatively inexpensive and cost effective, allowing complicated shapes to be made without the need for mechanical joints required of conventional aircraft materials; which acts as stress concentrations within aircraft structure.

The improved properties and performance attainable through use of FRPC materials has seen their use in both primary and secondary structure of aircraft platforms increase in the past 40 years. With this increase comes the need to consider through-life support of such materials, with this leading to the increased use of Bonded Composite Repairs (BCRs) as opposed to scrapping of costly large composite assemblies [1].

Epoxy resins are the most widely used polymer resin systems in aircraft structures, because of their excellent chemical and mechanical properties, low shrinkage, good compatibility with a range of different reinforcing fibres and relatively high glass transition temperatures (T_g) [2]. This later property results from the high cross-linking density of the polymer. Unfortunately this also translates to poor fracture toughness, poor resistance to crack propagation and low impact and peel strengths [3].

Extensive research has been conducted over the past few decades to improve the toughness of epoxy resins. This has focused on two main areas [4], (i) reduction of cross linking density, and, (ii) addition of modifiers to the epoxy resin system. Reducing the cross linking density reduces both strength and T_g, both of which are unfavourable for bonded repair. Through the mixing of secondary components into the adhesive, both strength and T_g of the epoxy system can be retained, whilst also improving the toughness of the system.

Most of the modifiers used to toughen epoxy resin systems are elastomers or thermoplastics [5], although reactive diluents and inorganic/hybrid modifiers are also used [3]. Elastomers such as liquid rubbers provide significant improvements to the fracture toughness of epoxy systems [6], however, these can lead to reductions in the T_g and modulus, and undesirable mechanical and chemical performance at elevated temperatures [3, 6]. Furthermore, the benefits of elastomeric modifiers decrease as the cross-linking density of the epoxy resin system increases [7].

In contrast, thermoplastic particles employed as toughening modifiers can lead to improvements in epoxy fracture toughness without sacrificing the thermal properties and strength of the system [7]. The thermal advantage arises because the thermoplastic particles are tough, ductile, chemically and thermally stable and have relatively high T_g's compared to elastomeric modifiers. However the toughness improvements achieved

through thermoplastic modifiers are generally not as good as that achieved through use of elastomeric modifiers [8], particularly where high T_g thermoplastic modifiers are used [9].

Typically, particle sizes for elastomeric or thermoplastic modifier tougheners are in the order of 1-5 μm in diameter, with a resin volume fraction of 5-20%. These particle sizes lead to substantial increases in the uncured resin viscosity, reducing processing ability, particularly for liquid molding techniques. In addition, these relatively large particle sizes prohibit the use of such systems with infusion processes, where the toughening modifiers could be filtered from the resin by the small gaps within the reinforcing material [10].

The use of nanoparticle modifiers has been shown to provide improvements in both modulus and fracture toughness performance of parent epoxy systems, with limited impact on the processability. A variety of different particles have been trialled in research, including carbon black and nano-clay [11], nano-silica [12] and block copolymers [9, 11, 13-19].

Block copolymers are particularly unique, as their toughening properties arise from the formation of unique nanostructures within the epoxy matrix, which provide improvements in toughness with minimal impact on T_g and modulus. The formation of these nanostructures is a more efficient toughening mechanism, with lower volume fractions required for equivalent toughening when compared to other particle types. The ability to dissolve such copolymers with a host monomer is also advantageous, providing consistent dispersion with minimal effort. The small size of the nanostructures formed also allows their use in composites with small inter-fibre spacing, thin bond-line adhesives and in resin transfer molding (RTM) applications where other particles may be filtered by the composite fibres during the infusion process.

In the research conducted for this report, the effect of two commercially available tri-block copolymers on the mechanical performance of two different epoxy resin systems was evaluated. The aim was to identify toughened low temperature cure epoxy resin systems that would be suitable for the following BCR applications:

1. room temperature vacuum bag cure wet lay-up repair applications
2. low temperature vacuum bag cure pre-preg repairs.

2. Experimental Methods

2.1 Materials

Two commercially available resin systems were used in this study. The first, Renlam Kit K3600 manufactured by Huntsman, was a low-temperature cure two-part epoxy system. The second, Araldite LY 556 also manufactured by Huntsman, was a pre-preg system designed for low temperature cure with a chemical B-stage, and is composed of four components: (i) Araldite LY 556 epoxy resin, (ii) Aradur 1571 hardener paste, (iii) LME 10188 accelerator paste and (iv) XB 3403 polyamine hardener.

To each these epoxy systems, two different tri-block copolymers were added, both manufactured by Arkema as part of their Nanostrength® range. The first was a copolymer of Polystyrene, 1,4-polybutadiene and syndiotactic poly (Methyl methacrylate) as seen in Figure 1, also known as SBM, with the E21 formulation used in this research. The second was a symmetric copolymer with a centre block of poly (butyl methacrylate) surrounded by two blocks of poly(methyl methacrylate) as seen in Figure 2, known as a MAM, with the M51 grade investigated.

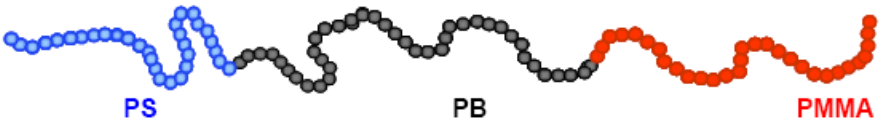

Figure 1 – SBM triblock copolymer comprised of three different blocks, Polystyrene, polybutadiene and poly (Methyl methacrylate).

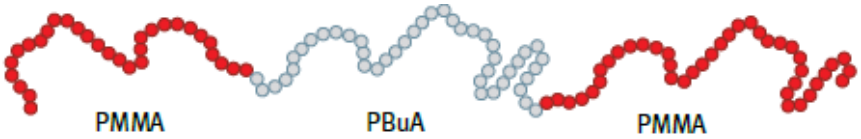

Figure 2 – MAM symmetric triblock copolymer with a centre block of poly (butyl methacrylate) surrounded by two blocks of poly (methyl methacrylate)

When mixed with an epoxy resin, both the PB (polybutadiene) and PBuA (poly [butyl acrylate]) blocks provide a soft immiscible rubber phase for toughening, whilst the PMMA (poly[methyl methacrylate]) block ensure compatibility with the epoxy monomer. Varying compatibility of each copolymer block means the blocks self-organise to minimise interactions between the non-miscible blocks and the epoxy monomer, giving rise to unique nanostructures prior to curing. Upon curing, these structures are locked into the epoxy, with the final structure depending upon the chemical nature of the cross-linker (hardener), and the chemical composition of the block copolymer utilised. These final structures modify the mechanical performance of the original epoxy resin system.

In order to investigate the performance of the resin systems within FRPC, several carbon fibre reinforced test coupons were manufactured, along with a variety of neat resin

specimens. For the carbon fibre reinforced specimens, two different fabrics were used: (i) a unidirectional IM7 3k carbon fabric manufactured by Hexcel known as HexTow IM7 [20], and (ii) a 3k carbon plain-weave fabric, 195 grams per square metre (gsm), known as RC200P, manufactured by SP systems [21].

2.2 Specimen manufacture

Each of the triblock copolymers (SBM E21 and MAM M51) were dispersed and dissolved within each of the epoxy resin systems with a loading of 10% parts by weight (PBW) of the total epoxy and copolymer mixture (including epoxy accelerator and catalyst components).

Prior to mixing, the copolymers were dried at 110 °C for 3 hours, and then ground using a laboratory mortar and pestle. The copolymer was then added to the epoxy resin and dispersed using a laboratory mixer and low torque mixing head at room temperature. Heat was then applied to the mixture via a temperature controlled hot plate, and the mixture stirred at 80 °C until complete dissolution was observed, usually after 3-4 hours. This mixture was then combined with the remaining components of the resin to initiate cross-linking.

A wet lay-up procedure with a fibre to resin ratio of 1:1 Parts-By-Weight (PBW) was used to manufacture all mechanical test coupons for both the K3600 and LY556 resin systems, with the lay-up illustrated in Figure 3. For the short beam shear (SBS) and four-point bend specimens, 16 plies of the plain weave fabric specified in Section 2.1 were used, stacked with each of the warp ply directions parallel. For the DCB specimens, 16 plies of the unidirectional fabric specified in Section 2.1 were used, stacked to form a completely uni-directional panel. Further details on the double cantilever beam (DCB) specimen manufacture are provided in Section 2.4.4.

Following lay-up and vacuum bagging, a -70 to -80 kPa vacuum pressure was applied for at least 1 hour to consolidate the lay-up. Following this, each lay-up was cured in an electric oven under the vacuum consolidation pressure using the relevant manufacturer specified resin cure profile. For the K3600 system, the cure was 24 hour at 25 °C, followed by a 3 hour post cure at 80 °C. For the LY556, the cure was 8 hours at 80 °C. As this is a pre-preg system, a b-stage of 25 °C for 24 hours can be applied to partially cure the resin, which improves its handling and processability before the final cure (or A-stage). This step was not performed on the coupons manufactured and tested in this study, but should be considered for any follow-on coupon manufacture and testing.

From the produced panels, mechanical testing coupons were cut to size using a Computer Numerically Controlled (CNC) water jet cutter, and all other specimens (for thermal conditioning and analysis) were cut using a water lubricated diamond saw, and polished using abrasive paper as necessary.

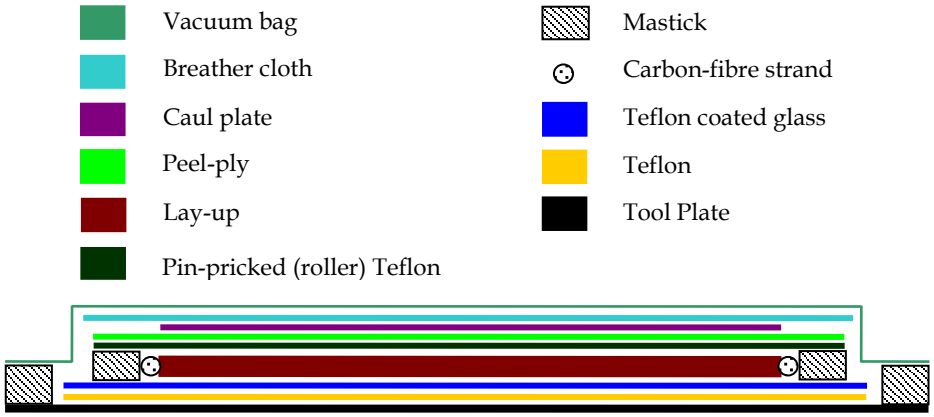

Figure 3 – Wet lay-up sequence for panel manufacture

In order to verify the quality of produced laminate, acid digestion was applied to off-cuts of the K3600 specimens, which yielded specimen average void volume (v_v) and fibre volume fraction (v_f) (see section 2.3). A theoretical tensile modulus was also calculated for each of the manufactured specimens using the rule of mixtures [22] as shown in Equation 1.

$$E_c = (1 - v_f)E_m + v_f E_f \quad \textbf{(1)}$$

Where:

v_f = Fibre volume fraction of specimen via acid digestion

E_m = Elastic modulus of matrix (specified in manufacturer's technical data sheet)

E_f = Elastic modulus of fibre (specified in manufacturer's technical data sheet)

2.3 Acid digestion

Acid digestion was performed on three specimen off-cuts from each of the neat, E21 toughened and M51 toughened K3600 specimens in order to measure the quality of the laminate manufactured.

The acid digestion procedure involved chemical digestion of the composite matrix using hot sulphuric acid, then oxidation and removal of the matrix through use of hydrogen peroxide. Measurement of specimen weight and volume before and after digestion allowed calculation of the lay-up fibre volume fraction (v_f), matrix volume fraction (v_m) and void volume (v_v) to be made as shown in Equations 2 to 4. All weight measurements were performed using a Shimadzu AUW220 analytical balance.

$$v_f = \left(\frac{M_f}{M_i}\right) \times \left(\frac{\rho_c}{\rho_f}\right) \quad \textbf{(2)}$$

$$v_m = \left(\frac{M_i - M_f}{M_i}\right) \times \left(\frac{\rho_c}{\rho_m}\right) \quad \textbf{(3)}$$

$$v_v = 1 - (v_f + v_m) \quad \textbf{(4)}$$

Where:

M_f = final mass of specimen after chemical digestion (g)

M_i = initial mass of the specimen before chemical digestion (g)

ρ_c = density of the specimen (g/ml)

ρ_f = density of the fibre reinforcement (g/ml)

ρ_m = density of the matrix (g/ml)

2.4 Mechanical testing

2.4.1 Short Beam Shear (SBS)

The SBS test was chosen to quantify any change in the SBS Strength (SBSS) of the two toughened resin systems. The test was performed in accordance with ASTM D 2344/D 2344M [23]. The SBSS (F_{SBS}) was calculated using Equation 5.

$$F_{SBS} = 0.75\left(\frac{P_m}{b \times h}\right) \quad \textbf{(5)}$$

Where:

P_m = maximum load observed during the test

b = measured specimen width

h = measured specimen thickness

A free body diagram for the SBS test is shown in Figure 4. In accordance with the ASTM standard, the support span was set to equal four times the specimen thickness, and the specimen machined to a width and length equal to two and six times the thickness respectively.

The test was performed using an INSTRON 1185 electromechanical universal testing machine with a 100 kN load cell, running with a cross-head rate of 1 mm/min. Load and cross-head displacement were recorded throughout the test until specimen failure, a load drop-off of 30%, or until the cross-head travel exceeded the specimen thickness.

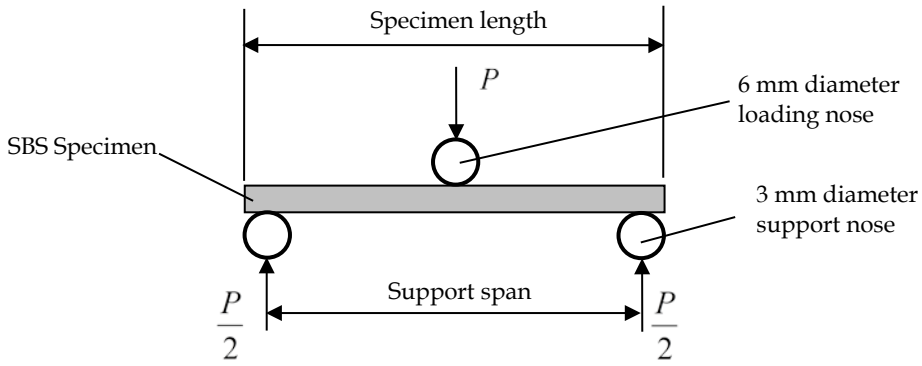

Figure 4 – Free body diagram for SBS showing details of the loading geometry

A minimum of five coupons per material set were tested. In addition, a second specimen set exposed to high temperatures for up to 100 hours were also tested. This was to determine any impact thermal extremes may have on the SBSS of each of the respective resin systems and copolymer additives. Section 3 outlines the results of thermal degradation trials, arriving at a suitable exposure condition of 180 °C for 100 hours for this second SBS specimen set.

2.4.2 Thick Adherend Lap-Shear (TALS)

To determine adhesive shear stress-strain properties and to support the SBSS results, a Thick Adherend Lap Shear (TALS) test was performed using the neat K3600 and K3600 toughened with E21 to the specifications of Section 2.2. TALS specimen manufacture and testing was performed in accordance with ASTM standard D 5656-04 [24].

The test involved surface preparation and bonding of two 9.53 mm thick 2024-T3 aluminium alloy plates using the adhesive of interest. These plates were then machined into 24.5 mm width coupons, incorporating a surface notch on either face to permit shear loads to be applied directly to a portion of the test adhesive. A schematic of the specimen can be seen in Figure 5, with the full specimen specifics detailed in the ASTM standard [24]. During testing, deflection in the specimen was measured by two extensometers attached either side of the bond area of the specimen, with the result averaged for calculations.

Three specimens of each of the neat and E21 toughened systems were tested. To minimise experimental uncertainty, particular care was taken in surface preparation of the specimens prior to bonding, and ensuring correct adhesive mixture ratios were used. The TALS specimen manufacture procedure is detailed in Appendix A.

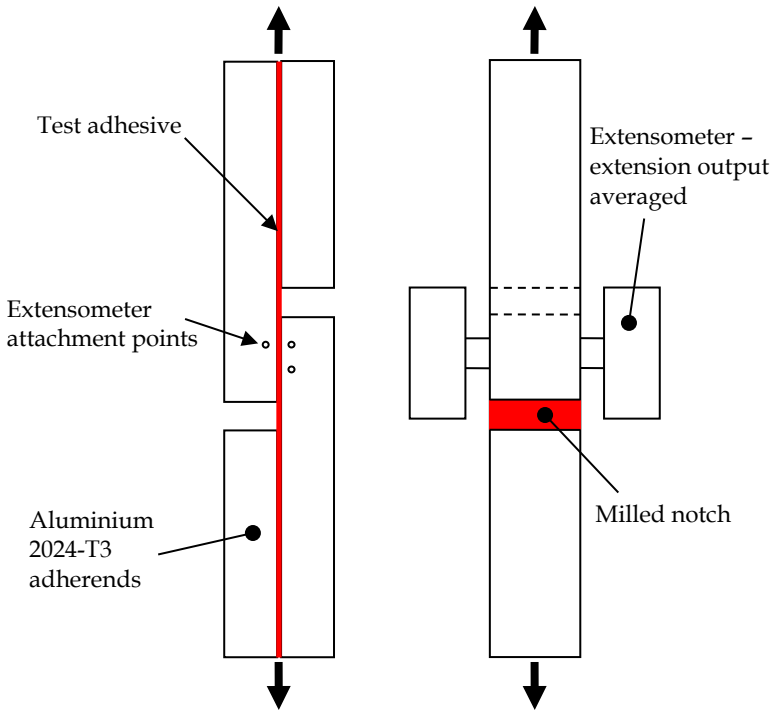

Figure 5 – Schematic of thick Adherend Lap Shear (TALS) specimen.

2.4.3 Four Point Flexural Strength Testing

A four point bend test was used to characterise the flexural strength (F_{4PB}) and tangent flexural modulus in bending (E_B) of each of the toughened resin systems when incorporated within a carbon fibre reinforced lay-up.

The flexural strength was defined as the maximum stress in the outer fibre of the specimen at the moment of break, and was determined using Equation 6. This maximum fibre stress will occur directly below the loading noses on the underside of the specimen at the centre of the support and load spans as depicted in Figure 6.

$$S = \frac{PL}{bd^2} \quad \textbf{(6)}$$

Where:

S = fibre stress (MPa)

P = load applied at break (N)

b = specimen width (mm)

d = specimen thickness (mm)

L = support span (mm)

For all measurements, L was set equal to sixteen times the specimen thickness, and the loading span set equal to one third of the support span. Five specimens per material combination were tested.

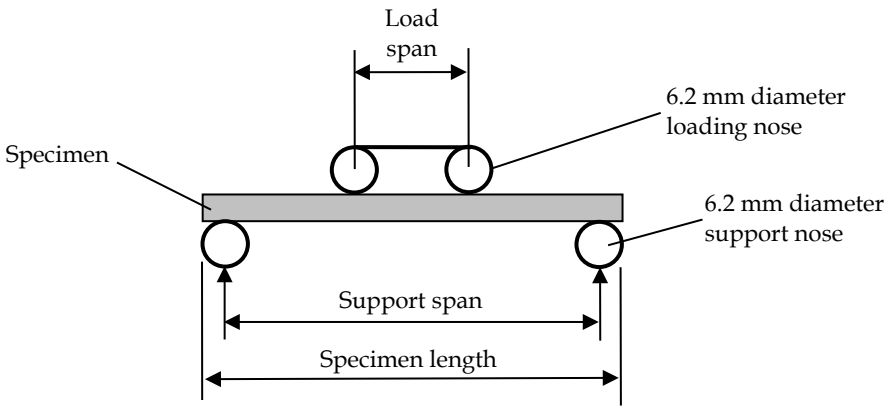

Figure 6 – Four point bend configuration.

In order to avoid failure due to stress concentration directly under the loading nose, 6.2 mm diameter loading noses were used (a loading nose of up to 1.6 times the specimen thickness is permitted according to the ASTM standard [25]), and a sheet of silicon placed between each loading nose and the specimen. The silicon allowed for a more evenly distributed load, reducing localised stresses at each of the loading nose locations on the top surface of the specimen.

The tangent flexural modulus in bending (E_B) was calculated by using Equation 7. In this equation, the gradient, *m*, was calculated as the slope of a tangent drawn to the steepest initial straight-line portion of the four point bend applied load to mid-span deflection.

$$E_B = 0.21L^3 \frac{m}{bd^3} \tag{7}$$

Load was applied to each specimen using an INSTRON 1185 electromechanical universal testing machine equipped with a 100 kN load cell. A constant cross head displacement rate (R) was calculated for each specimen set tested using Equation 8.

$$R = 0.185Z\frac{L^2}{d} \quad (8)$$

Where:

Z = rate of straining of outer fibre of specimen, set at 0.01 mm/mm

d = Specimen thickness (mm)

L = Support span (mm)

Simultaneous measurement of applied load and mid-span deflection were recorded throughout the test until the mid-span deflection (D) had caused strain in the outer fibres to reach 0.05 mm/mm (calculated using Equation 9, or until the specimen had failed. The mid-span deflection was measured using a linear variable differential transformer (LVDT) placed on the top surface of each specimen and connected to a Yokogawa WE7000 data acquisition unit, sampling at 10 Hz.

$$D = 0.21r\frac{L^2}{d} \quad (9)$$

Where:

D = mid-span deflection (mm)

r = strain (mm/mm)

2.4.4 Double cantilever beam

The Double Cantilever Beam (DCB) test was used to determine the mode I fracture toughness of both carbon fibre reinforced SBM and MAM toughened epoxy resin materials. This was performed in accordance with ASTM standard D 5528 – 01 [26].

The specimens for the test were manufactured using the wet lay-up technique described in Section 2.2 with a uni-directional IM7 fabric used to produce a 16 ply uni-directional panel. At the mid-plane of the specimen during lay-up, a 25 µm Teflon insert was placed to form an initiation site for delamination growth following load application. Load was then applied to the specimen by way of bonded aluminium hinges as shown in Figure 7, and the crack propagation length, a_0, recorded using a travelling microscope. An INSTRON 1185 electromechanical universal testing machine with a 100 kN load cell was used to apply the load at a constant rate of 2mm/min, with the applied load and cross head displacement recorded during load application.

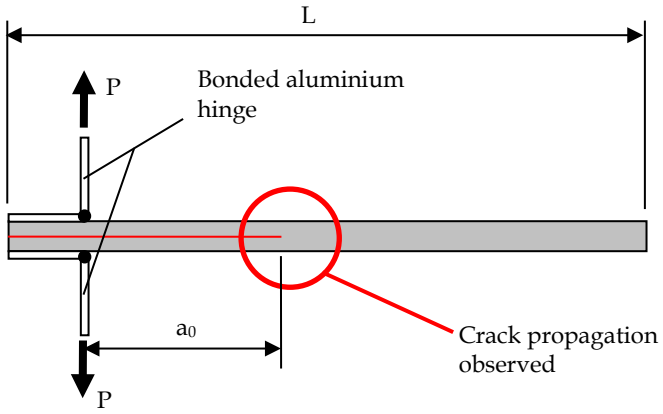

Figure 7 – Double Cantilever Beam (DCB) test configuration

To compare the performance of the toughened and neat epoxy resin systems, the resistance to crack growth was characterised by the strain energy release rate of crack propagation, that is, the rate at which energy is absorbed by the growth of the crack. For crack propagation to occur, this strain energy release rate must exceed a critical value, which is known as the critical strain energy release rate, G_{Ic}. For mode I crack propagation in a material, G_{Ic} is considered to be the materials fracture toughness.

The critical strain energy release rate can be calculated using a Beam Theory method via Equation 10.

$$G_{Ic} = \frac{3P\delta}{2ba} \tag{10}$$

Where:

G_{Ic} = Mode I interlaminar fracture toughness (J/m²)

P = applied load (N)

δ = cross-head displacement (m),

b = specimen width (m)

a = delamination length (m)

This equation assumes that the DCB specimen is perfectly clamped at the delamination front. In practice this is not the case, and rotation of the delamination front may occur. In order to account for this in the calculation of the strain energy release rate, the ASTM standard [26] recommends use of a slightly longer delamination front, $a + |\Delta|$, where Δ is computed using the technique outlined in Appendix B for each tested specimen. This gives rise to the Modified Beam Theory (MBT) method, for which G_{Ic} is expressed as,

$$G_{Ic} = \frac{3P\delta}{2b(a+\Delta)} \tag{11}$$

The point on the sample load/deflection curve at which Equation 11 is applied will affect the value of GIc obtained. Three different points are considered in the ASTM standard [26]:

1. The point of deviation from linearity on the load-displacement plot (NL).
2. The point at which delamination is visually observed on the edge of the specimen following the pre-crack (VIS).
3. Drawing a line from the origin and offset by a 5% increase in compliance from the Hookean region of the load-deflection curve, the intersection of this point with the load-deflection curve is another possible calculation point. If this point occurs after the maximum load point, the maximum load point is to be used. This criterion is known as the 5%/MAX point.

Calculations for all three points were made, however NL and 5%/MAX points were found to provide the lowest error. In order to correlate applied load and crack propagation length, a digital camcorder was used to simultaneously monitor the INSTRON load and displacement values and the travelling microscope output. This experimental set-up can be seen in Figure 8. By reviewing the recorded video the VIS, NL and MAX points could be recorded and compared. The full set of specimen results are presented in Appendix G.

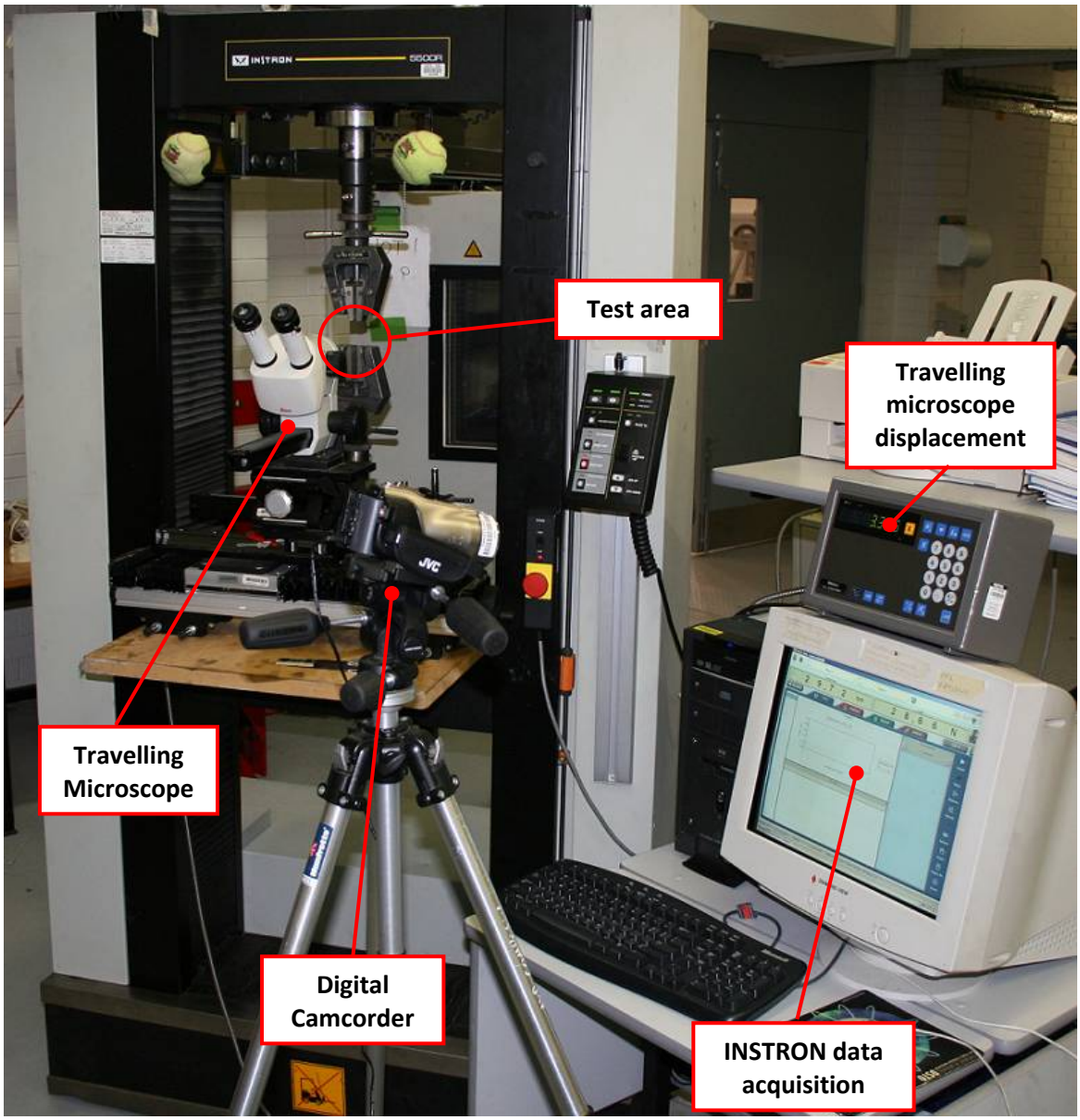

Figure 8 – Experimental set-up for double cantilever beam testing

2.4.5 Dynamic Mechanical Thermal Analysis

Dynamic Mechanical Thermal Analysis (DMTA) was used to determine the glass transition temperature, T_g, for the toughened and neat K3600 system, and also to determine an appropriate mix-ratio and cure profile for the LY556 resin system.

Testing was performed using a Polymer Laboratories Mark III Dynamic Mechanical Thermal Analyser, with the storage and loss moduli recorded as a function of specimen temperature. All specimens were loaded in a single cantilever bending mode (flexure) with 1, 10 and 15 Hz oscillatory frequencies applied.

The DMTA provides outputs for the tested material loss moduli (E″) to storage moduli (E′). The ratio of E″ to E′ provides an indication of the dampening behaviour of the material tested, and is equal to the tangent of the phase angle shift (δ) between stress and strain vectors as shown in Equation 12. This phase difference can equivalently be considered as the phase shift between the oscillatory mode applied to the specimen, and the displacement response of the specimen.

$$\frac{E''}{E'} = \tan(\delta) \tag{12}$$

The glass transition temperature of the specimen is observed by a peak in this $\tan(\delta)$ response for a given oscillatory frequency, and also by a sudden and considerable change in the materials storage moduli (E′). This storage modulus is equivalent, but not equal to, the elastic modulus of the material being tested in that it represents the materials elastic performance under cyclic loading conditions as opposed to static loads.

The specimen temperature was commonly ramped from 40 °C to a maximum of 200 °C at a ramp rate of 3 °C/min, with the temperature ranges chosen depending upon the expected glass transition temperature. For a number of the specimens, several consecutive runs were performed to provide an indication of the degree of cure and the associated shift in the characteristic peak in the $\tan(\delta)$ response.

2.5 Thermal degradation

Military aircraft are using increasingly larger amounts of composite materials to meet the high thermal and mechanical demands imposed during flight. The availability of Bismaleimide resin technologies has also encouraged this, offering service temperatures of up to 245 °C. Consequently, knowledge of the performance of any bonded composite repair resin system following exposure to elevated temperatures is significant.

To investigate this, five sets of 3 coupons for each resin system (30 coupons in total) were initially dried in an electric oven set to 70 °C, with their weight periodically measured until a dry equilibrium was reached (weight change of less than 0.1%). The oven temperature was then increased to 180 °C, and three coupons from each resin system removed and weighed at 5, 9, 24, 48 and 100 hour intervals. To quantify any degradation in mechanical strength resulting from exposure to the 180 °C environment, SBS testing was performed on the 100 hour conditioned coupons. These SBS results were then compared to as-cured resin material coupons.

3. Results and discussion

3.1 Assessment of Specimen Constituent Content

The results of acid digestion applied to the K3600 specimen off-cuts are shown in Figure 9 and Figure 10.

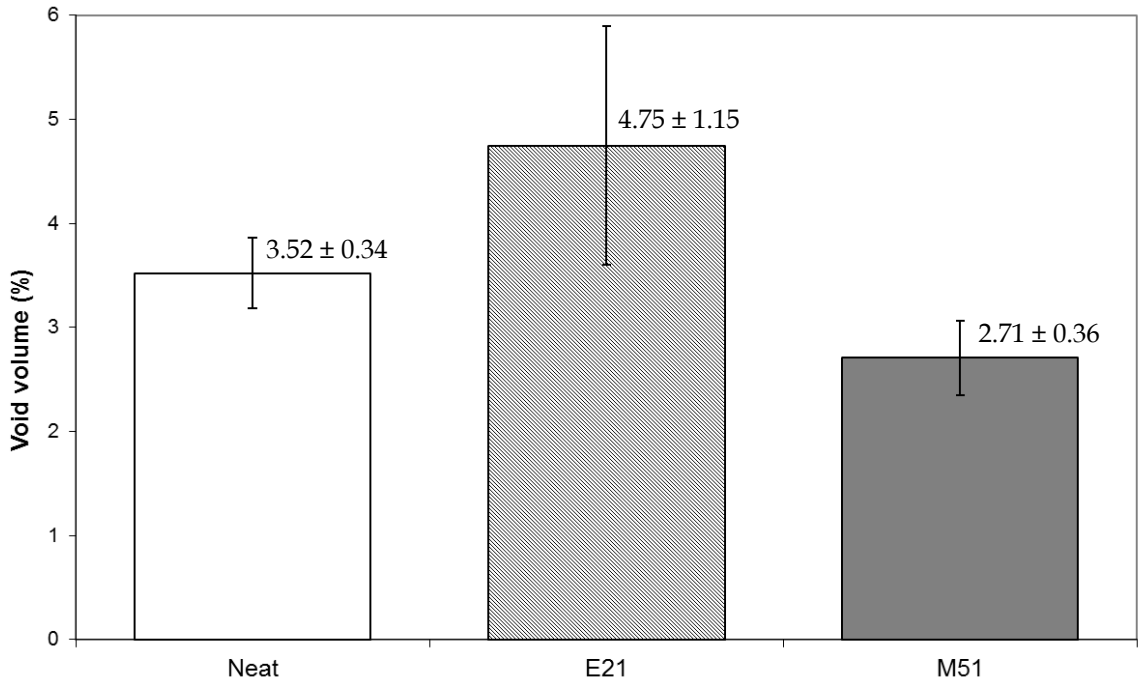

Figure 9 – Average void volume for K3600 wet lay-up laminates with and without copolymer additives. Error as shown (standard deviation).

The void volume for each of the three different specimens tested appeared roughly equal. The voiding was thought to arise primarily from mechanical entrapment of air during the wet lay-up and also from volatiles and vaporised moisture which was locked into the matrix during cure. The application of vacuum to consolidate the lay-up served to remove gross porosity accessible from the outside of the lay-up, however was thought to also cause dilation of trapped voids in the laminate, contributing to an increased void volume following cure.

The observed variation in the fibre volume fraction was thought to be a result of differences in resin viscosity. Lower resin viscosities permit flow and additional resin bleeding during consolidation and cure, thus leading to a higher fibre volume fraction in the final cured part. The K3600 neat system exhibits a viscosity of between 200 and 400 mPa.s at the cure temperature of 25 °C [27]. This compares with technical data sheet viscosities of 1060 mPa.s and 400 mPa.s for the E21 and M51 copolymers mixed at 10% PBW in Diglycidyl ether of bisphenol-A (DGEBA) at 80 °C [28, 29]. As a result, the neat

K3600 system experienced the highest fibre volume fraction, followed by the M51 and then E21 toughened K3600 samples.

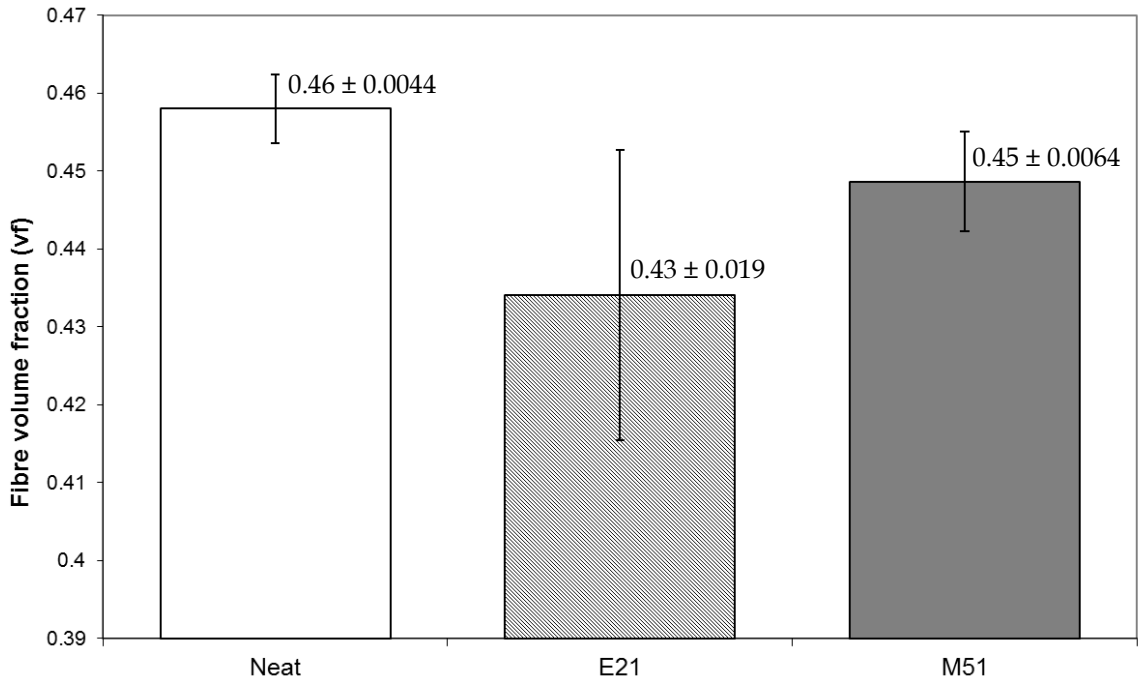

Figure 10 - Average fibre volume fraction for K3600 wet lay-up laminates with and without copolymer additives. Error as shown (standard deviation).

The substitution of the vacuum pressure for positive pressure during consolidation and cure is recommended as a means of reducing average void volumes. High positive pressures could also lead to improvements in the fibre volume fraction of the cured specimens. The use of an autoclave would achieve this aim, or in a repair situation, application of pressure by way of mechanical clamps or a double vacuum bagging technique. The double vacuum bagging technique (as opposed to the single vacuum bagging technique used in this study) permits removal of porosity, prevents dilation of internal voids and enables consolidation and compaction of the lay-up.

3.2 Glass transition temperature (T_g) analysis

Figure 11 shows the elastic moduli (E′) and dampening behaviour of the K3600 system combined with each of the two copolymers investigated for a 1 Hz bending mode oscillation via DMTA. Similar trends are observed for higher oscillatory frequencies (5 and 10 Hz), with the full results provided in Appendix C.

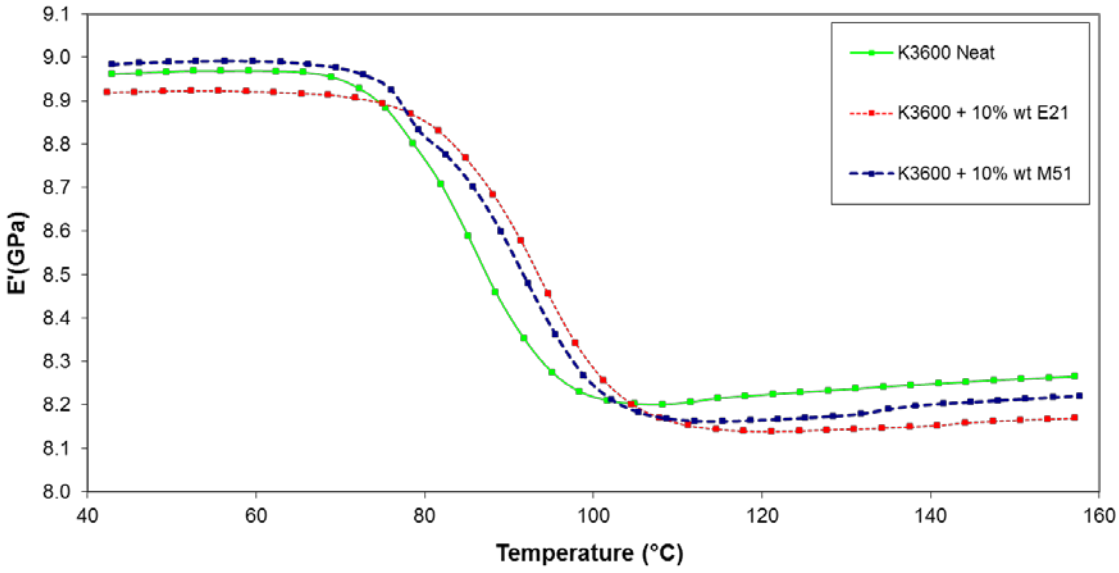

(a)

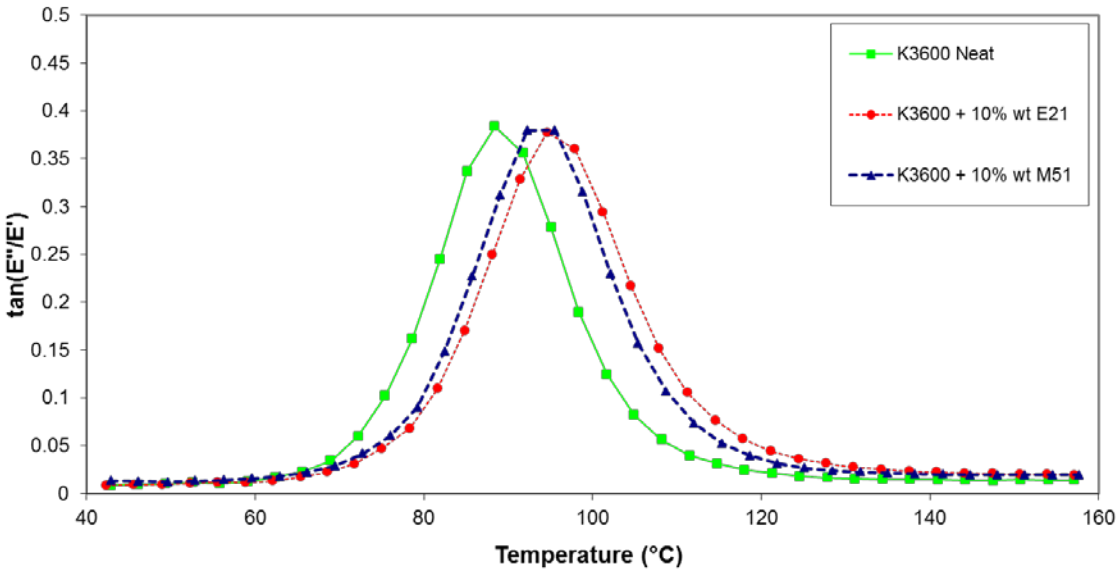

(b)

Figure 11 – DMTA results for a 1 Hz oscillatory frequency applied to mixtures of K3600 and E21 or M51 copolymers: (a) Change in storage modulus as a function of temperature, and (b) change in dampening behaviour as a function of temperature.

The T_g, when defined as the peak in the tan(E″/E′) profile, increases with the addition of both 10% PBW E21 and 10% PBW M51 copolymers. This point occurs at 88 °C for the neat K3600, at 95 °C for K3600 with E21 and 92 °C for K3600 with M51. The neat K3600 glass transition temperature compares well with the manufacturers technical data sheet value of 90 °C [27].

To determine a mix ratio that yielded the highest T_g for the LY556 system, DMTA was applied to several different neat LY556 specimens of different mix ratios and cure times (at 80 °C). Of the four components comprising the resin, Aradur 1571 is primarily required to crosslink with the resin component (Araldite 556), whilst LME 10188 is required to accelerate the rate of cross-linking, and thus both directly impact the final cured properties and T_g. The technical data sheet [30] suggests three possible mix ratios:

1. **100** LY556 : **23** Aradur 1571 : **3** LME 10188 : **12** Hardener XB 3403
2. **100** LY556 : **23** Aradur 1571 : **5** LME 10188 : **12** Hardener XB 3403
3. **100** LY556 : **23** Aradur 1571 : **7** LME 10188 : **12** Hardener XB 3403

The effect of variations in the amount of Aradur 1571 content in the mixture (with all other quantities held constant) is shown in Figure 12. This plot shows Aradur 1571 content had little effect on T_g (approximately equal to 120 °C) when cured for 8 or 12 hours at 80 °C. For a 4 hour cure, the T_g drops to approximately 80 °C, and remains mostly independent of the Aradur 1571 content.

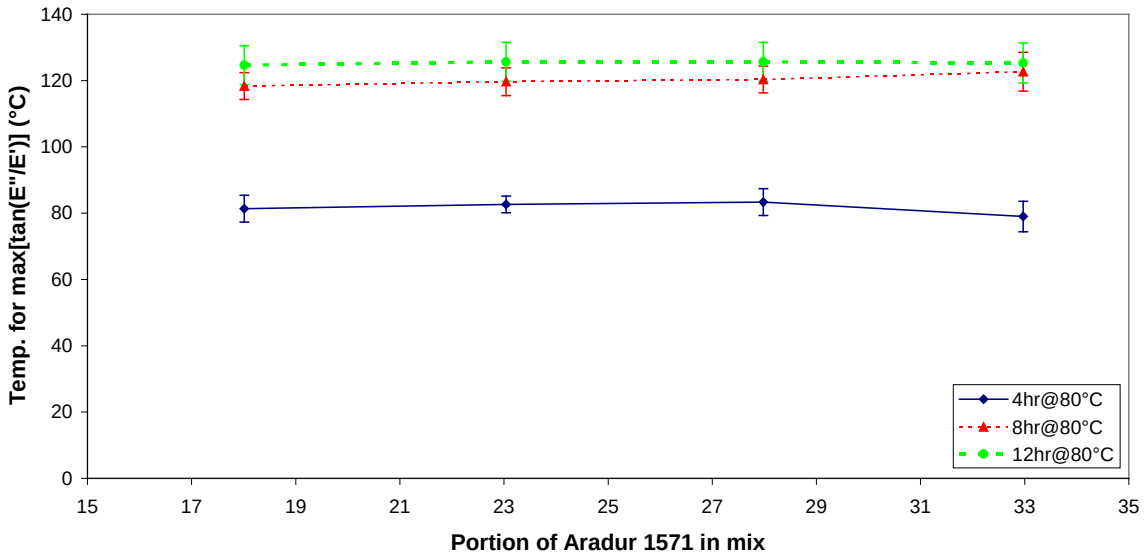

Figure 12 – The effect of Aradur 1571 content on T_g for LY556 resin (error bars equal to standard deviation across frequencies analysed). Respective portions of LY556, Aradur1571, LME10188 and XB3403 are 100:x:7:12.

Figure 13 shows the effect of variations of LME 10188 content on T_g for the LY556 resin system. This figure shows increasing amounts of LME 10188 in the mixture provided an increase in the T_g for all cure times investigated.

For the resin considered, LME 10188 was used to accelerate cross-linking. Reducing content of the LME 10188 in the resin mixture thus reduces the rate of cross-linking and hence quantity of cross-linking for a fixed cure time. This impacts directly on the final cured T_g. For lower cure times (i.e. 4 hours) this effect is more pronounced, as limited time is provided for cross-linking to occur. In some instances, two peaks in the tan(E″/E′) response were noted, indicating more than one phase in the tested material; this can be seen in Figure 14. As the amount of LME 10188 was increased, the multiple peaks in the

tan(E″/E′) response become one clearly defined peak, indicating material homogeneity and progression toward complete cross-linking within the sample.

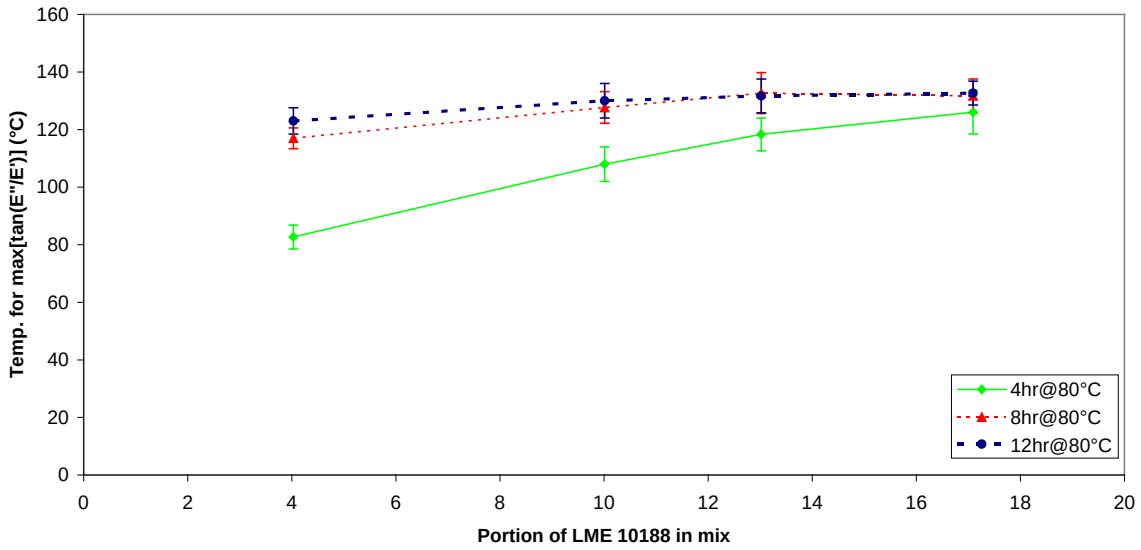

Figure 13 - The effect of LME 10188 content on T_g for LY556 resin (error bars equal to standard deviation across frequencies analysed). Respective portions of LY556, Aradur1571, LME10188 and XB3403 are 100:23:x:12.

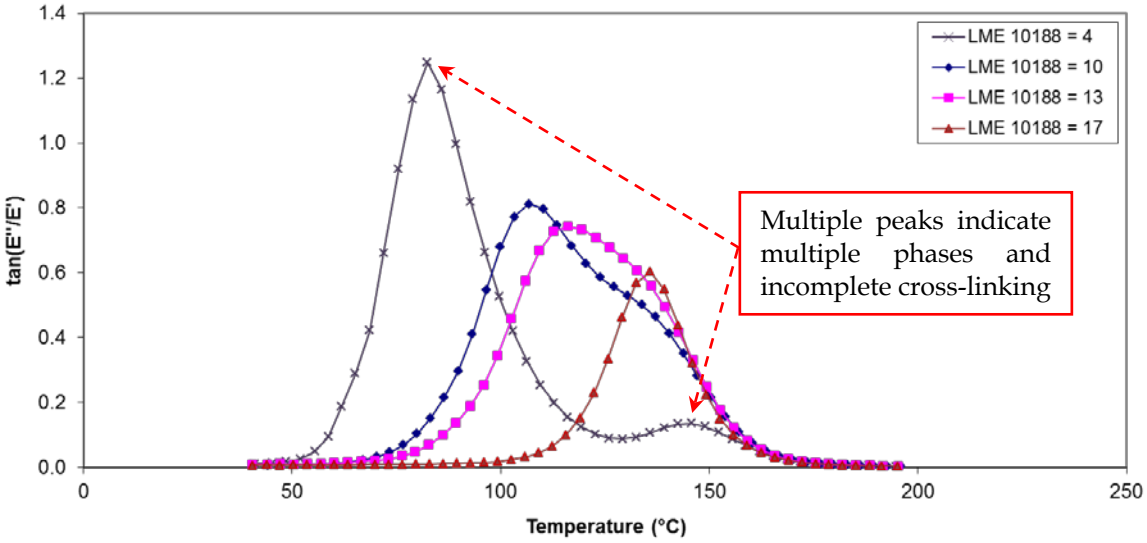

Figure 14 – Effect of LME 10188 content on tan(E″/E′) response averaged over 1, 5 and 10 Hz oscillatory frequencies for LY556 resin. Mixtures were cured for 4 hours at 80 °C. Respective portions of LY556, Aradur1571, LME10188 and XB3403 are 100:23:x:12.

From this investigation, system 3 of the manufacturers technical data sheet [30] was chosen as the mix ratio for the LY556 resin mixture; The cure schedule chosen was a b-stage of 24 hours at 23 °C, followed by 8 hours at 80 °C. Figures 12 and 13 show that this cure time and mixture yields a T_g of 120±4.2 °C, similar to the longer 12 hour cure cycle, and slightly higher than the 110-115 °C T_g range specified in the technical data sheet [30].

This reduced cycle time is advantageous for composite repair applications where time of repair is critical for platform turn-around.

3.3 Thermal degradation

Figure 15 shows the residual weight for each of the two resin systems investigated as a function of exposure time at 180 °C. As can be seen, less than 3% weight loss was experienced by the K3600 system after the 100 hour exposure time (excluding drying), with the four part LY556 system experiencing less than 2% weight loss. Typical military fighter aircraft flying at around 2000 km/h at an altitude of 15000 m will experience skin temperatures of approximately 100 °C* [31]. The use of the 180 °C is thus an extreme conditioning environment for the mechanical SBS coupons and the minimal weight loss after 100 hour exposure to this condition is encouraging.

One significant result to note from the weight loss trend of Figure 15 is the 1% weight loss experienced by the K3600 system following only 5 hours of exposure. This compares to a loss of 0.2% in the LY556 resin over the same time period. This difference is thought to be a result of differing thermal oxidation rates of the two systems. Work by Buch et al. [32, 33] suggests weight loss of epoxies subject to heating is a result of chain scission within the epoxy, and subsequent liberation of degradation products, decreasing the weight of the specimen. This theory is further supported by the colour and opacity change during conditioning as shown in Figure 16. These changes suggest chemical modification occurring in the outer regions of the resin due to thermo-oxidation.

* This temperature assumes isentropic flow, and is for stagnation points in the air flow around the aircraft such as wing leading edges, and the tip of the nose cone where local flow velocities are zero.

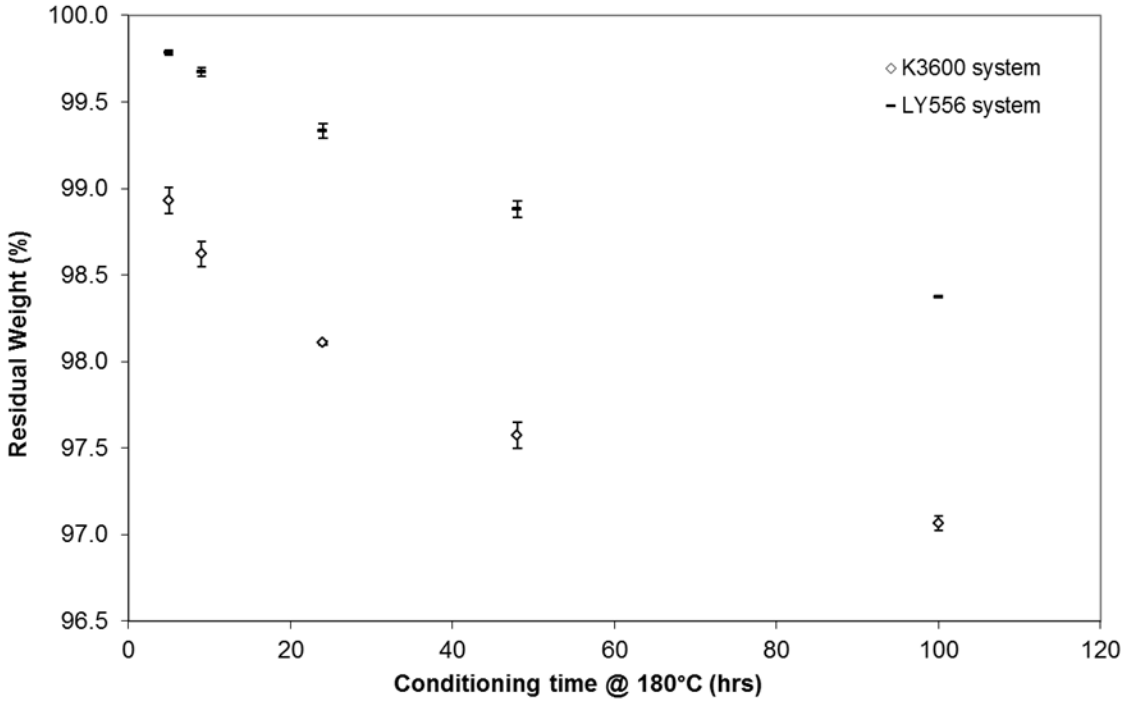

Figure 15 – Sample weight loss for neat K3600 and LY556 epoxy resin system coupons as a function of conditioning time at 180 °C (dried prior to testing). Error bars represent standard deviation in measurement.

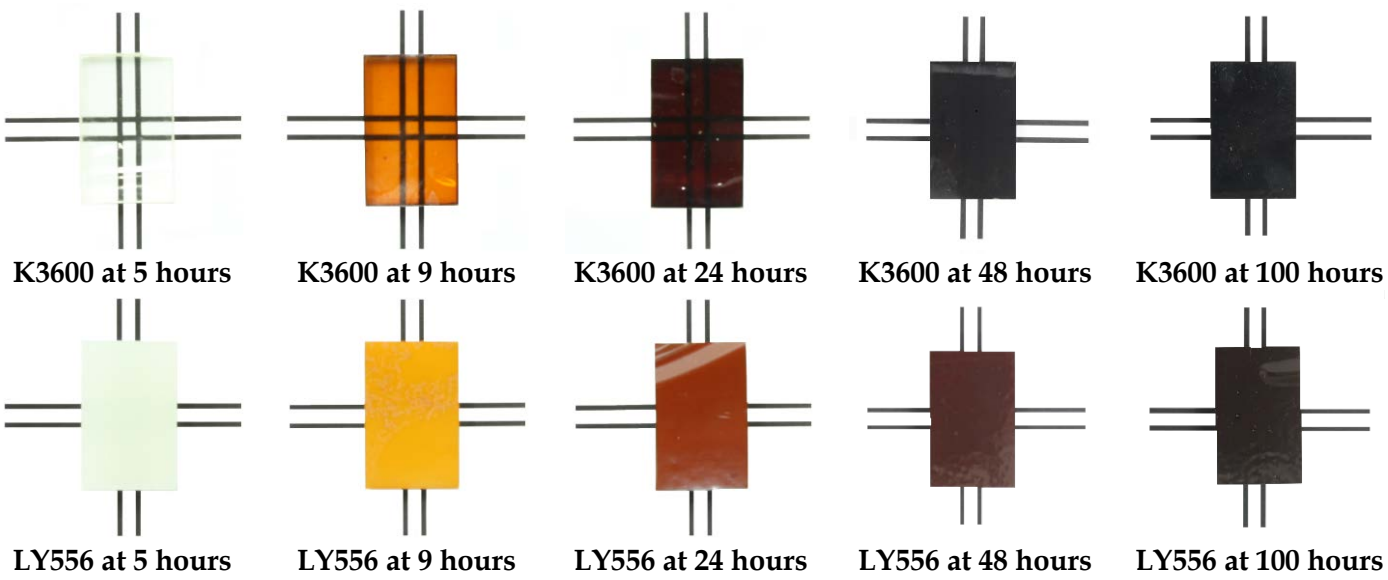

Figure 16 – Change in specimen colour and opacity as a function of exposure time. Black targets behind specimens used to highlight change in opacity.

3.4 Short Beam Shear strength

3.4.1 Unconditioned Results

The SBSS of the K3600 and LY556 resin systems neat and with the addition of E21 and M51 copolymers are shown in Figure 17. The full set of results is shown in Appendix D. In general, both resin systems experienced a 10-12% reduction in SBSS following the addition of the either of the copolymers.

The use of the SBS method is ideally suited for the comparative assessment of SBSS performance within a specimen set of similar geometry and properties. Although shear is the dominant load applied during loading in the method, the internal stresses are complex, and a number of modes of failure can occur. Of particular significance is the localised shear, in-plane and transverse stress occurring at the contact point between loading nose and the specimen. This can give rise to matrix crushing, and a subsequent compression failure on the top surface of the specimen and/or tensile failure on the bottom face. For the specimens tested in this research, failure was dominated by a combination of compressive failure at the point of loading nose contact with the specimen, and interlaminar shear failure. During manufacture, the use of higher consolidation pressures (through use of an autoclave or higher vacuum pressures) is suggested as a way to reduce the proportion of compressive failure occurring in the specimens. Uniformity of failure mode between the specimens tested in this study justifies the use of the results for comparative purposes.

The observed reduction in SBSS for the toughened resin systems is thought to be partly a result of the lower fibre volume fractions (v_f) observed in these coupons (see Section 3.1). A lower v_f correlates to a reduction in tensile and compressive strength due to the lowered density of axial fibres to carry an applied load. This in-turn translates to a reduction in coupon flexural strength. As noted previously, the SBS coupons tested in this study experienced a combination of compression and interlaminar shear failure, and it is likely that the compression failure accentuated the reduced flexure strength. Although a consistent reduction in SBSS was observed for both resin systems investigated in this research, other work in literature has shown varied shear performance with the addition of copolymer additives. Work by Quaresimin and Varley [34] indicated a substantial reduction in Interlaminar Shear Strength (ILSS) following the introduction of an SBM copolymer to a four part epoxy resin system. The copolymer, AF-X E20, supplied by Arkema, was mixed at 10% PBW into the four part epoxy resin system, and used to pre-impregnate a unidirectional carbon tape, which in turn was used to manufacture the SBS specimens. The substantial reduction in ILSS (up to 61%) was attributed to entrapment of solvents during cure (used to introduce the copolymer into the epoxy), causing excessive voiding, and subsequently reducing fibre volume fraction whilst also restricting formation of nanostructures in the matrix.

In contrast to this, work by Barsotti et al. [35] for Arkema indicated varied improvement in lap shear strength with the addition of MAM copolymers to DGEBA epoxy resin cured with dicyandiamide (DICY), polyetheramines (Jeffamine D230) or diethylene triamine (DETA) hardeners. Equivalent lap shear strength to the neat epoxy was noted for the DICY

and D230 cured epoxies, whilst the DETA cured epoxy experienced an improvement in lap shear strength of approximately 45%. Justification as to these observations were not provided in the research, however it is thought that varied compatibility between copolymer additive and each of the host resin systems could account for the varied performance.

The compatibility of the copolymer to the host resin is thought to drive the type, extent and morphology of nano-structure formed within the resin by the copolymer. These nano-structures can lead to changes in the mechanical performance of the resin once cured, and so an understanding of the copolymer compatibility to the resin in question is essential. For this reason, for each of the copolymer/resin combinations investigated in this work, microscopy was used to interrogate the type of nano-structuring present, with the results of this work presented in Section 3.8.

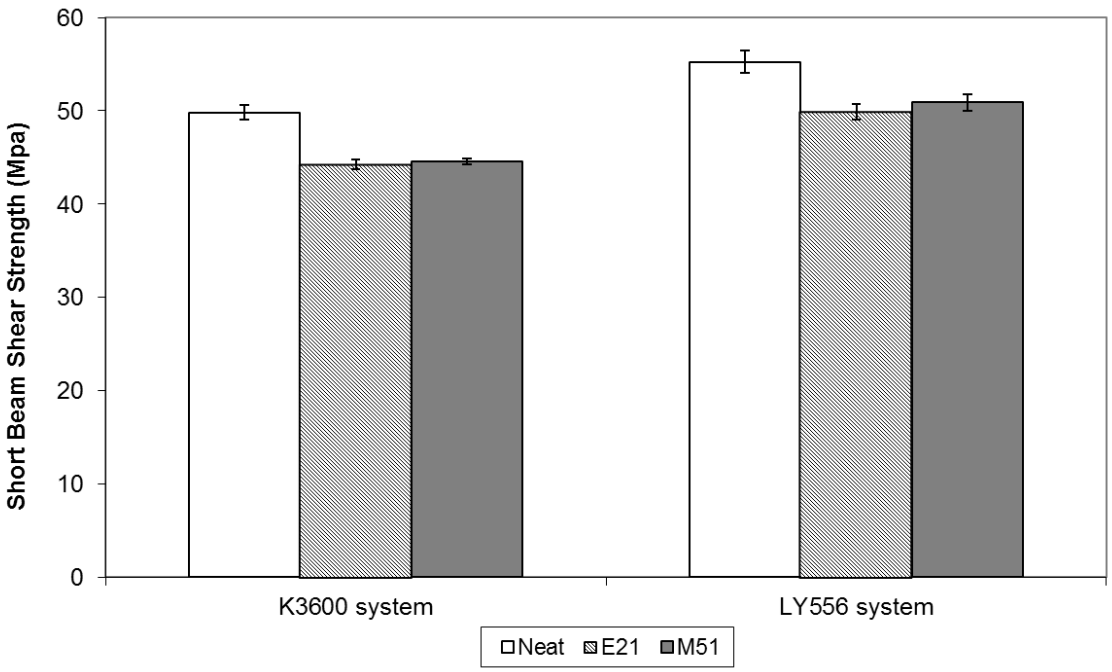

Figure 17 – SBSS for K3600 and LY556 systems neat, and with the addition of E21 and M51 copolymers. Error bars shown represent standard deviation in the specimen set tested.

3.4.2 Conditioned for 100 hours at 180 °C

As outlined in Section 2.4.1, a second SBS specimen set was exposed to 180 °C for 100 hours, and then tested. A comparison of the unconditioned and conditioned coupon SBSS's is shown in Figure 18 for the K3600 resin system and Figure 19 for the LY556 resin.

Given the weight changes observed following conditioning in Section 3.3, a reduction in SBSS was expected for both resin systems. As can be seen in the results, all systems (toughened and un-toughened) exhibited a less than 10% reduction in SBSS, with most

presenting a negligible reduction (within error). Like the unconditioned SBS coupons tested, failure in the conditioned coupons was dominated by a combination of compressive failure at the point of loading nose contact with the specimen, and interlaminar shear failure.

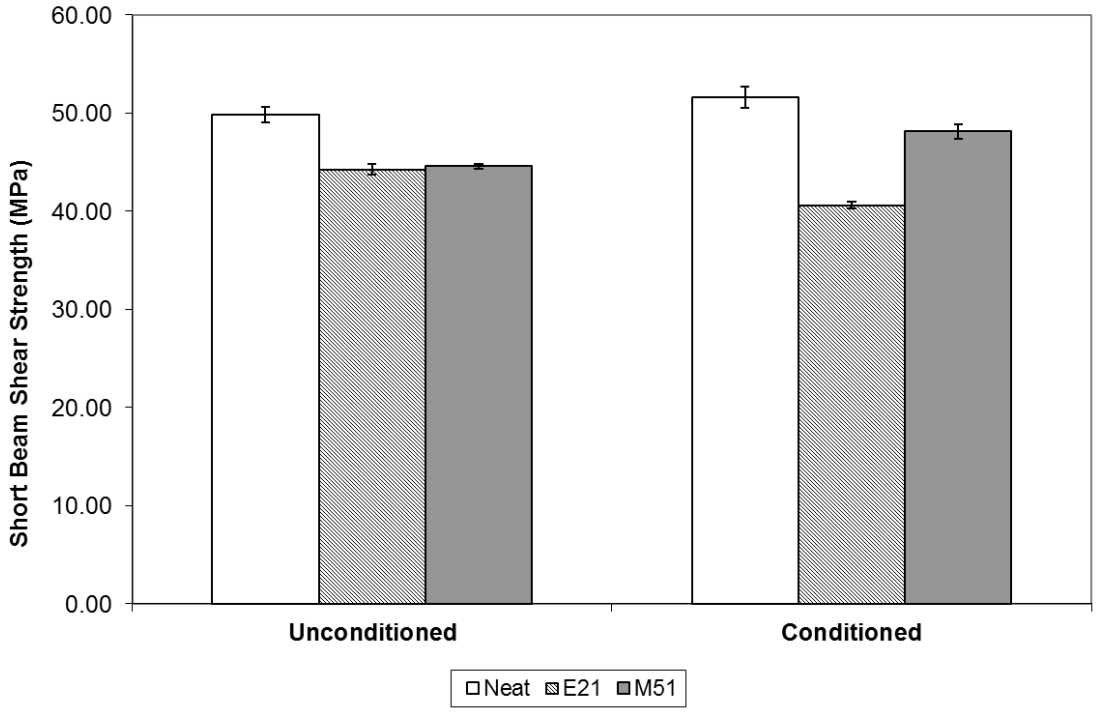

Figure 18 – SBSS for K3600 toughened and neat resin systems prior to and following exposure to 180 °C for 100 hours. Error bars shown represent standard deviation in the specimen set tested.

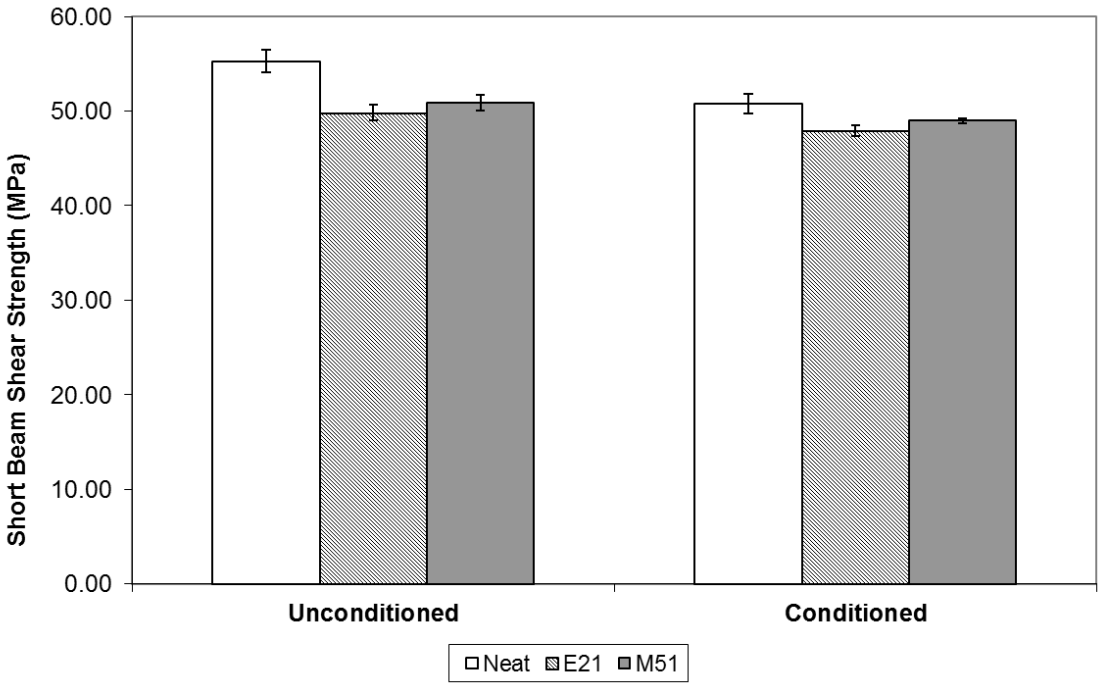

Figure 19 – SBSS for LY556 toughened and neat resin systems prior to and following exposure to 180 °C for 100 hours. Error bars shown represent standard deviation in the specimen set tested.

This result is in-line with other work presented by Ozcelik et al. [36], which also indicated a slight reduction in SBSS following conditioning of a carbon fibre reinforced epoxy material. The study concluded that reductions in SBSS due to exposure of carbon/epoxy composites to elevated temperatures results from oxidation of the specimen, and accompanying degradation of the matrix. Furthermore, increasing exposure temperatures, up to and in excess of the matrix T_g, leads to increased degradation rates, and corresponding reductions in SBSS. For the AS4/3501-6 specimens tested in the study, SBSS reductions of around 15% ± 4% occurred for a conditioning temperature of 200 °C for 100 hours, ~20 °C above the systems T_g.

3.5 Thick Adherend Lap-Shear

For the TALS specimens tested, consistent bond-line thicknesses and bond areas were measured, with all specimens failing due to cohesive failure in the bond-line. A summary of the results obtained through TALS testing can be seen in Table 1, with further results detailed in Appendix E.

Table 1 – TALS results for K3600 system and comparison with SBSS values.

Material	Ultimate shear strength	Ultimate shear strain	Shear modulus
	MPa	*mm/mm*	*MPa*
Neat K3600	42.13 ± 0.92	0.35 ± 0.02	431.10 ± 50.27
K3600 + E21	38.78 ± 0.64	0.77 ± 0.12	406.67 ± 40.41

As can be seen in Table 1, a slight reduction, approximately 7%, in the resins ultimate shear strength occurred with the introduction of the E21 toughener, however the ultimate shear strain increased by approximately 120%. In a bonded joint, this high strain to failure, particularly with a limited knockdown in strength, is advantageous as it improves the energy absorption capacity of the joint, and provides greater resistance to damage in service.

The high strain to failure for the toughened resin system (when compared with the un-toughened system) is evident in the stress-strain relationship of Figure 20. As can be seen from the figure, the large area under each of the E21 toughened specimen curves indicates a substantial improvement in the toughness modulus for this system, from approximately 1.3 MJ/m^3 to 3.2 MJ/m^3. Despite this, a reduction in the toughened resins yield stress, coupled with a slight reduction in the toughened resins shear modulus (the gradient of the elastic region of the curve), suggests a reduction in the resins resilience, quantified by the area under the stress-strain curve within the elastic region.

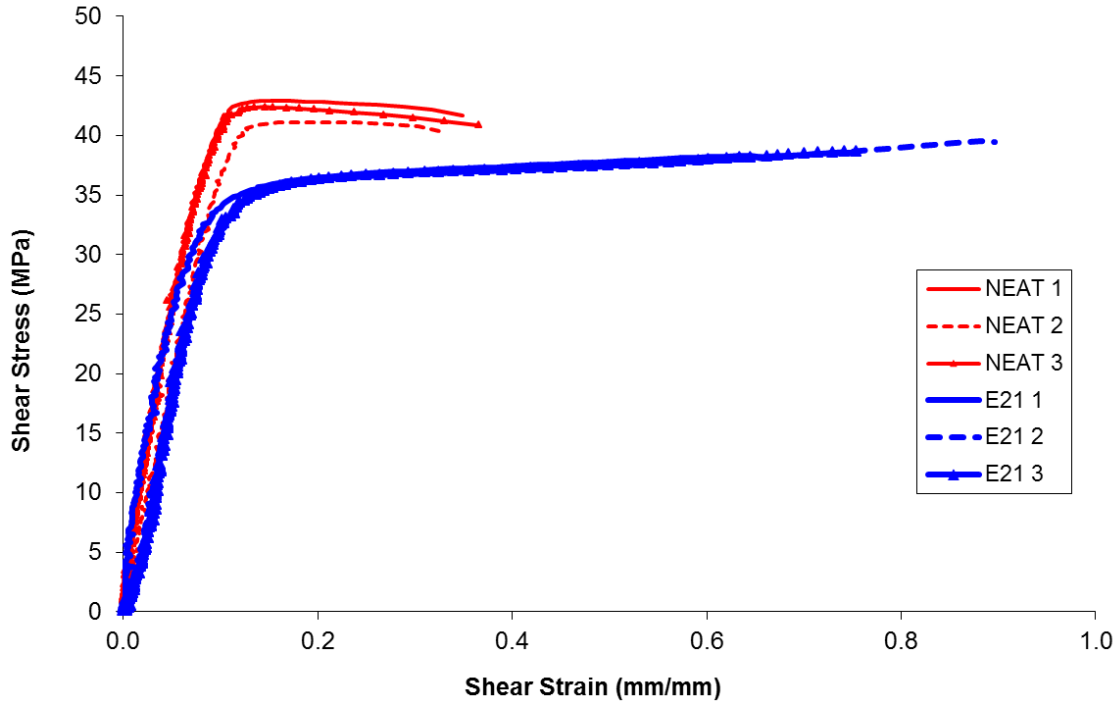

Figure 20 – Shear stress vs. shear strain for the three neat K3600 TALS coupons (NEAT 1, NEAT 2 and NEAT 3) and three E21 toughened TALS coupons (E21 1, E21, 2 and E21 3).

3.6 Flexural strength

The average flexural strength calculated by four-point bend testing for each of the two resin systems with and without the addition of each copolymer can be seen in Figure 21, with the full results presented in Appendix F. This flexural strength is considered the maximum fibre stress at the moment of break (using equation 6), which should theoretically occur at the underside (tensile face) midpoint of the specimen. Unfortunately, many of the specimens tested experienced other undesirable failure modes that invalidated the test results.

For the coupons tested, two dominate failure modes were observed:

1. Compression failure of the matrix directly below the loading noses due to nose bearing on the specimen surface (see Figure 22 and Figure 24 [i]).
2. Tensile failure and fibre breakage at the midpoint on the bottom surface combined with small amounts of compressive failure between loading noses on the top surface (see Figure 23 and Figure 24 [ii]).

The matrix compression failure on the top surface of the specimens was mitigated by inclusion of a thin strip of silicon which locally distributed the applied load about the contact region of the loading nose on the specimen as seen in Figure 23. In doing this, subsequent tests produced tensile dominated failure at the specimen midpoint with small amounts of matrix compression failure on the top surface (again at the specimen midpoint). This undesirable compression failure, which is indicative of poor matrix

compressive properties, is thought to result from the relatively high void content observed in the laminates following cure.

As shown in Section 3.1, void volume content for the laminates manufactured were found to be between 2.71% and 4.75%. For aerospace applications, void volume contents below 1% are considered acceptable, and numerous studies ([13, 18] for example) have demonstrated a close correlation between void content and composite laminate mechanical properties, particularly matrix dominated properties such as compression.

In order to reduce the laminate void contents observed, an increase in the consolidation pressure during cure is required as discussed in Section 3.1. However, to progress with the vacuum bag cured coupons, only those coupons which experienced midpoint tensile dominated failure (be it with small amounts of midpoint compression failure) were included in the flexural strength and modulus calculations.

From these results, the K3600 system presented a 22% reduction in average flexural strength following the addition of E21, and a 16% reduction with the addition of M51. For the LY556 system, the average flexural strength results indicate slight improvements, however a relatively large spread of results (shown as standard deviation error in Figure 21) was observed within each of the specimen sets tested, and it is likely that little to no improvement was actually realised. Further testing with a lower dispersion of results is required to clarify this, and this is likely to be achieved using specimens manufactured with higher laminate consolidation pressures.

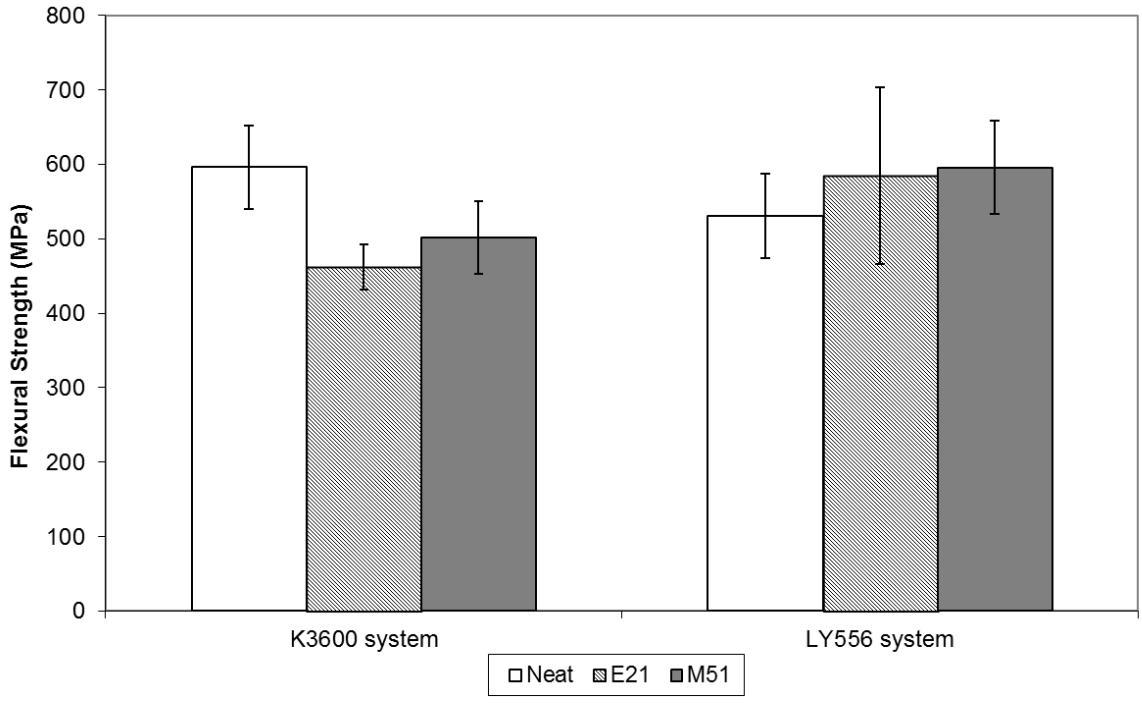

Figure 21 - Flexural strength of K3600 and LY556 systems as determined using the four-point bend test. Error bars indicate standard deviation within the specimen set.

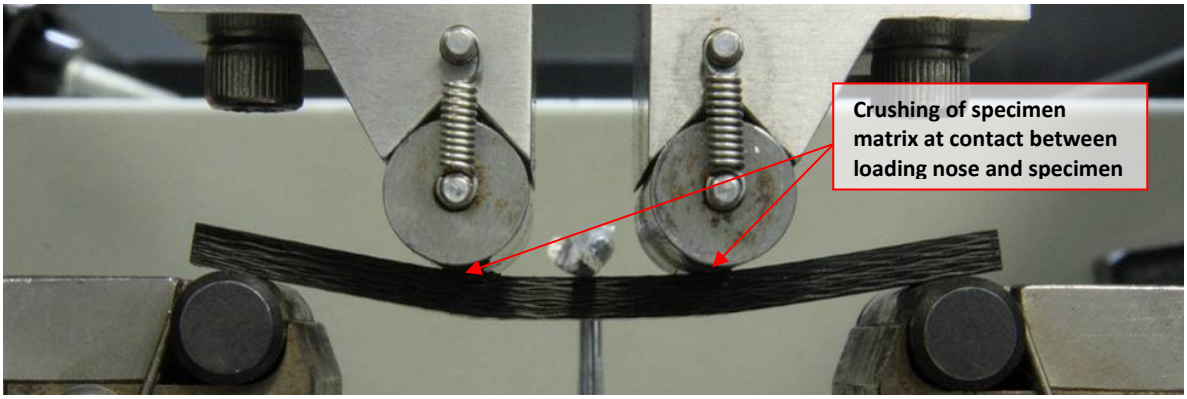

Figure 22 - Example specimen failure for four-point bend loading without the use of a silicon rubber sheet to locally disperse load into the specimen about each loading nose.

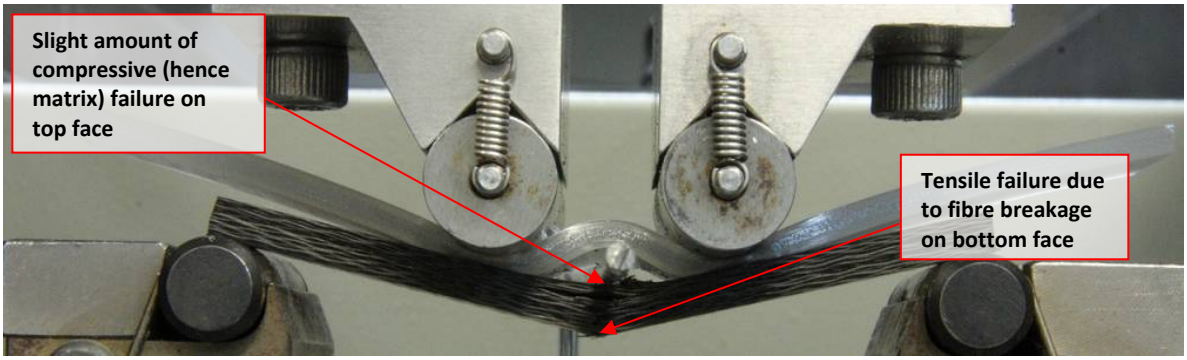

Figure 23 – Example specimen failure for four-point bend loading. A silicon sheet is used to disperse the applied load underneath either loading nose.

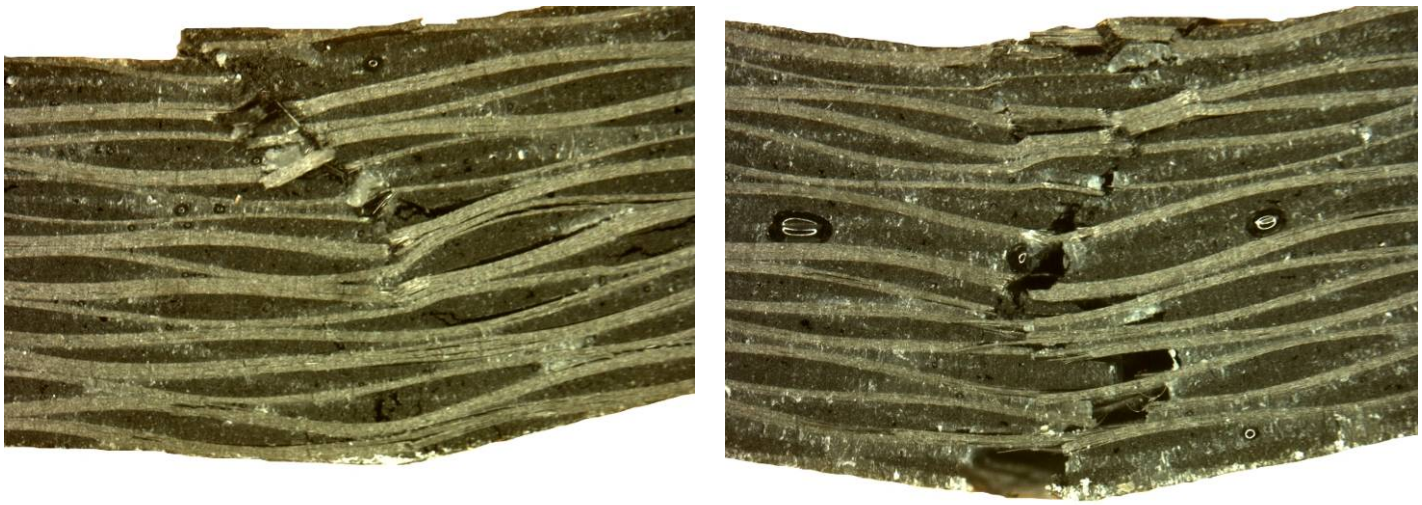

(i) **(ii)**

Figure 24 – Micrographs showing (i) compressive failure due to bearing on the top face of the specimen, and (ii) tensile dominated failure on the bottom of the specimen, which is the desired failure mode for the four point bend test.

For those specimens which flexural strength was calculated, the tangent flexural modulus was also determined, with these results shown in Figure 25. These results indicated the flexural modulus of the K3600 system to be slightly higher than that of the LY556, with the neat K3600 giving a value of 38 GPa ± 1.5 and the neat LY556 giving a value of 33 GPa ± 2.6. The toughened average flexural moduli of either system was approximately equal, with K3600 + E21 and LY556 + E21 providing values of 36 GPa ± 5.9 and 36 GPa ± 4.0 respectively, and K3600 +M51 and K3600 + M51 giving values of 34 GPa ± 2.6 and 34 GPa ± 5.7 respectively.

These four-point bending results suggest that the impact of either copolymer on the flexural properties of both resin systems is negligible, however, further testing on higher consolidation pressure cured laminates is required to improve the observed specimen failure mode, and thus yield more representative results.

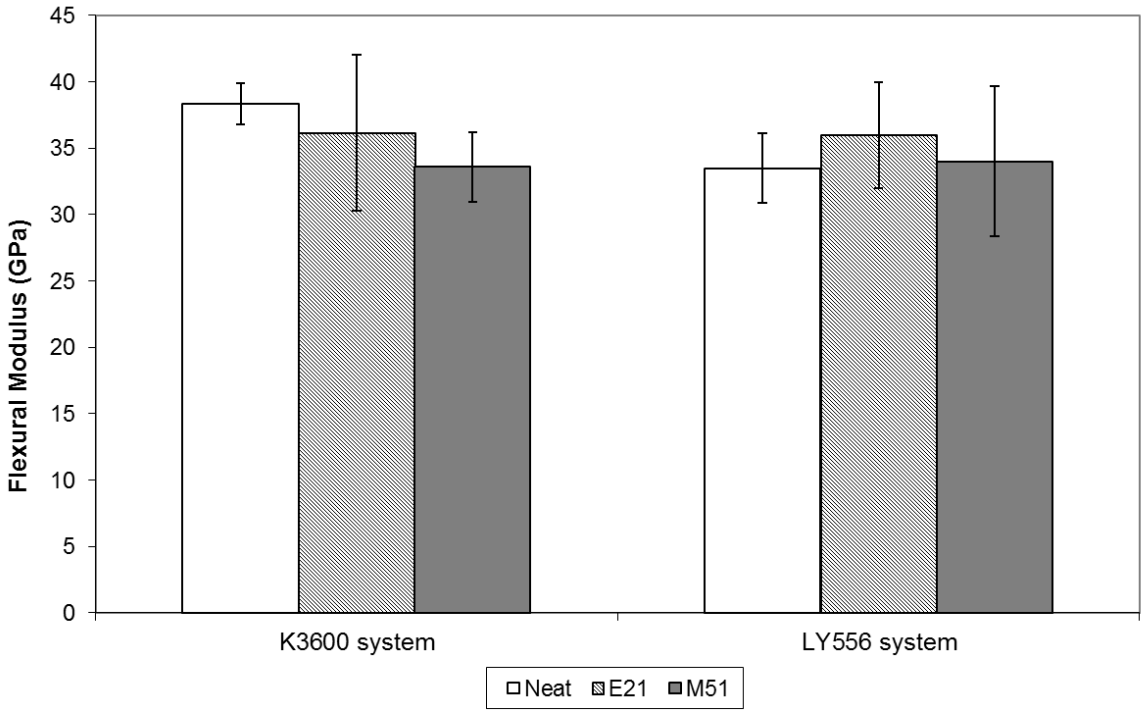

Figure 25 – Tangent flexural modulus determined for each of the tested specimens.

3.7 Mode I interlaminar fracture toughness

From the DCB testing, all specimens failed as expected, with the crack propagating cleanly from the Teflon insert. Of the three possible G_{Ic} values determined for each specimen set (VIS, NL and 5%/MAX as outlined in Section 2.4.4), the averaged NL and 5%/MAX values exhibited the lowest standard deviation within each specimen set, and thus the most consistent fracture toughness results for comparison. The NL and 5%/MAX values are shown in Figures 26 and 27 and were computed using the Modified Beam Theory (MBT) method outlined in Section 2.4.4.

The low standard deviation for NL and 5%/MAX results is supported by work conducted by O'Brien et al. [37], indicating that crack initiation can often occur within the specimen, and hence may not be visually observable at the edges of the DCB specimen width. The initiation energy is, however, observed by non-linearity in the load-displacement plot. Thus for both NL and 5%/MAX points, as they are driven by observations from the load-displacement plot, should provide low deviation results for specimens of the same material. Due to this, and the fact that the NL value is less than the 5%/MAX value, the NL fracture toughness value is commonly used for generating failure criteria in durability and damage tolerance analysis of composite structures.

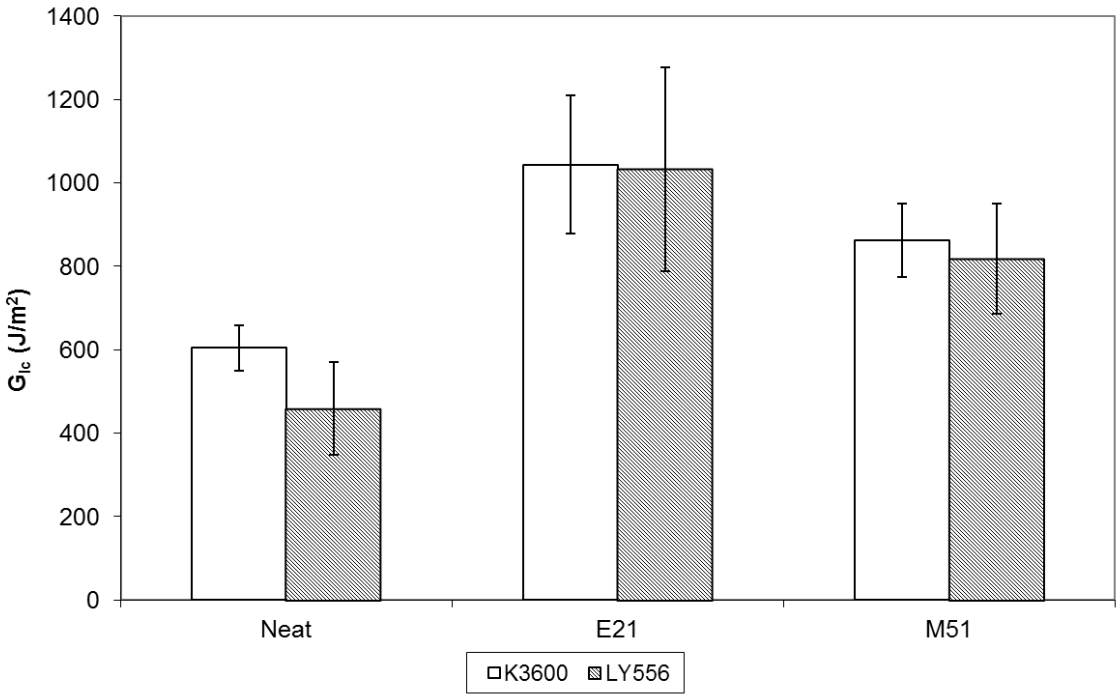

Figure 26 – Interlaminar fracture toughness values determined using DCB and measured at the NL point of respective sample load-displacement plots.

From the results (a full listing of which is provided in Appendix G), a marked improvement in interlaminar fracture toughness can be seen for both copolymers in either of the two resin systems. For the K3600 system, the E21 copolymer performed extremely well, roughly doubling the neat NL fracture toughness value of 604.91 J/m² ± 55 to 1043.45 J/m² ± 166. When incorporated within the LY556 system, the E21 copolymer provided a similar improvement over the neat system, increasing the fracture toughness from 459.34 J/m² ± 111.67 to 1033.09 J/m² ± 245.

The M51 copolymer showed slightly less improvement than the E21 modified samples, despite providing fracture toughness improvements to both resin systems. For the K3600 system, the M51 copolymer increased the NL fracture toughness from 604.91 J/m² ± 55 to 862.05 J/m² ± 88, and for the LY556 system, an improvement from 459.34 J/m² ± 111.67 to 767.63 J/m² ± 77 in the NL fracture toughness was observed.

The neat fracture toughness values can be compared to other experimental results achieved in earlier Long Crack Extensions tests, and values provided by the adhesive technical data sheets. For the K3600 system, the Defence Science and Technology Organisation has previously performed work to characterise the fracture toughness of this system using a Long Crack Extension (LCE) mechanical testing method, the details of which are provided in Appendix H. Using this method, a fracture toughness value of 329.71 J/m² ± 109.02 was determined, using the same cure profile and mix ratios as detailed in Section 2.2 for the neat K3600 system. For the neat LY556 system, a fracture toughness value of 150 - 160 J/m² is provided in the manufacturers technical data sheet [30], this being for the neat resin cured for 2 hours at 120 °C (following the b-stage detailed in Section 2.2), and tested using a bend notch standard method PM 258-0/90.

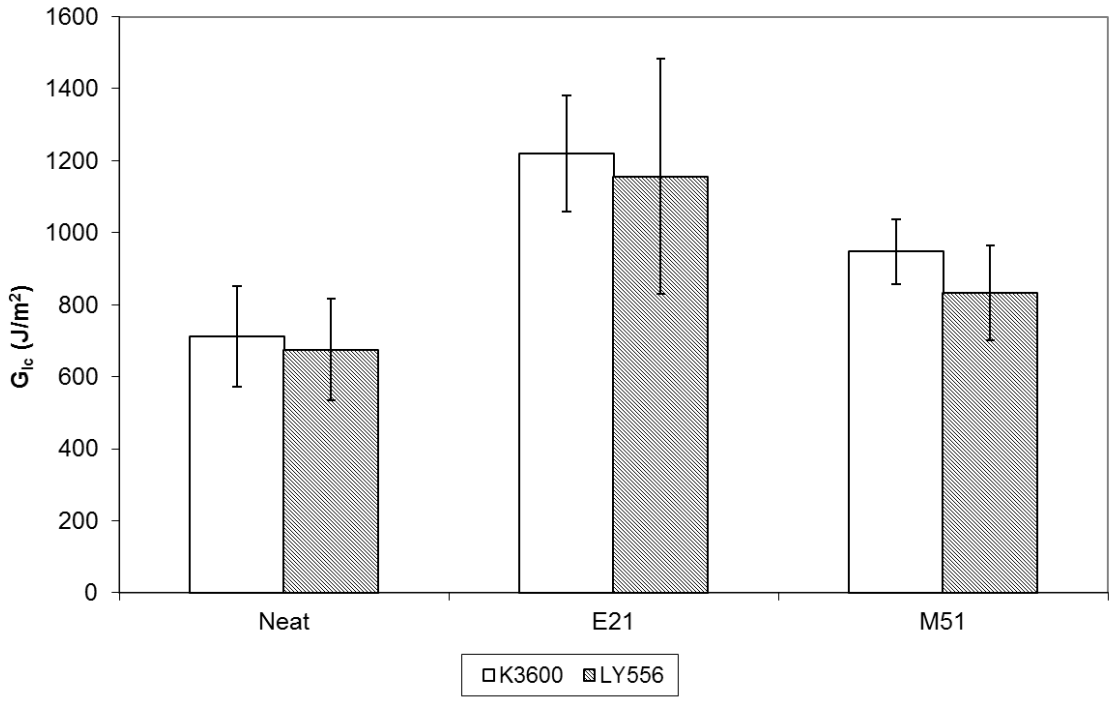

Figure 27 – Interlaminar fracture toughness values determined using DCB and measured at the 5%/MAX point of respective sample load-displacement plots.

Both of these results are significantly lower than those determined using the DCB method described here. This difference is thought to be a result of the interaction of the crack front with the fibres, namely through fibre bridging across the crack opening [38, 39]. An example of this can be seen in Figure 28 for one of the DCB specimens tested in this study. The fibre bridging results from growing the delamination between two 0° unidirectional plies, with the crack front switching from one fibre-matrix interface to an adjacent fibre-matrix interface, giving rise to a bridging fibre. These bridging fibres provide traction forces which increase the observed toughness during testing.

Figure 28 – Example of fibre bridging occurring along the crack front of a K3600 + E21 DCB specimen.

This theory is supported by the observed relationship between fracture toughness and crack length, depicted in the form of a resistance curve (or R-curve) as seen in Figure 29 for the K3600 system and Figure 30 for the LY556 system. These figures show fracture toughness (G_{Ic}) increasing as a function of crack propagation length, and then levelling out at a constant value larger than both the MAX and NL values indicated.

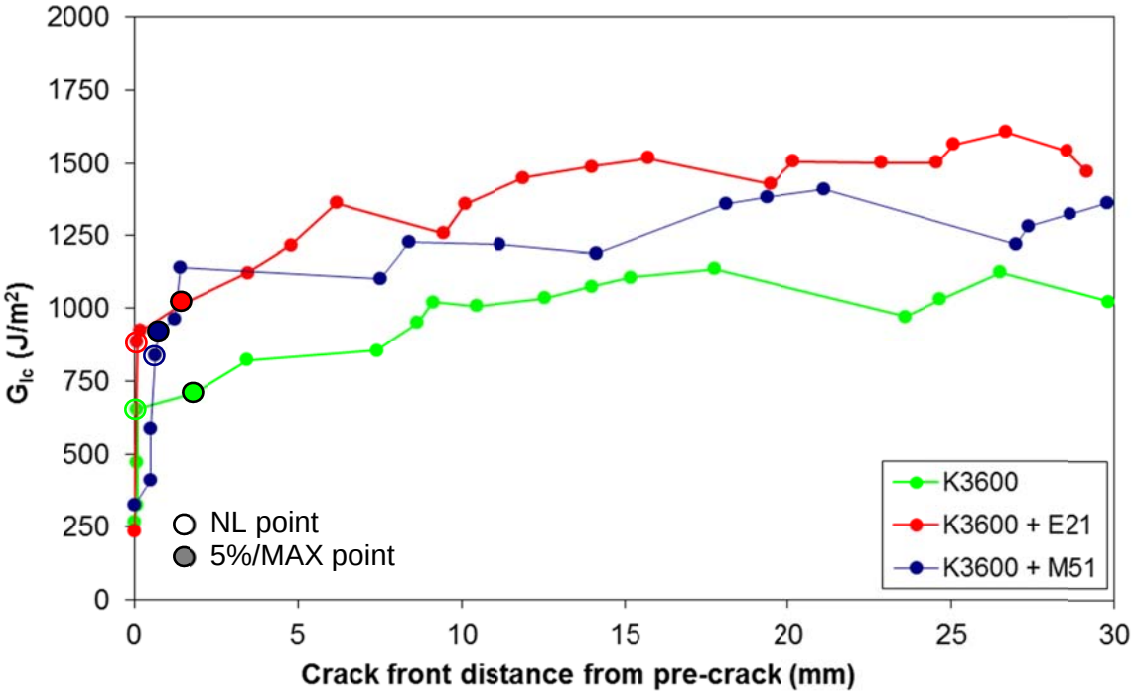

Figure 29 – Delamination Resistance Curve (R-curve) for the K3600 system via DCB.

In laminate composite structures, delaminations typically form between plies of dissimilar orientation, limiting the likelihood of fibre bridging. For this reason, fibre bridging is considered to be an artefact of the DCB test itself, and the validity of fracture toughness measured beyond the initiation values (NL and 5%/MAX) is questionable.

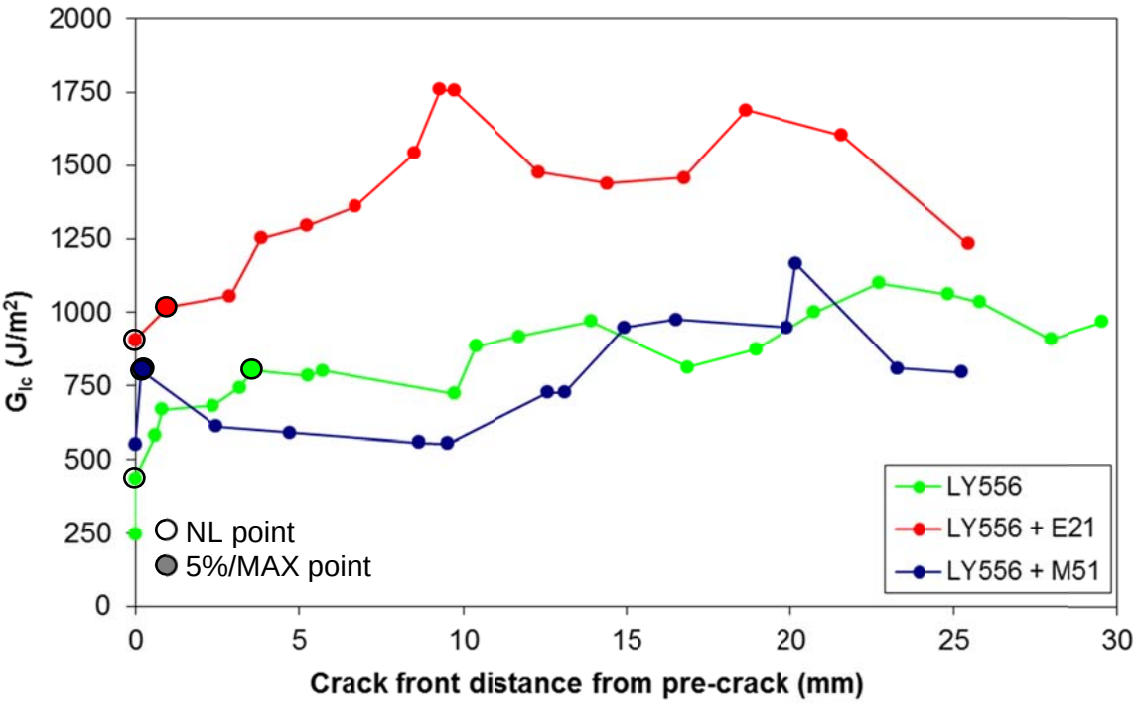

Figure 30 – Delamination Resistance Curve (R-curve) for the LY556 system via DCB.

3.8 Microscopy

The morphology of the nanostructures formed by the tri-block copolymers (either SBM or MAM) when combined with an epoxy monomer and cured, is heavily dependent upon a number of factors including [15, 16, 40]:

- Compatibility (solubility) of the PMMA block(s) with the epoxy monomer and hardener.
- Complete immiscibility of the PB (for SBM copolymer) and PBuA (for MAM polymer) blocks with the epoxy monomer.
- Chemical nature of the cross-linker (hardener).
- Chemical composition of the copolymer used (respective molecular weights of each block in the tri-block).
- Concentration of copolymer in the epoxy blend.

For these reasons, a number of different morphologies can be formed when a tri-block copolymer is combined with an epoxy monomer, and this morphology can change following cure of the epoxy. A number of authors have presented work investigating the various morphologies obtained for SBM and MAM copolymers in combination with epoxy [9, 13, 16, 18]. Morphologies obtained by other tri-block, di-block and block copolymer blends have also been researched [17, 35, 41]. Examples of typical morphologies seen for SBM and MAM block copolymers in epoxy can be seen in Figure 31.

blends have also been researched [17, 35, 41]. Examples of typical morphologies seen for SBM and MAM block copolymers in epoxy can be seen in Figure 31.

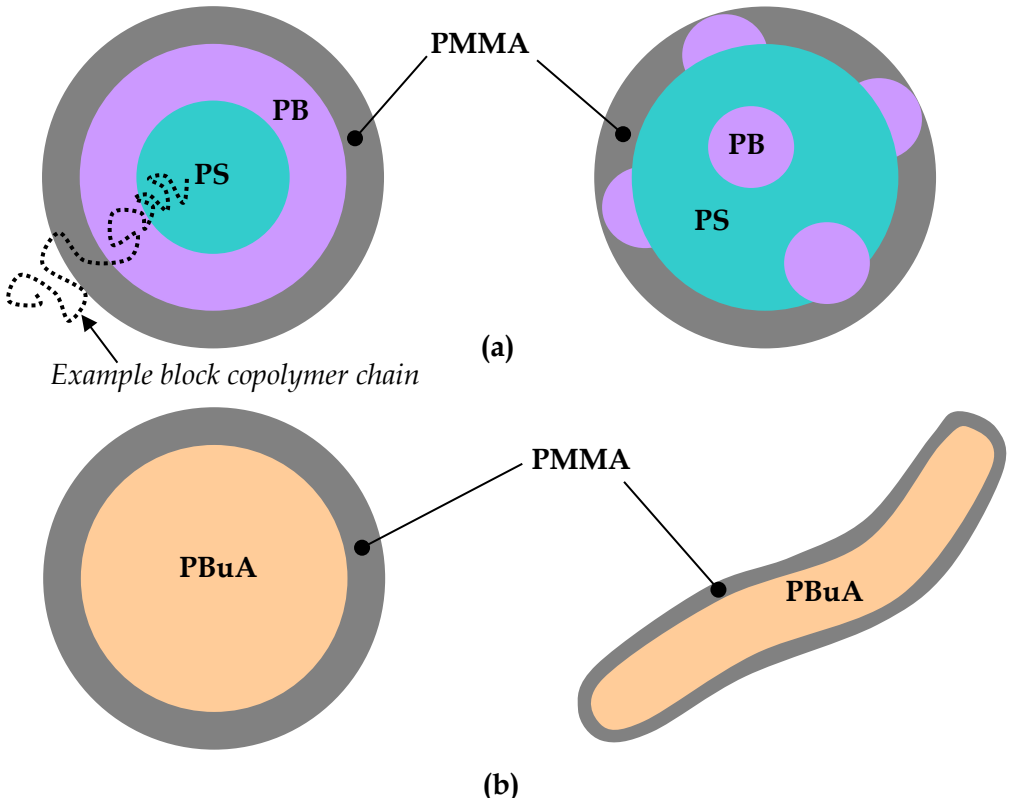

Figure 31 – Examples of various copolymer morphologies when combined with epoxy resin: (a) polystyrene-block-polybutadiene-block-poly-(methyl methacrylate) (SBM), and (b) polymethylmethacrylate-block-polybutylacrylate-block-polymethylmethacrylate (MAM). An example block copolymer chain is provided in (a) to visualise the formation of the copolymer domains presented.

The type of morphology formed in the cured epoxy will affect the mechanical performance of the epoxy as shown by the results in Sections 3.3 to 3.7. To better understand the reasoning behind the varying mechanical results observed, Field Emission Scanning Electron Microscopy (FESEM) of a number of specimens was performed.

Samples of neat K3600, K3600 + 10% PBW E21 and K3600 + 10% PBW M51 were manufactured. These were then cooled using liquid nitrogen and broken to form a fracture surface for interrogation. Redundant material from the specimen was then removed using a micro-saw and the specimen mounted onto metallic mounting stubs using graphite paint. Each specimen was then sputter coating with a 2nm thick iridium coating to prevent charging. The targets were then interrogated using a LEO 1530VP FESEM.

Micrographs for the K3600, K3600 + 10% E21 and K3600 + 10% M51 specimens can be seen in Figures 32, 33 and 34 respectively.

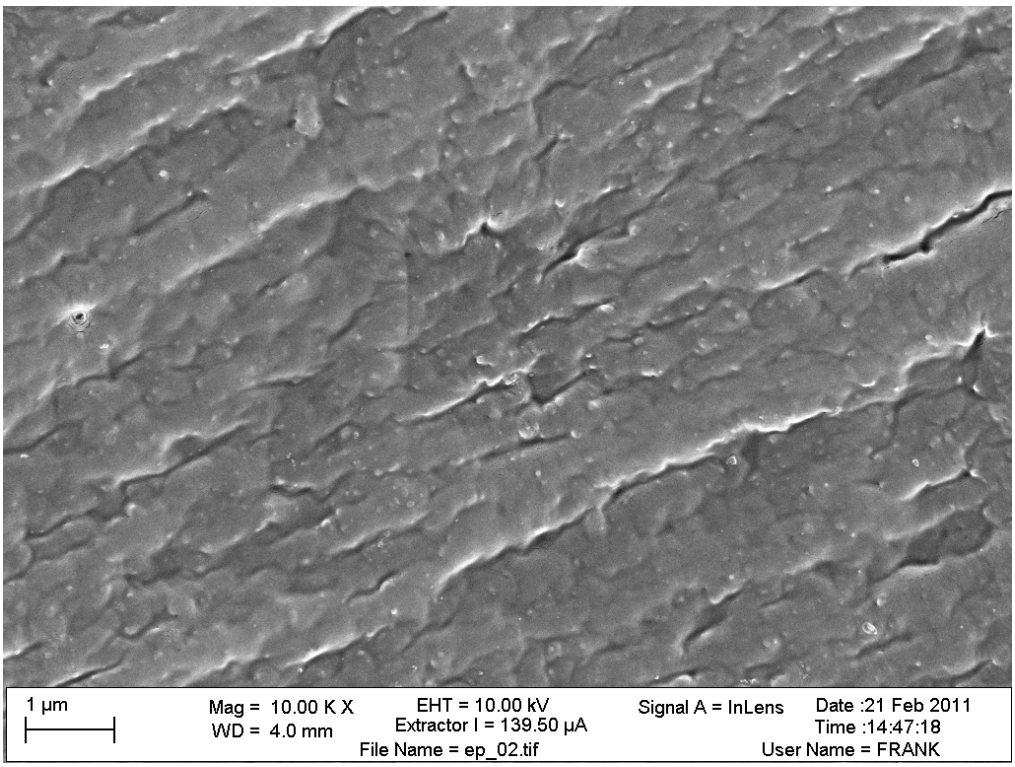

Figure 32 – Micrograph of neat K3600 fracture surface

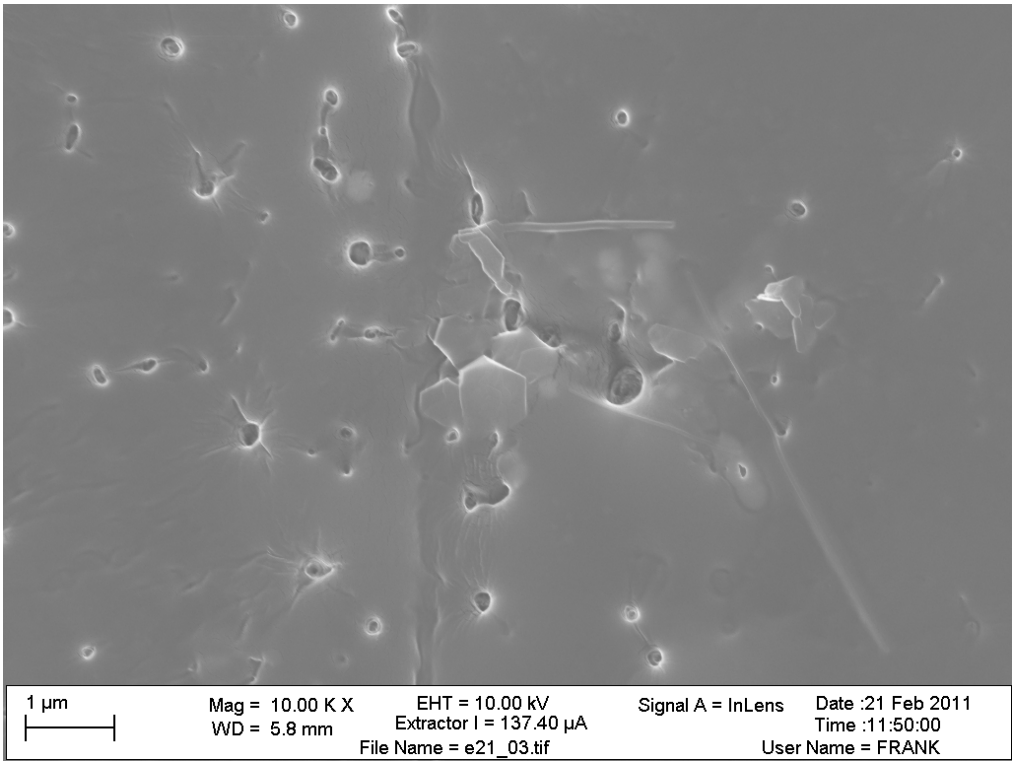

Figure 33 – Micrograph of K3600 + 10% E21 fracture surface

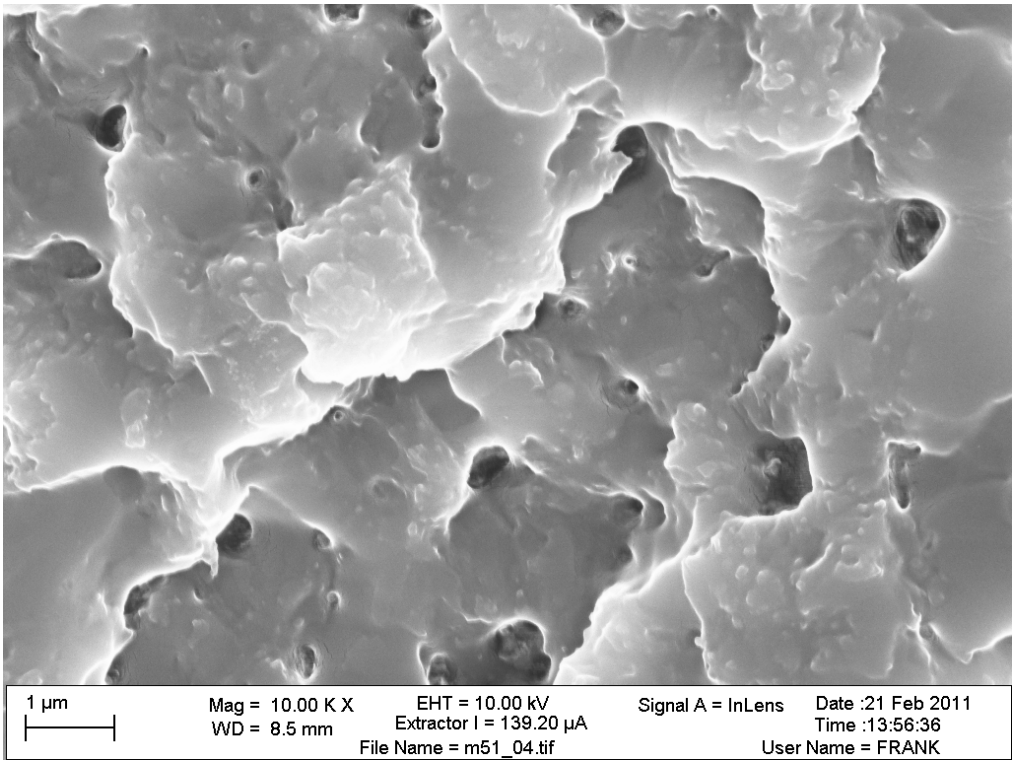

Figure 34 - Micrograph of K3600 + 10% M51 fracture surface

As shown in the two copolymer toughened epoxy images, regions of cavitation can be seen, ranging in size from 100 to 200 nm. These cavities are thought to arise during the

formation of the fracture surface, in doing so, removing parts of the formed copolymer structures, examples of which were shown in Figure 31. In the case of the SBM copolymer (E21), it is thought that upon fracturing, the miscible PMMA blocks remain associated with the epoxy, whilst the immiscible PB blocks of the chain become exposed, connected to the also immiscible PS blocks. Removal of the PS blocks from the epoxy is thought to give rise to the cavitation.

A number of other authors have also reported similar failure surface cavitation. Work by Dean et al. [17] in which a number of different di-block copolymers were combined in varying ratios with an epoxy resin (poly(bisphenol A-coepichlorohydrin)) and hardener (4,4'-methylenedianiline) showed cavitation of room temperature compact tension coupon failure surfaces. Work by Hydro et al. [14] with E20 Arkema SBM copolymer (a variant of the E21 used in this study) combined in an epoxy resin system (DGEBA–DER 331 epoxy resin and amine based hardener) also presented similar results. Room temperature three-point bend single edge notch (SEN) testing was performed on cast coupons, and the fracture surface analysed using a SEM. Cavitation was observed on the failure surface, with small amounts of de-bonded particles, hypothesised to be the PS phase of the SBM copolymer.

For the SBM toughened epoxy in this study, fine filaments (approximately 30 – 50 nm in diameter) of material were found to litter the fracture surface in a number of regions, uniformly distributed across the sample surface. An example of this can be seen in

Figure 35. These filaments are thought to be remnants of the PB blocks from the SBM copolymer, seen as a section of the chain filament shown as 'example block copolymer chain' in (a) of Figure 31. In the work conducted by Dean et al. [17], similar 'drawn fibrillar structures' are reported to exist between the debonded visicle structures of the failure surface, and the host epoxy, however appear to be much shorter in length than those observed in the current work. No conclusions were made as to the composition of these structures, however it was hypothesised that they are formed from either the host epoxy material, or by deformation/extrusion of a copolymer bi-layer formed around the nano-structure, specific to the block copolymers used in the research.

In the case of the MAM toughened epoxy, it is thought that no filaments are observed due to the absence of the PS block in the symmetrical chain. Cavitation is however observed, thought to result from removal of the PBuA blocks, similar in fashion to the removal of the PS blocks from the SBM toughened epoxy.

For cavitation to occur, chemical and mechanical bonds between the epoxy and the respective copolymer blocks (PS and PB for an SBM copolymer, and PBuA for a MAM) must be severed. In order for this to occur, energy in addition to that required to break cross-linking polymer bonds must be provided. If this energy is provided by way of mechanical force, additional mechanical loading will be required, effectively improving the toughness of the epoxy. This toughness will however depend on the morphology (if any) of nanostructure formed, and the compatibility of the nano-phase with the host epoxy.

The variation in mechanical performance achieved for the two different copolymers, as seen in Sections 3.3 to 3.7, highlight this dependence on copolymer compatibility to the epoxy and type of nanostructure formed. For example, the SBM copolymer (E21) combined with K3600 resin provided a mode I fracture toughness value of 1043.45 J/m^2 ± 166, whilst the MAM (M51) provided a value of 862.05 J/m^2 ± 88. This variation in fracture toughness could be attributed to a 'stringing' effect of the SBM copolymer whereby the PB blocks, thought to be seen as elongated filaments in

Figure 35, bridge the crack front during propagation, reducing the stress concentration at the crack tip. In the case of the MAM copolymer, the absence of this block means no stringing can occur, and a comparatively lower fracture toughness results.

Further investigation is required to confirm these hypotheses, namely confirmation of the morphologies formed, and the mechanisms at play during fracturing of the specimen. Nevertheless, these images provide confirmation of the existence of structuring within the epoxy from the addition a copolymer.

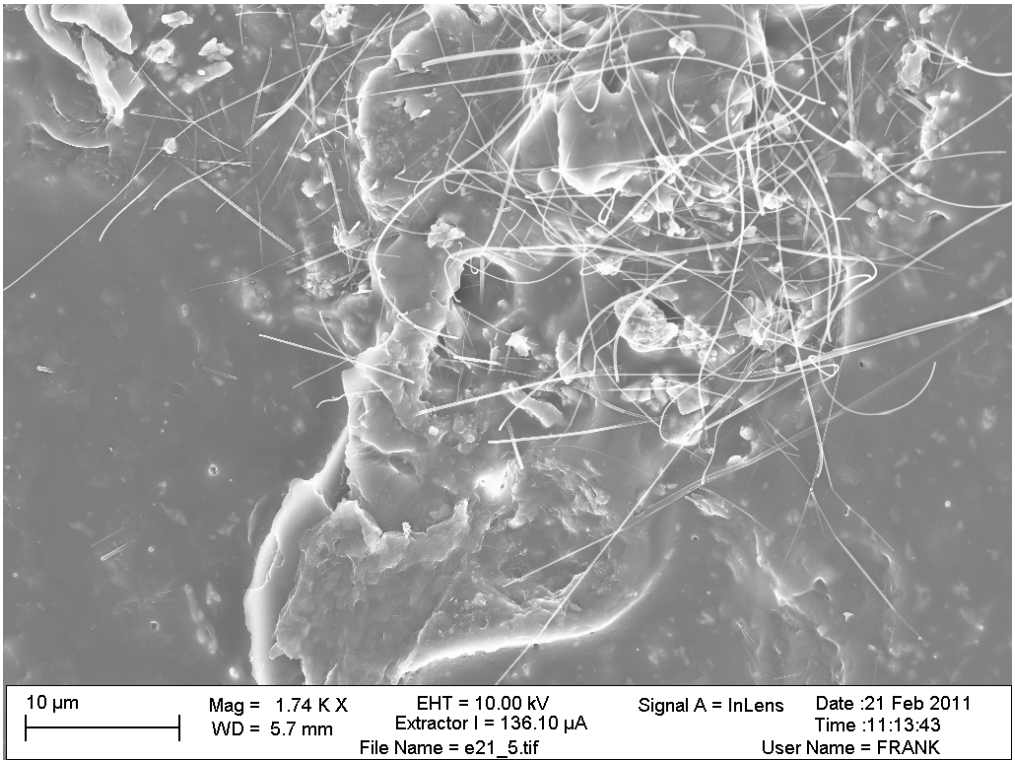

Figure 35 – Micrograph of filaments observed on surface of SBM (E21) toughened K3600 epoxy.

4. Conclusion

The use of tri-block copolymer additives offers potential to improve the fracture toughness of low temperature cure epoxy resin systems, without increasing resin viscosity and lowering glass transition temperature or compromising the tensile properties observed in rubber-toughened systems.

In this research, two commercially available tri-block copolymers were investigated: (i) Nanostrength® SBM, E21 and, (ii) Nanostrength® MAM, M51. These were combined with two low-temperature-cure epoxy resin systems: (i) K3600 and, (ii) a pre-preg system comprising an Araldite LY 556 epoxy resin. The performance of each combination was examined using Short Beam Shear (SBS), Four Point Flexure and Double Cantilever Beam (DCB) testing. In addition, Dynamic Mechanical Thermal Analysis (DMTA) was used to quantify glass transition temperature and thermal degradation.

SBS testing indicated a 5 MPa reduction in SBSS with the addition of either copolymer to either resin system. Conditioning of the SBS specimens for 100 hours at 180 °C indicated negligible change in the interlaminar strength when compared to the unconditioned specimens, varying by no more than 10% and potentially some enhancement for the MAM and K3600 combination.

Four point bend testing of the K3600 system showed a 22% reduction in flexural strength following the addition of E21, and a 16% reduction with the addition of M51. Conversely, the LY556 system experienced improvements in flexural strength for both copolymers, 10% with the addition of the E21, and 12% with the addition of the M51. Unfortunately, the four point bend specimens tested exhibited undesirable failure mode characteristics, possibly the result of high void levels in the laminates. Further testing with laminates containing less than 1% volume will be required to validate the results obtained. Additionally, due to the influence of the block copolymer addition on the resin viscosity, each of the laminates had varying fibre volume fractions, which is known to have a significant effect on the SBS and flexural strengths of carbon/epoxy laminates.

Double Cantilever Beam testing indicated dramatic improvements in the mode I interlaminar fracture toughness for either of the two copolymers in both resin systems. The E21 copolymer performed the best, improving fracture toughness values by 72 % for the K3600 system, and 125% for the LY556 system. Slightly less improvement was noted for the M51 copolymer, however still yielding an average improvement of 55%.

DMTA analysis of the K3600 system showed improvements to the systems glass transition temperature following the addition of either copolymer, increasing from 88 °C to 95 °C and 92 °C for the E21 and M51 copolymers, respectively. DMTA analysis was also used to determine a suitable mix ratio and cure schedule for the four part LY556 resin which maximised the resins glass transition temperature, whilst minimizing cure time and temperature. The mix ratio and cure schedule chosen, 8 hours at 80 °C cure, provided a neat resin glass transition temperature of 120 °C.

Thermal degradation analysis, involving exposure of both cured neat resin systems to 180 °C for 100 hours showed negligible cumulative weight change due to oxidation. The K3600 system lost approximately 3% of its initial weight whilst he LY556 lost approximately 1.5% of its initial weight, both following the full exposure period.

5. References

1. Alan A. Baker and R. Jones, *Bonded repair of aircraft structures*. 1988: Martinus Nijhoff publishers.
2. Alan A. Baker, Stuart Dutton, and D.W. Kelly, *Composite materials for aircraft structures*. 2004: American Institute of Aeronautics and Astronautics.
3. Man, Z., *A Review of the Epoxy Resin Toughening*, in *Department of Chemical Engineering and Materials Science*. 2003, Syracuse University: Syracuse.
4. Min, B.G., et al., *Quantitative analysis of the cure reaction of DGEBA/DDS epoxy resins without and with thermoplastic polysulfone modifier using near infra-red spectroscopy.* Polymer, 1993. **34**(17): p. 3620-3627.
5. G. Cicala, et al., *Development of Epoxy/Hyperbranched Blends for Resin Transfer Molding and Vacuum Assisted Resin Transfer Molding Applications: Effect of Reactive Diluent.* Polymer Engineering and Science, 2009. **49**(3): p. 577-584.
6. Ratna, D., A.K. Banthia, and P.C. Deb, *Toughening of epoxy resin using acrylate-based liquid rubbers.* Journal of Applied Polymer Science, 2000. **78**(4): p. 716-723.
7. Ruthnakornpituk, M., *Thermoplastic Toughened Epoxy Networks and Their Toughening Mechanisms in Some Systems.* Naresuan University Journal, 2005. **13**(1): p. 73-83.
8. K. P. Unnikrishnan and E.T. Thachil, *Toughening of Epoxy Resins.* Designed Monomers and Polymers, 2006. **9**(2): p. 129-152.
9. N. Passade-Boupat, et al., *Improving composites properties with acrylic block copolymers.* International SAMPE Technical Conference, 2005. **2005**.
10. B.B. Johnsen, et al., *Toughening mechanisms of nanoparticle-modified epoxy polymers.* Polymer 2007. **48**: p. 530-541.
11. Kim, B.C., S.W. Park, and D.G. Lee, *Fracture toughness of the nano-particle reinforced epoxy composite.* Composite Structures, 2008. **86**(1-3): p. 69-77.
12. Soon-Chul Kwon and T. Adachi, *Strength and fracture toughness of nano and micron-silica particles bidispersed epoxy composites: evaluated by fragility parameter.* Journal of Materials Science, 2007. **42**(14): p. 5516-5523.
13. Sergio Frascino Muller de Almeida and Zabulon dos Santos Nogueira Neto, *Effect of void content on the strength of composite laminates.* Composite Structures, 1994. **28**: p. 139-148.
14. Ryan M. Hydro and Raymond A. Pearson, *Epoxies toughened with triblock copolymers.* Journal of Polymer Science. Part B, Polymer Physics, 2007. **45**(12): p. 1470-1481.
15. S. Ritzenthaler, et al., *ABC Triblock Copolymers/Epoxy−Diamine Blends. 1. Keys To Achieve Nanostructured Thermosets.* Macromolecules, 2002. **35**(16): p. 6245-6254.
16. S. Ritzenthaler, et al., *ABC Triblock Copolymers/Epoxy−Diamine Blends. 2. Parameters Controlling the Morphologies and Properties.* Macromolecules, 2003. **36**(1): p. 118-126.
17. Dean, J.M., et al., *Mechanical properties of block copolymer vesicle and micelle modified epoxies.* Journal of Polymer Science Part B: Polymer Physics, 2003. **41**(20): p. 2444-2456.
18. Ling Liu, et al., *Effects of Cure Pressure Induced Voids on the Mechanical Strength of Carbon/Epoxy Laminates.* Journal of Material Science and Technology, 2005. **21**(1): p. 87-91.

19. Gerard, P., et al., *Toughness Properties of Lightly Crosslinked Epoxies Using Block Copolymers.* Macromolecular Symposia, 2007. **256**(1): p. 55-64.
20. Hexcel Corporation, *HexTow IM7 Carbon Fiber Product Data Sheet*. 2010, Hexcel Corporation,.
21. SP Systems, *SP Systems Composite Materials Handbook*. SP Systems: United Kingdom.
22. D. Hull and T.W. Clyne, *An Introduction to Composite Materials, Second Edition*. Cambridge Solid State Science Series. 1996, Cambridge: Press Syndicate of the University of Cambridge.
23. ASTM International, *Standard Test Method for Short-Beam Strength of Polymer Matrix Composite Materials and Their Laminates, ASTM D2344/D2344M-00*. 2006, ASTM international.
24. ASTM International, *Standard Test Method for Thick-Adherend Metal Lap-Shear Joints for Determination of the Stress-Strain Behavior of Adhesives in Shear by Tension Loading, D 5656–04*. 2005, ASTM International.
25. ASTM International, *Standard Test Method for Flexural Properties of Unreinforced and Reinforced Plastics and Electrical Insulating Materials by Four-Point Bending, ASTM D6272-02*. 2002, ASTM international.
26. ASTM International, *Standard Test Method for Mode I Interlaminar Fracture Toughness of Unidirectional Fiber-Reinforced Polymer Matrix Composites, ASTM D5528-01*. 2001, ASTM international.
27. Huntsman Advanced Materials Pty Limited, *Araldite Kit K3600 Technical Data Sheet.* 2005, Huntsman Advanced Materials Pty Limited.
28. Arkema, *Nanostrength E21 for Epoxies - Technical Data Sheet*. 2009, Arkema.
29. Arkema, *Nanostrength M51 for Epoxies - Technical Data Sheet*. 2009, Arkema.
30. Huntsman Advanced Materials Pty Limited, *Araldite LY 556 Aradur 1571/LME 10188/Hardener XB 3403 - Provisional Technical Data Sheet*. 2009, Huntsman Advanced Materials Pty Limited.
31. National Aeronautics and Space Administration. *AtmosModeler Simulator*. 2008 [cited 2010 30th March]; Available from: http://www.grc.nasa.gov/WWW/K-12/airplane/atmosi.html.
32. X. Buch and M.E.R. Shanahan, *Influence of the Gaseous Environment on the Thermal Degradation of a Structural Epoxy Adhesive.* Journal of Applied Polymer Science, 1999. **76**(2000): p. 987-992.
33. X. Buch and M.E.R. Shanahan, *Thermal and thermo-oxidative ageing of an epoxy adhesive.* Polymer Degradation and Stability, 2000. **68**(2000): p. 403-411.
34. M. Quaresimin and R. J. Varley, *Understanding the effect of nano-modifier addition upon the properties of fibre reinforced laminates.* Composites Science and Technology, 2008. **68**: p. 718-726.
35. Robert Barsotti, et al., *Nanostrength Block Copolymers for Epoxy Toughening*, in *Meeting of the Thermoset Resin Formulators Association*. 2008: Hilton Suites Chicago Magnificent Mile in Chicago, Illinois, USA.
36. *O. Ozcelik, L. Aktas,* and *M.C. Altan, Thermo-oxidative degradation of graphite/epoxy composite laminates: Modeling and long-term predictions.* eXPRESS Polymer Letters, 2009. **3**(12): p. 797-803.
37. T. K. O'Brien and R.H. Martin, *Round Robin Testing for Mode I Interlaminar Fracture Toughness of Composite Materials.* Journal of Composites Technology and Research, 1993. **15**(4): p. 269-281.

38. Spearing, S.M. and A.G. Evans, *The role of fiber bridging in the delamination resistance of fiber-reinforced composites.* Acta Metallurgica et Materialia, 1992. **40**(9): p. 2191-2199.
39. Johnson, W.S. and P.D. Mangalgiri, *Investigation of fiber bridging in double cantilever beam specimens [microform] / W. S. Johnson and P. D. Mangalgiri.* NASA technical memorandum ; 87716. 1986, Hampton, Va. :: National Aeronautics and Space Administration, Langley Research Center.
40. S. Ritzenthaler, et al., *ABC Triblock Copolymers/Epoxy - Diamine Blends. 2. Parameters Controlling the Morphologies and Properties.* Macromolecules, 2003. **36**: p. 118 - 126.
41. Goldacker, T., V. Abetz, and R. Stadler, *Blends of block copolymers.* Macromolecular Symposia, 2000. **149**(1): p. 93-98.
42. ASTM International, *Standard Test Method for Fracture Strength in Cleavage of Adhesives in Bonded Metal Joints, ASTM D3433 - 99*. 2005, ASTM International.
43. ASTM International, *Standard Test Method for Adhesive-Bonded Surface Durability of Aluminum (Wedge Test), ASTM D3762 - 03(2010)*. 2010, ASTM International.
44. Boeing Aircraft Company, *Specification for Adhesive Joint Durability Testing, BSS 7208*.

Appendix A: TALS Specimen Manufacture

1. The surface was abraded in one direction using Scotch-Brite 3M No. 447 for a minimum of 2 minutes, and then abraded in a direction 90° to the original until all original scratches were removed. The area was kept wet with methyl ethyl ketone (MEK) whilst abrading.
2. The adherend was then cleaned with lanoline and lint free tissues soaked in MEK in the most recent Scotch-Brite abrade direction to remove debris from the previous action. This was repeated using a single wipe and discard technique until the tissues came up clean.
3. Step 1 was repeated using distilled water in place of MEK.
4. Step 2 was repeated using distilled water in place of MEK.
5. A water break test was then applied for 15 seconds to ensure a contaminant free surface. The surface was held at 45° and a squeeze bottle was used to apply distilled water, and its flow observed for any breaks (to indicate surface contamination). If any breaks were observed, steps 1 to 4 were repeated.
6. The adhered was then dried in an air circulating oven for 20 minutes at 80 °C.
7. The adherend was then allowed to dry to at least 35 °C.
8. The adherend bonding surface was then grit blasted with 50µm aluminium oxide grit using dry nitrogen gas as a propellant, with a pressure of approximately 450kPa.
9. The adherend was then submerged in a one percent aqueous solution of γ-glycidoxypropyl trimethoxy silane (γ-GPS) for 10 minute. This solution consists of 1% γ-GPS + 99% distilled water, stirred for 1 hour prior to use.
10. The adherend was then dried in an air circulating oven for one hour at 110°C, and cooled to below 35°C.
11. Parts A and B of the K3600 resin were combined (part A containing a 10% PBW of E21) and mixed using a THINKY planetary mixer running at 1350 RPM.
12. The adhesive was then applied equally to both plate mating surfaces using a plastic applicator.
13. A 130µm nylon scrim was placed on one of the mating surfaces, and the two mating surfaces joined.
14. 150µm brass shim was positioned near the end of both plates to assist with bond-line thickness uniformity, and the adherends aligned using locator pins positioned through the plate holes.
15. The assembly was cured in an environmental chamber at 25 °C and 38%RH (as measured by an independent probe) for 24 hours. Pressure was applied for curing by way of two 0.9 kg cylindrical dead weights placed upon the assembly.
16. After 24 hrs, the plate assembly was post cured for 4 hrs at 80 °C in a free standing oven (no dead weights applied).
17. The specimens were then cut from the plate using a mill, and then mechanically tested.

This page is intentionally blank

Appendix B: Double Cantilever Beam Strain Energy Release Rate Calculation

Using the Modified Beam Theory (MBT) approach to calculate the strain energy release rate assumes the delamination front to be perfectly built-in. In practice however, rotation of the delamination front exists, and to accommodate for this, the ASTM standard [26] recommends perturbing the delamination front by a small amount to $a+|\Delta|$, hence providing a strain energy release rate as in Equation 11.

$$G_{Ic} = \frac{3P\delta}{2b(a+|\Delta|)} \quad \textbf{(13)}$$

Where:

P = load (N)

δ =load point displacement

b = specimen width

a = delamination length

Δ can be determined experimentally by plotting the cubed root of compliance, $C^{1/3}$, as a function of delamination length observed on the edge of the specimen during testing. The compliance, C, is the ratio of the load point displacement to the applied load, δ / P. The magnitude of the x-intercept of a linear fit to this plot is Δ for use in Equation 11, and an example of this can be seen in Figure following.

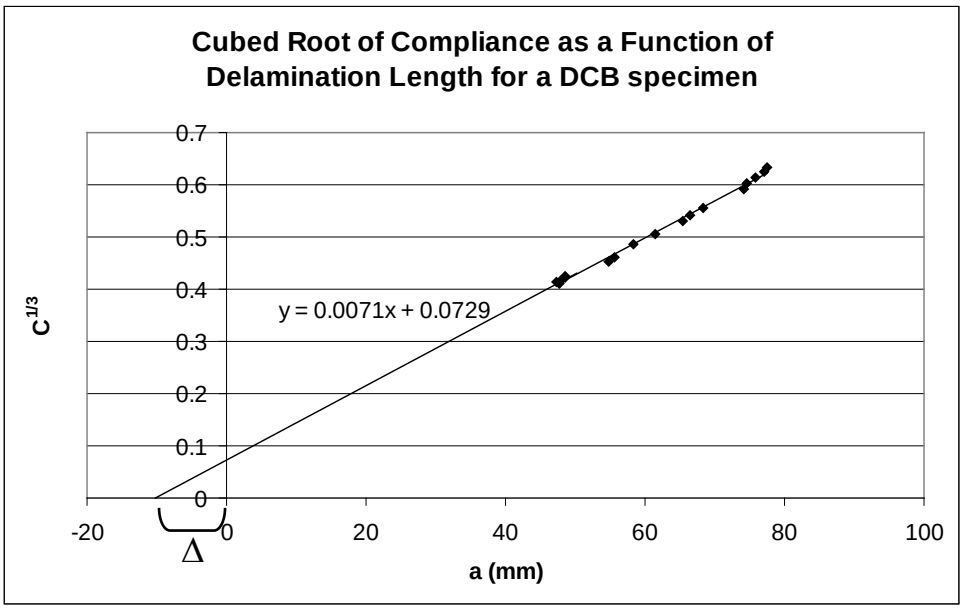

Figure B-1 – Plot of cubed root of compliance vs. delamination length, used to determine the correction factor in the MBT method.

This page is intentionally blank

Appendix C: Dynamic Thermal Mechanical Analysis Results

C.1. K3600 system results

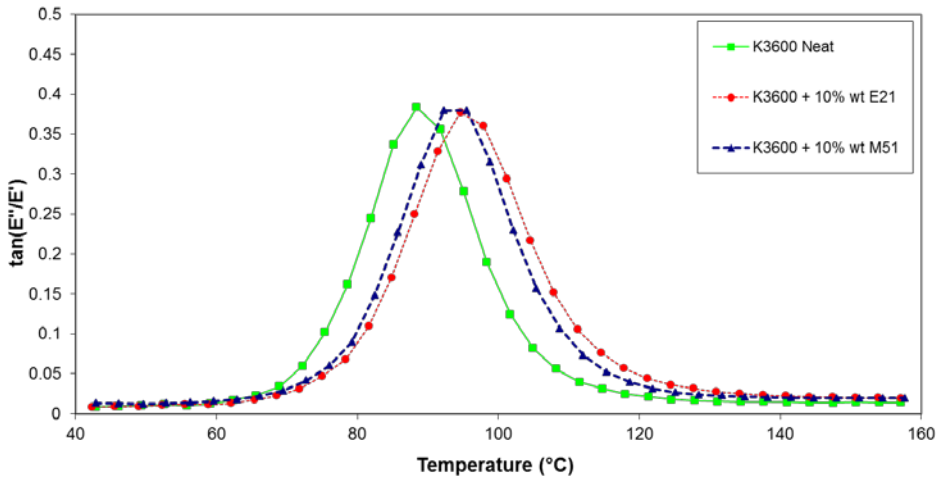

Figure C-1 – K3600 with E21 and M51 DMTA dampening behaviour results for a 1 Hz oscillatory frequency

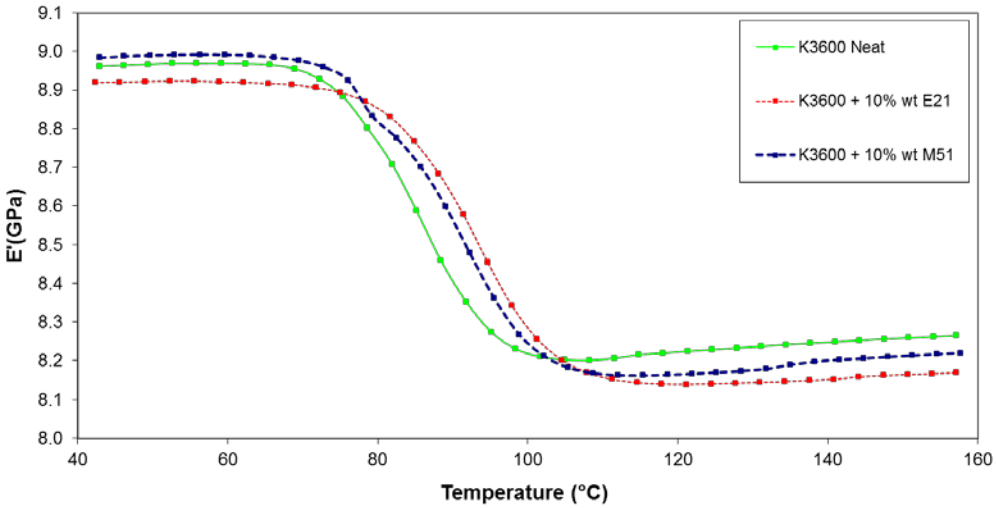

Figure C-2 – K3600 with E21 and M51 DMTA storage modulus results for a 1 Hz oscillatory frequency

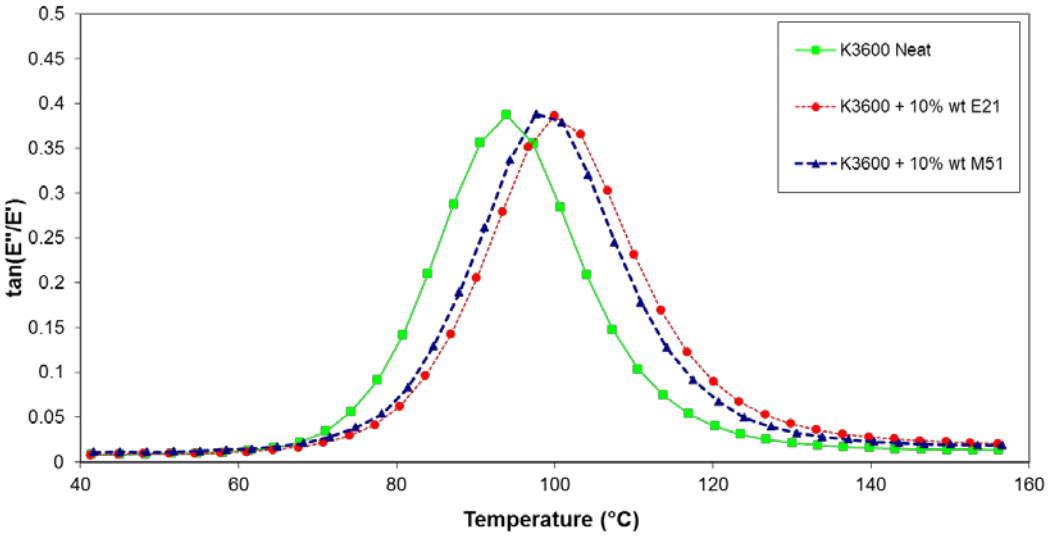

Figure C-3 – K3600 with E21 and M51 DMTA dampening behaviour results for a 5 Hz oscillatory frequency

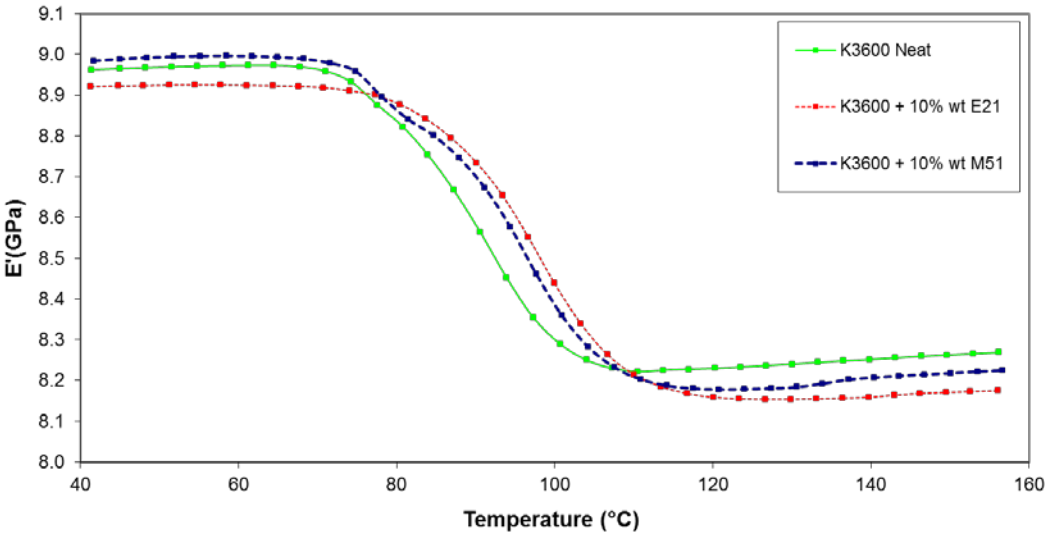

Figure C-4 – K3600 with E21 and M51 DMTA storage modulus results for a 5 Hz oscillatory frequency

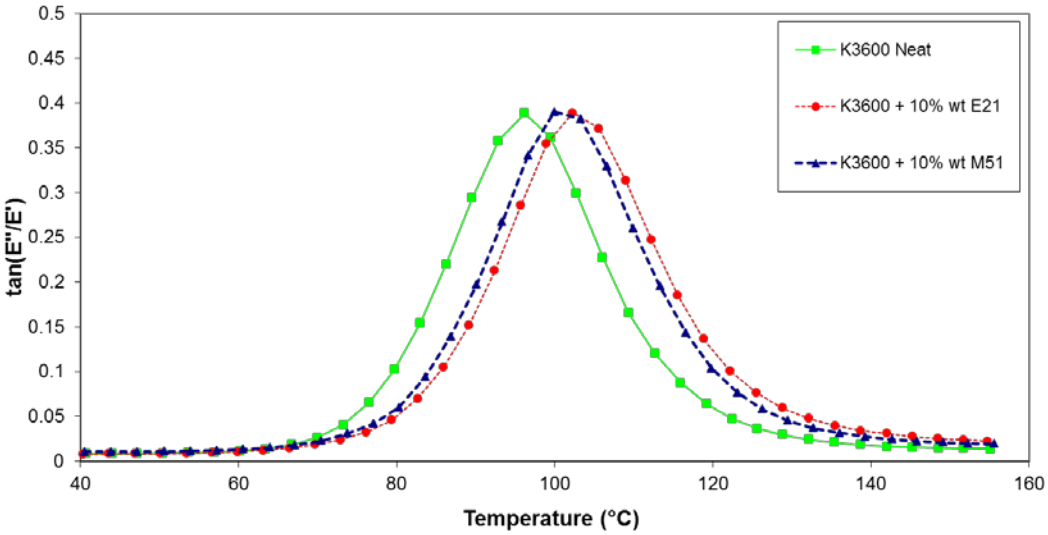

Figure C-5– K3600 with E21 and M51 DMTA dampening behaviour results for a 10 Hz oscillatory frequency

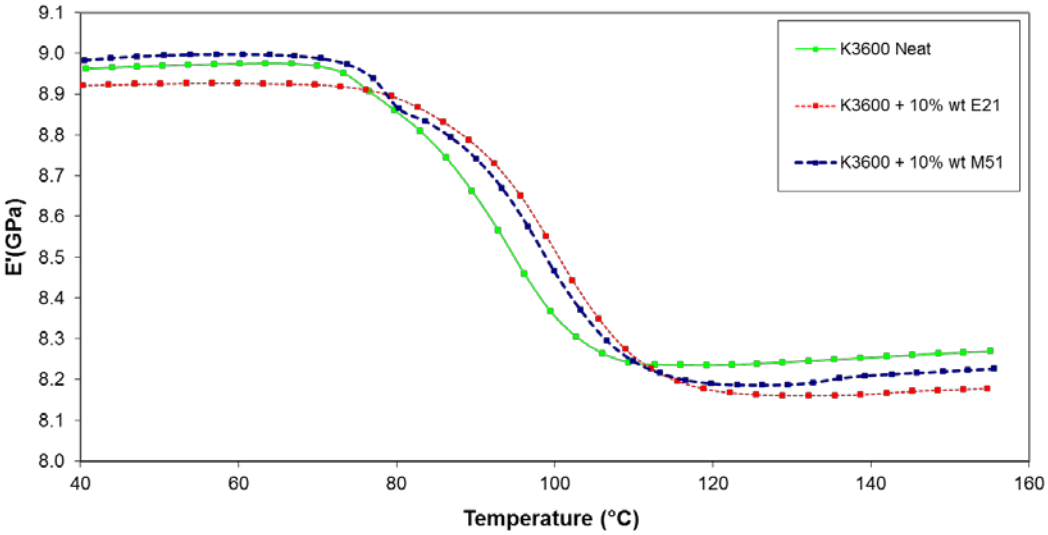

Figure C-6– K3600 with E21 and M51 DMTA storage modulus results for a 10 Hz oscillatory frequency

C.2. LY556 system results

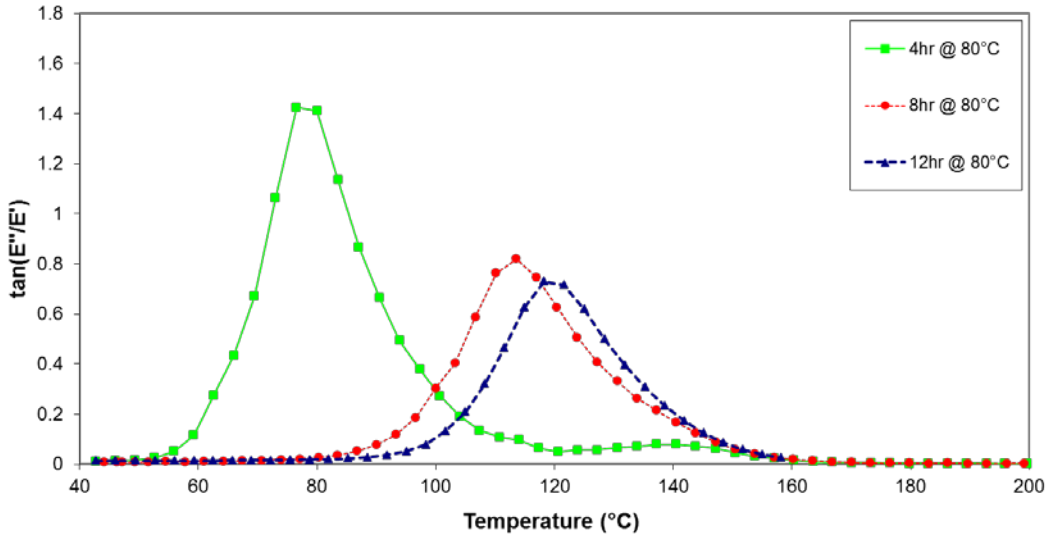

Figure C-7 – LY556 DMTA dampening behaviour results for a 100:18:7:12 mix and varying cure times

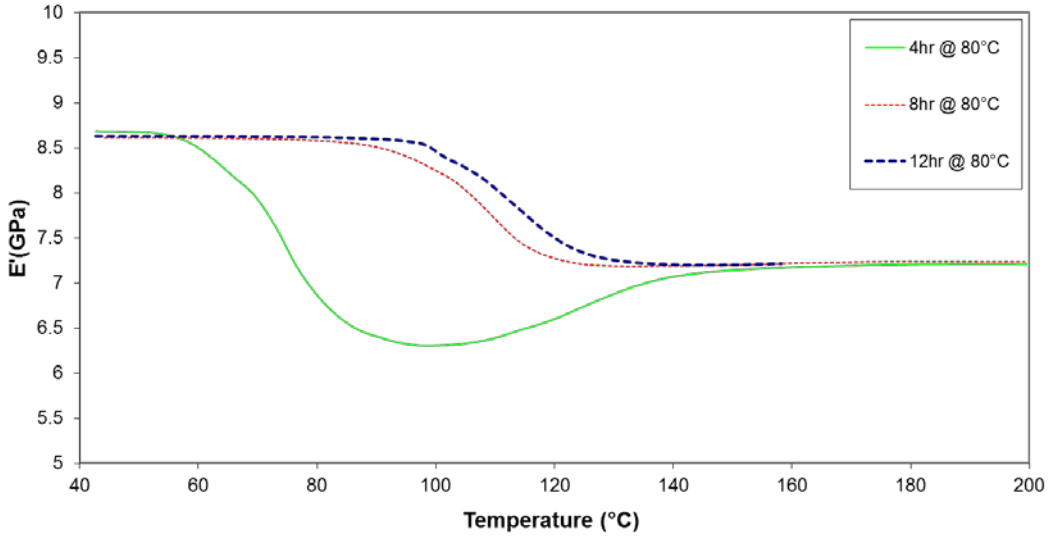

Figure C-8 – LY556 DMTA storage modulus results for a 100:18:7:12 mix and varying cure times

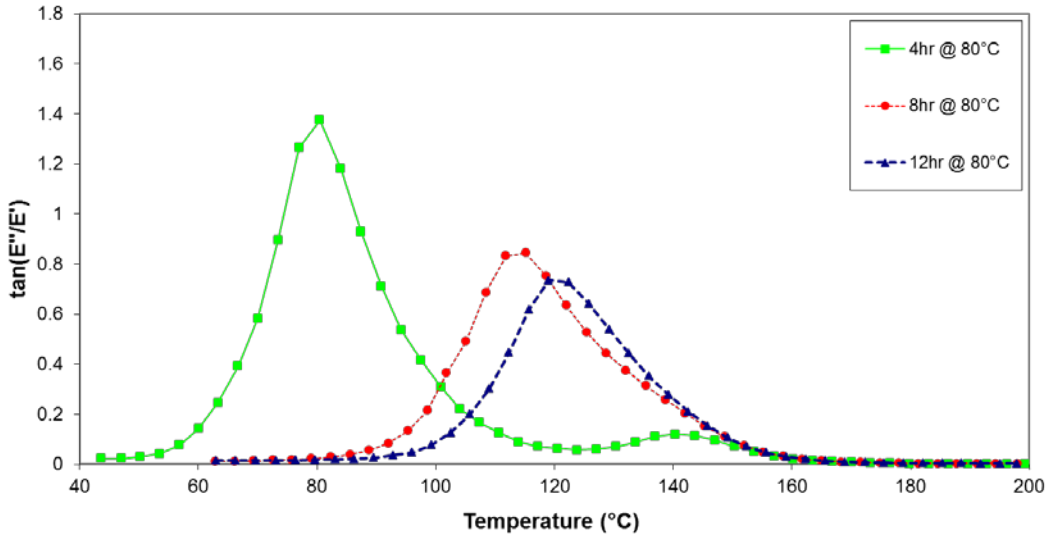

Figure C-9 – LY556 DMTA dampening behaviour results for a 100:23:7:12 mix and varying cure times

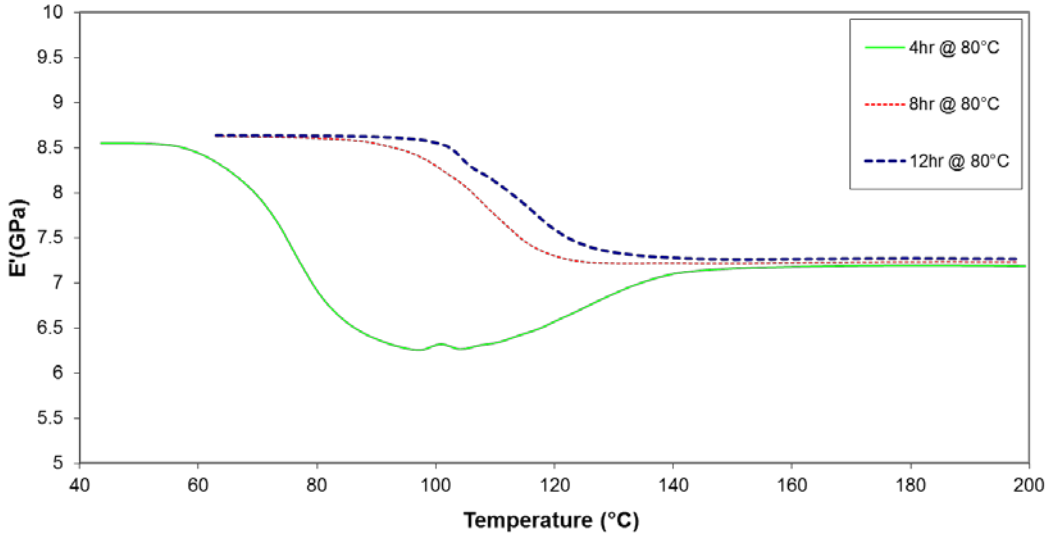

Figure C-10 – LY556 DMTA storage modulus results for a 100:23:7:12 mix and varying cure times

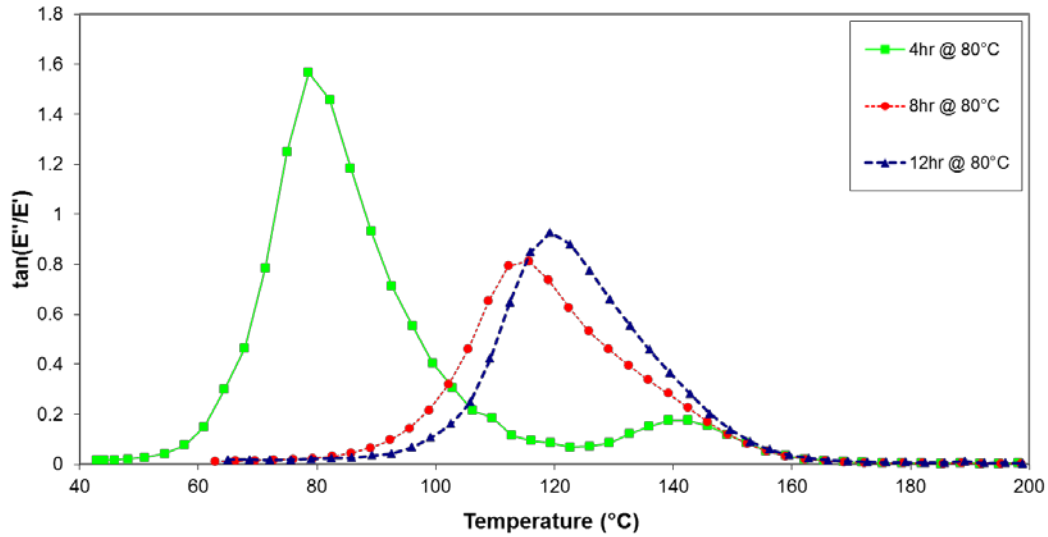

Figure C-11 – LY556 DMTA dampening behaviour results for a 100:28:7:12 mix and varying cure times

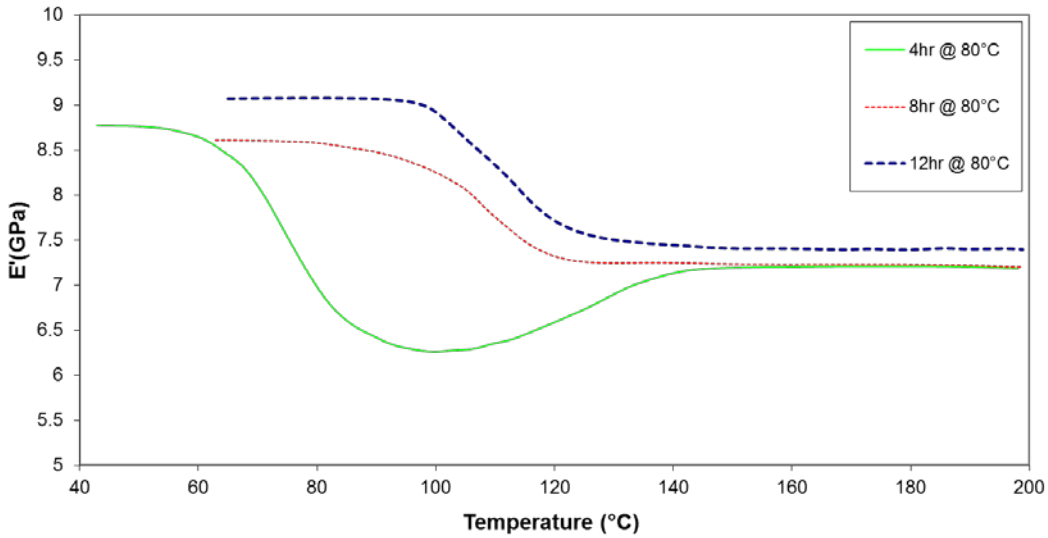

Figure C-12 – LY556 DMTA storage modulus results for a 100:28:7:12 mix and varying cure times

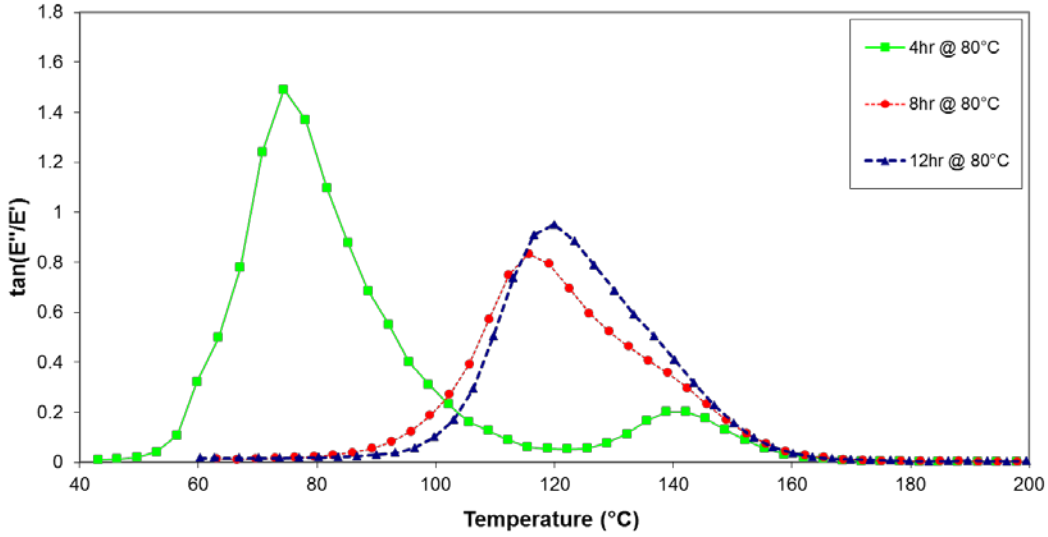

Figure C-13 – LY556 DMTA dampening behaviour results for a 100:33:7:12 mix and varying cure times

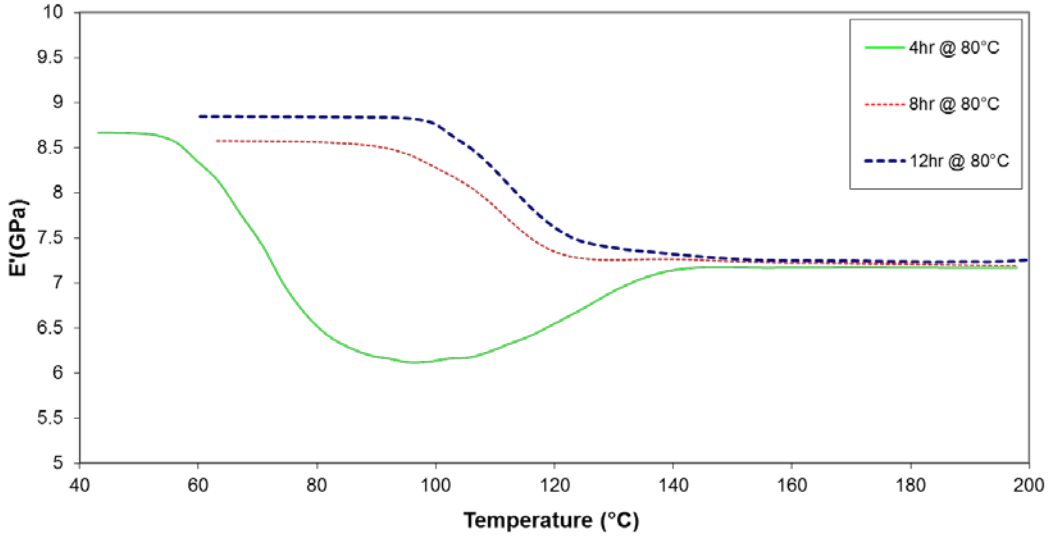

Figure C-14 – LY556 DMTA storage modulus results for a 100:33:7:12 mix and varying cure times

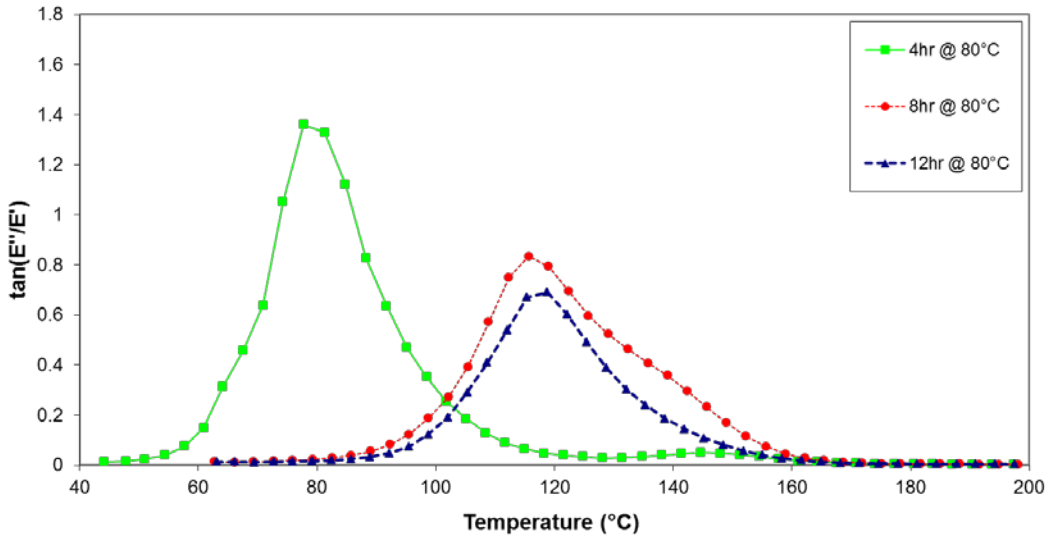

Figure C-15 – LY556 DMTA dampening behaviour results for a 100:23:4:12 mix and varying cure times

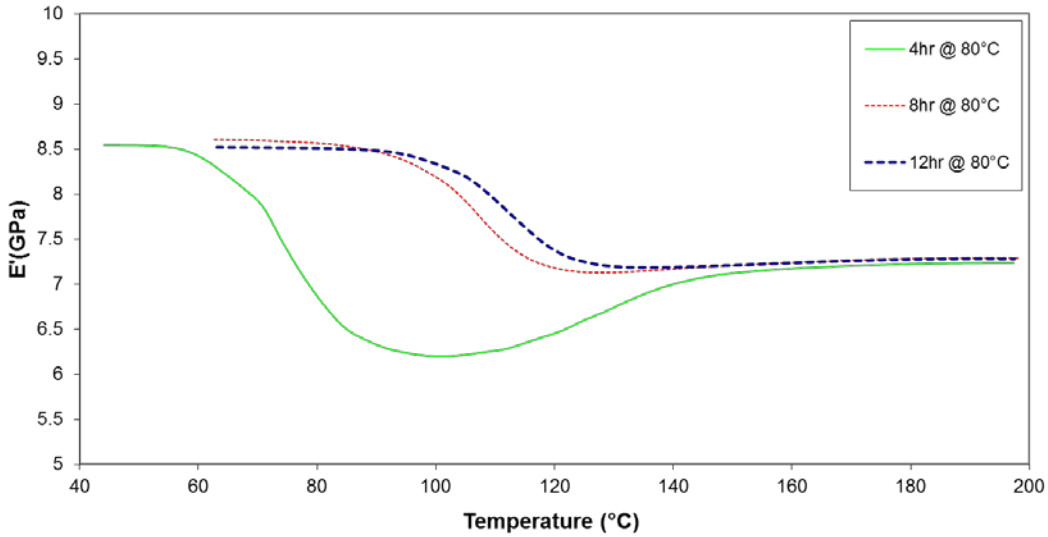

Figure C-16 – LY556 DMTA storage modulus results for a 100:23:4:12 mix and varying cure times

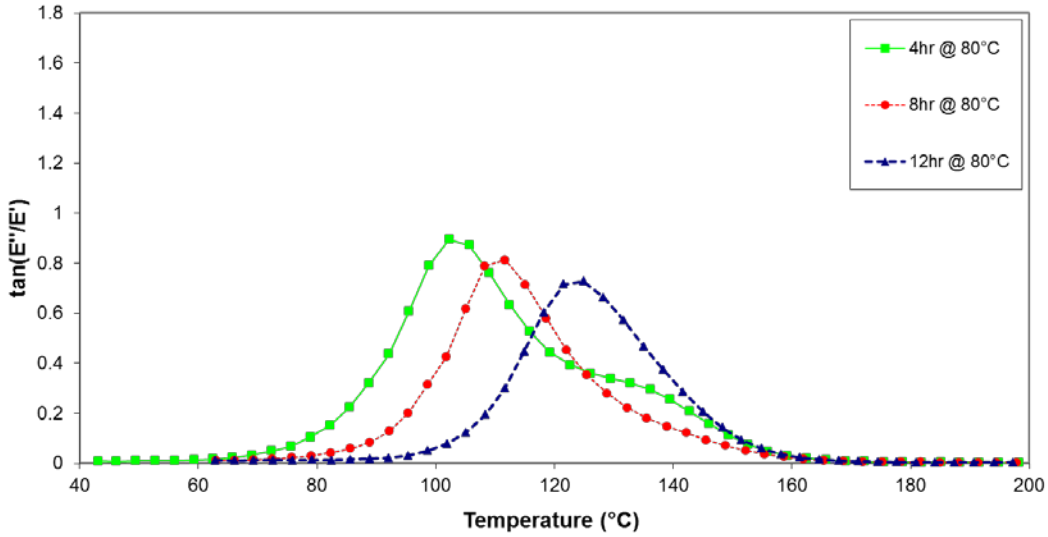

Figure C-17 – LY556 DMTA dampening behaviour results for a 100:23:10:12 mix and varying cure times

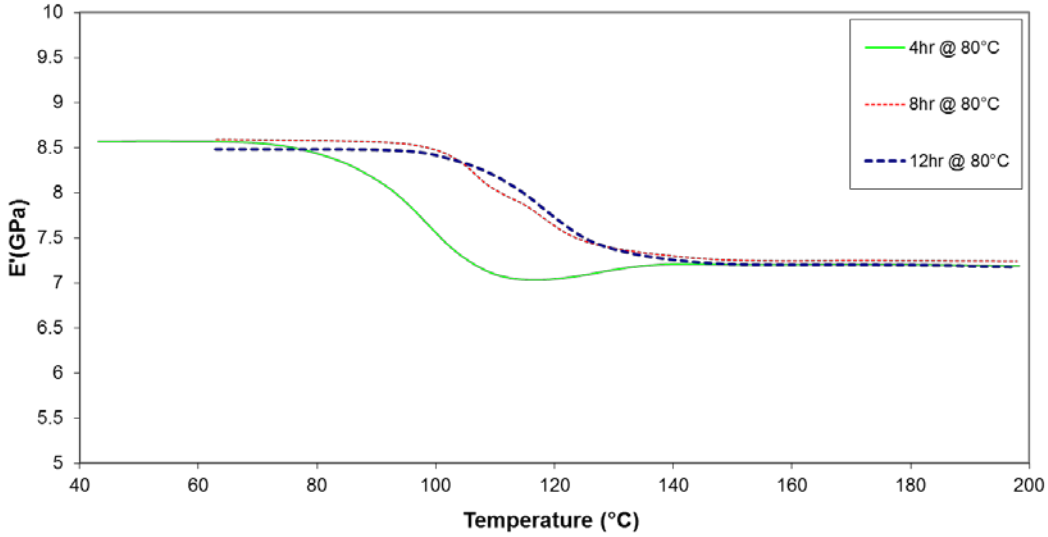

Figure C-18 – LY556 DMTA storage modulus results for a 100:23:10:12 mix and varying cure times

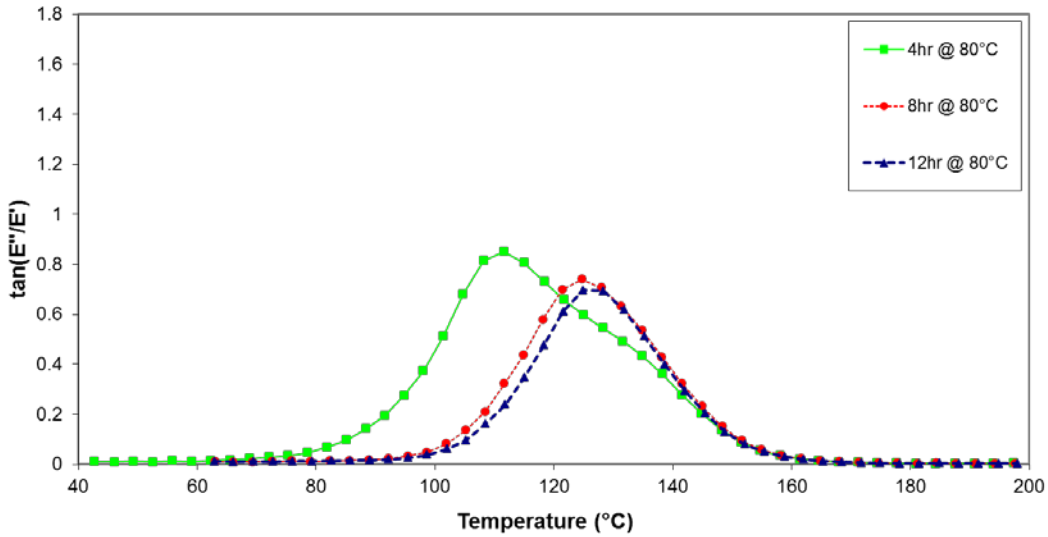

Figure C-19 – LY556 DMTA dampening behaviour results for a 100:23:13:12 mix and varying cure times

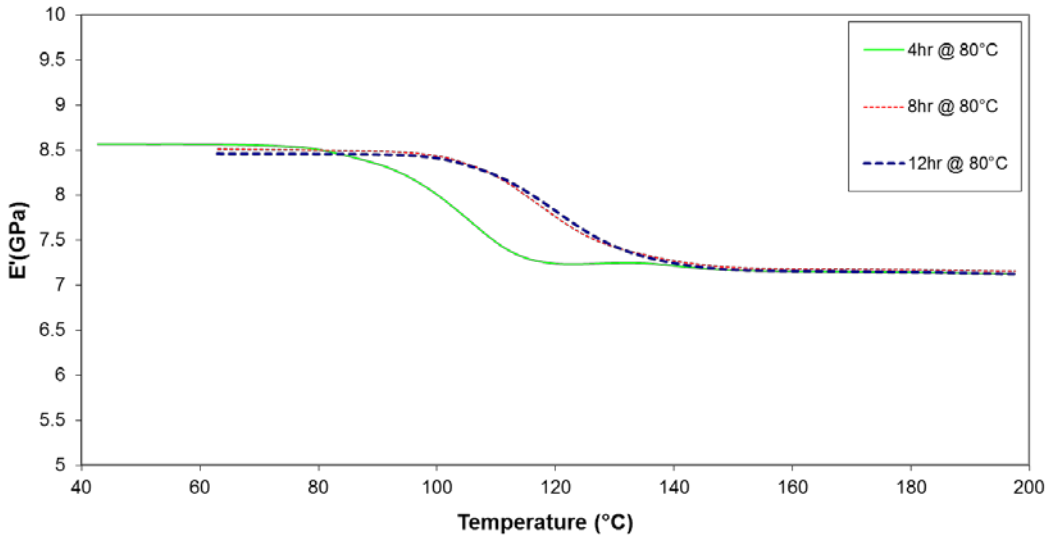

Figure C-20 – LY556 DMTA storage modulus results for a 100:23:13:12 mix and varying cure times

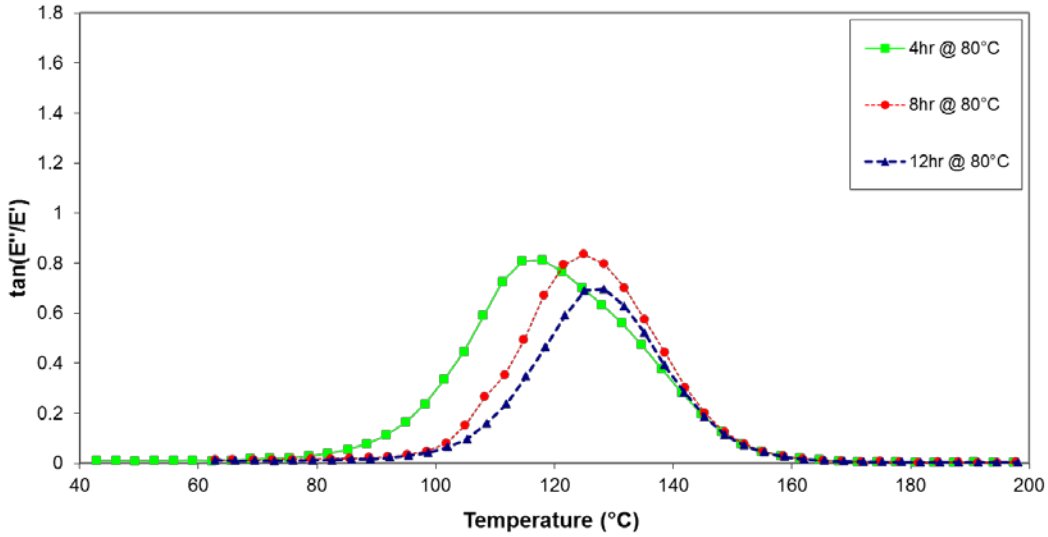

Figure C-21 – LY556 DMTA dampening behaviour results for a 100:23:17:12 mix and varying cure times

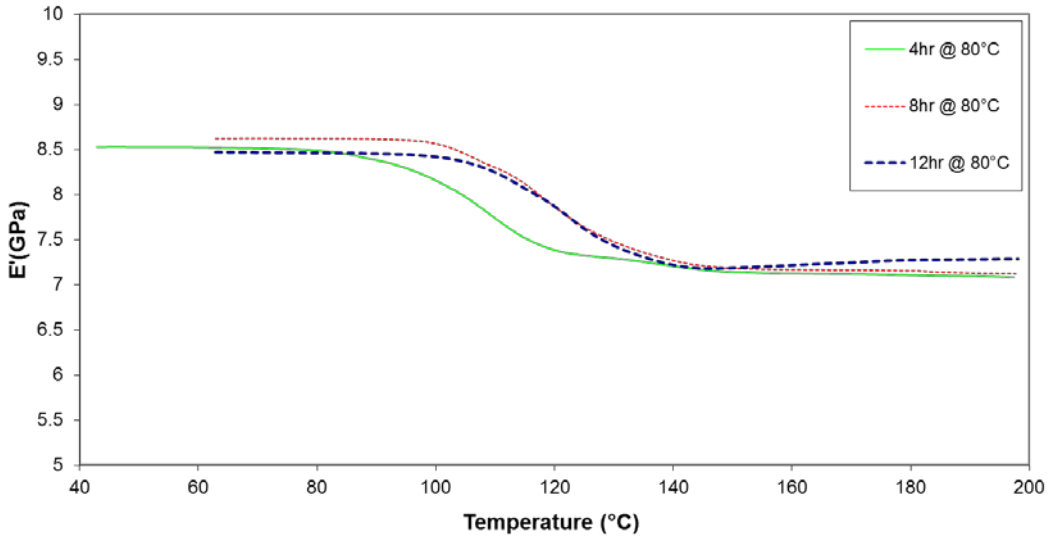

Figure C-22 – LY556 DMTA storage modulus results for a 100:23:17:12 mix and varying cure times

This page is intentionally blank

Appendix D: Short beam shear results

Table D-1 – Short beam shear specimen test results

Resin	Copolymer	Conditioning	Specimen thickness	Specimen width	Specimen length	Maximum load	Short beam strength	Average SBS strength (MPa)	Standard deviation (Mpa)
			mm	*mm*	*mm*	*N*	*MPa*	*MPa*	*MPa*
K3600	nil	nil	4.0	7.7	23.1	2079.3	50.6	49.8	0.8
			4.0	7.7	23.3	2072.8	50.3		
			4.0	7.7	23.2	2039.8	49.6		
			4.0	7.7	23.2	2074.7	51.0		
			4.0	7.7	23.2	1964.3	48.8		
			3.9	7.6	23.3	1948.3	49.1		
			3.8	7.7	23.2	1936.7	49.4		
			3.8	7.6	23.2	1914.6	49.6		
K3600	nil	100 h at 180 °C	3.9	7.7	23.0	2107.4	53.0	51.6	1.1
			3.9	7.6	23.1	2027.4	51.1		
			3.9	7.6	23.1	2059.2	51.8		
			3.9	7.6	23.1	1995.3	50.1		
			3.9	7.6	23.1	2059.2	51.9		
K3600	E21	nil	4.5	7.8	23.1	2066.7	44.2	44.3	0.5
			4.6	7.7	23.2	2116.5	45.0		
			4.6	7.7	23.2	2115.7	44.7		
			4.6	7.7	23.1	2094.7	44.3		
			4.5	7.7	23.2	2038.3	43.8		
			4.5	7.7	23.2	2029.0	44.3		
			4.3	7.7	23.1	1973.6	44.5		
			4.2	7.7	23.2	1856.8	43.3		

Table D-2 – Short beam shear specimen test results (continued)

Resin	Copolymer	Conditioning	Specimen thickness	Specimen width	Specimen length	Maximum load	Short beam strength	Average SBS strength (MPa)	Standard deviation (Mpa)
			mm	*mm*	*mm*	*N*	*MPa*	*MPa*	*MPa*
K3600	E21	100 h at 180 °C	4.2	7.7	23.0	1747.0	40.2	40.6	0.3
			4.3	7.7	23.1	1780.2	40.7		
			4.3	7.6	23.2	1756.1	40.2		
			4.3	7.7	23.2	1796.6	40.9		
			4.3	7.7	23.1	1795.4	40.9		
K3600	M51	nil	4.2	7.7	23.1	1906.7	44.8	44.6	0.3
			4.2	7.7	23.1	1900.6	44.6		
			4.2	7.7	23.1	1885.9	44.1		
			4.2	7.7	23.2	1926.0	44.6		
			4.3	7.7	23.2	1935.6	44.7		
			4.2	7.7	23.2	1915.1	44.3		
			4.2	7.6	23.2	1907.9	44.6		
			4.2	7.7	23.2	1920.3	45.0		
K3600	M51	100 h at 180 °C	4.0	7.7	23.2	1999.9	48.9	48.1	0.7
			4.0	7.7	23.2	1995.5	48.6		
			4.0	7.7	23.2	1988.3	48.4		
			4.0	7.7	23.1	1958.2	47.8		
			4.0	7.7	23.2	1912.3	47.0		
LY556	nil	nil	3.8	7.6	22.5	2123.4	55.4	55.3	1.2
			3.7	7.6	22.5	2128.1	57.1		
			3.8	7.6	22.5	2123.1	55.4		
			3.8	7.6	22.3	2061.8	54.1		
			3.7	7.6	22.5	2034.4	54.0		
			3.8	7.6	22.5	2069.8	54.3		
			3.8	7.6	22.4	2150.3	56.4		

Table D-3 – Short beam shear specimen test results (continued)

Resin	Copolymer	Conditioning	Specimen thickness	Specimen width	Specimen length	Maximum load	Short beam strength	Average SBS strength (MPa)	Standard deviation (Mpa)
			mm	*mm*	*mm*	*N*	*MPa*	*MPa*	*MPa*
LY556	nil	100 h at 180 °C	4.0	7.7	22.7	2050.3	50.1	50.8	1.0
			4.0	7.7	22.7	2087.2	51.1		
			3.9	7.7	22.9	2095.6	52.1		
			4.0	7.7	22.9	2022.4	49.5		
			4.0	7.7	23.0	2087.0	51.3		
LY556	E21	nil	4.1	7.7	22.8	2158.0	51.0	49.9	0.8
			4.1	7.7	22.6	2121.8	50.3		
			4.0	7.7	23.1	2001.6	49.4		
			4.0	7.7	23.0	2014.7	48.6		
			4.1	7.7	23.1	2097.9	49.8		
			4.1	7.7	23.1	2141.3	50.5		
			3.8	7.7	23.0	1925.5	49.5		
LY556	E21	100 h at 180 °C	3.9	7.4	22.0	1813.0	47.5	47.9	0.6
			3.9	7.4	22.2	1848.0	48.5		
			3.9	7.4	21.9	1813.0	47.2		
			3.9	7.4	22.3	1854.8	48.2		
			3.8	7.4	22.2	1829.6	48.3		
LY556	M51	nil	4.1	7.9	23.2	2240.2	51.5	50.9	0.9
			4.0	7.9	23.3	2190.7	51.6		
			4.2	7.9	23.4	2256.2	51.2		
			4.1	7.9	23.4	2258.9	51.8		
			4.2	7.9	23.2	2204.5	49.5		
			4.2	7.9	23.5	2245.0	50.4		
			4.2	7.9	23.3	2242.5	50.3		
LY556	M51	100 h at 180 °C	4.1	7.9	23.4	2146.0	49.5	49.0	0.3
			4.2	7.9	23.5	2139.0	48.9		
			4.1	7.9	23.0	2116.8	48.9		
			4.2	7.9	23.2	2138.8	48.9		
			4.2	7.9	23.5	2146.2	48.7		

This page is intentionally blank

Appendix E: TALS Test Results

Table E-1 – TALS specimen results for K3600 with and without the addition of the E21 copolymer toughener

Specimen	Average Bond-line Thickness	Bond Area	Shear Modulus	Shear Strength (ULT)	Shear Strength (KN)	Shear Strength (LL)	Ult. load	Shear Strain (ULT)	Shear Strain (KN)	Shear Strain (LL)
	µm	*mm²*	*MPa*	*MPa*	*MPa*	*MPa*	*N*	*mm/mm*	*mm/mm*	*mm/mm*
P2A-1	150.00	235.90	469.00	42.89	40.42	32.79	10,118	0.3488	0.0971	0.0662
P2A-2	149.00	236.30	374.00	41.11	38.71	28.95	9,714	0.3301	0.1129	0.0728
P2A-3	160.00	236.90	450.00	42.38	40.33	33.07	10,041	0.3654	0.0998	0.0694
E2110P2A-1	153.00	237.34	450	38.27	33.99	27.17	9,081	0.6593	0.0997	0.0558
E2110P2A-2	151.00	237.24	370	39.5	34.54	25.19	9,371	0.8965	0.1245	0.0678
E2110P2A-3	152.00	239.78	400	38.57	34.15	25.18	9,248	0.7539	0.1184	0.0694

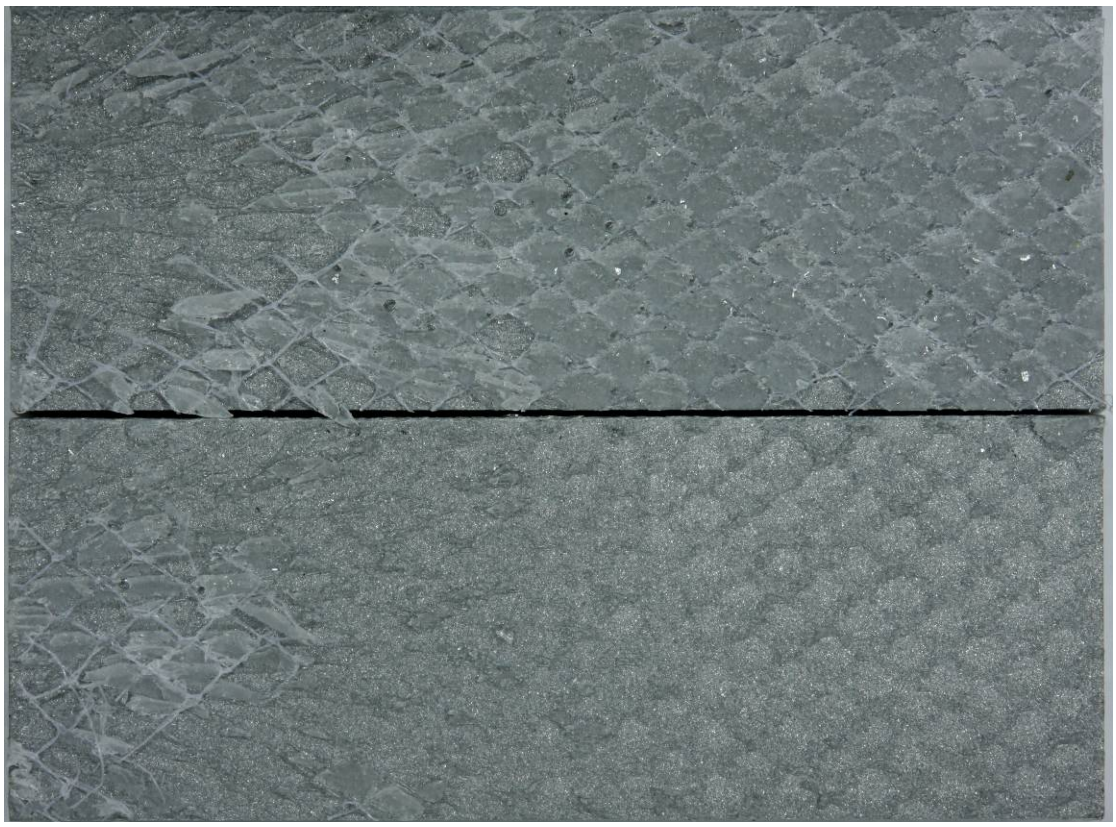

Figure E-1 – Neat K3600 TALS specimen (P2A-1) bond-line showing uniform cohesive failure across the bond area.

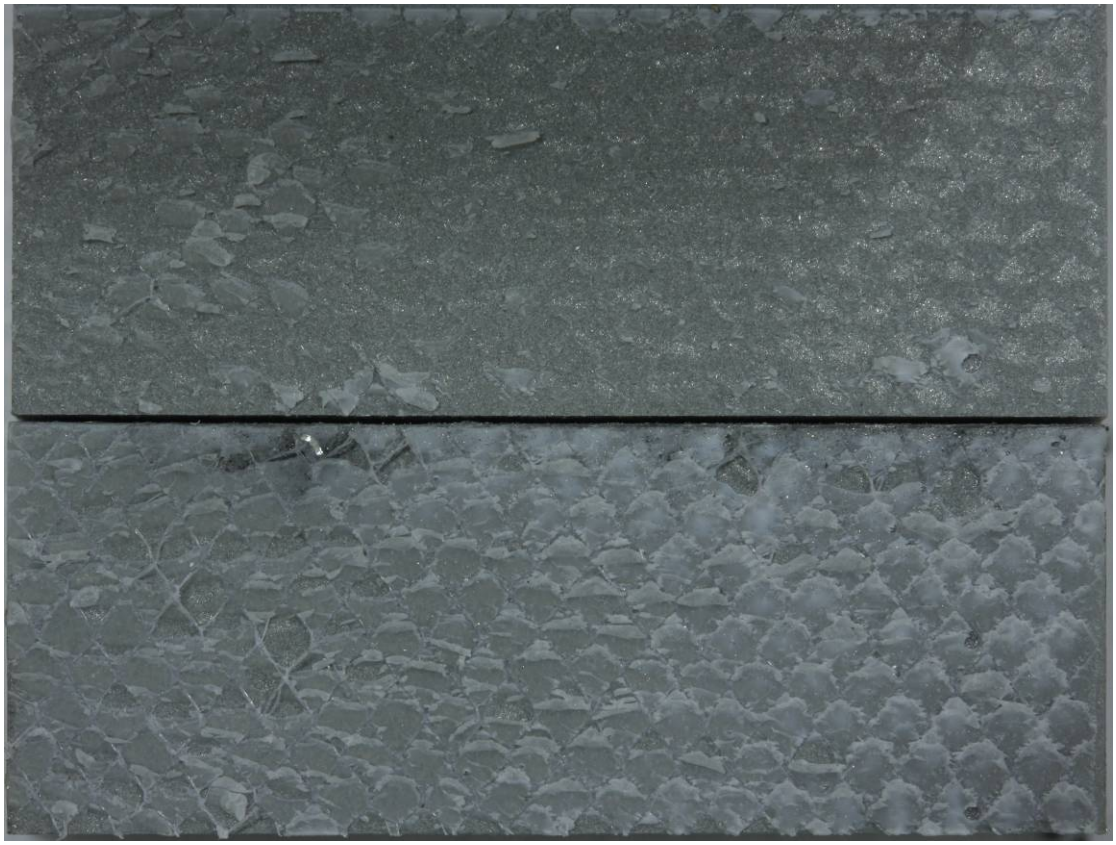

Figure E-2 – K3600 + E21 TALS specimen (E2110P2A-3) bond-line showing uniform cohesive failure across the bond area.

Appendix F: Four point bend results

Table F-1 – Four point bend specimen test results

Resin	Copolymer	Specimen thickness (centre of support span)	Specimen width (centre of support span)	Rate of cross head motion	Support span	Load span	Maximum compressive load	Flexural strength	Flexural modulus	Note
		mm	*mm*	*mm/min*	*mm*	*mm*	*N*	*MPa*	*GPa*	
K3600	nil	3.9	14.1	1.8	61.8	20.6	2218.1	625.0	52.0	Bearing failure at loading nose
		3.9	14.1	1.8	61.8	20.6				Damaged before testing
		3.9	14.1	1.8	61.8	20.6	2046.9	606.2	37.0	Single point tensile failure on underside of specimen
		3.8	14.0	1.8	61.8	20.6	1781.0	535.2	38.0	Single point tensile failure on underside of specimen
		3.8	14.0	1.8	61.8	20.6	2084.0	646.4	40.0	Single point tensile failure on underside of specimen
K3600	E21	4.7	14.1	2.0	71.4	37.3	3003.6	685.0	176.0	Tested at half load span, bearing failure at loading nose
		4.8	14.1	2.0	71.4	25.0	2264.6	505.4	44.6	Bearing failure at loading nose
		4.7	14.1	2.0	71.4	25.0	2280.1	516.0	37.0	Bearing failure at loading nose
		4.7	14.1	2.0	71.4	23.8	1882.1	440.7	40.3	Single point tensile failure on underside of specimen
		4.5	14.0	2.0	71.4	23.8	1886.4	483.2	32.0	Single point tensile failure on underside of specimen
K3600	M51	4.2	14.1	2.0	67.1	22.4	2261.2	625.3	52.0	Bearing failure at loading nose
		4.2	14.0	2.0	67.1	22.4	1605.5	437.4	51.0	Bearing failure at loading nose
		4.2	14.0	2.0	67.1	22.4	1905.9	516.8	34.0	Single point tensile failure on underside of specimen
		4.2	14.0	2.0	67.1	22.4	1843.0	498.1	36.0	Single point tensile failure on underside of specimen
		4.2	14.0	2.0	67.1	22.4	2026.0	553.2	30.8	Single point tensile failure on underside of specimen

Table F-2 – Four point bend specimen test results (continued)

Resin	Copolymer	Specimen thickness (centre of support span)	Specimen width (centre of support span)	Rate of cross head motion	Support span	Load span	Maximum compressive load	Flexural strength	Flexural modulus	Note
		mm	*mm*	*mm/min*	*mm*	*mm*	*N*	*MPa*	*GPa*	
LY556	nil	3.8	13.9	1.8	61.6	0.9	1570.6	481.0	32.0	Single point tensile failure on underside of specimen
		4.0	13.9	1.8	61.6	0.9	1924.3	545.4	34.0	Single point tensile failure on underside of specimen
		3.9	13.9	1.8	61.6	0.9	1701.9	492.3	31.0	Single point tensile failure on underside of specimen
		3.6	13.9	1.8	61.6	0.9	1808.2	603.5	37.0	Single point tensile failure on underside of specimen
		3.8	13.9	1.8	61.6	0.9	1778.2	533.3	34.0	Bearing failure at loading nose
		3.9	13.9	1.8	61.6	0.9	1832.1	524.6	33.0	Bearing failure at loading nose
		3.9	13.9	1.8	61.6	0.9	1831.0	524.2	32.0	Bearing failure at loading nose
LY556	E21	3.8	14.0	1.8	62.9	22.6	1724.2	530.4	32.0	Bearing failure at loading nose
		4.1	14.0	1.8	62.9	22.6	1824.6	477.9	32.0	Single point tensile failure on underside of specimen
		3.8	14.0	1.8	62.9	22.6	1878.5	577.9	36.0	Single point tensile failure on underside of specimen
		3.7	14.0	1.8	62.9	22.6	2293.8	752.2	40.0	Single point tensile failure on underside of specimen
		3.9	14.0	1.8	62.9	22.6	1695.5	513.5	37.0	Bearing failure at loading nose
		4.0	14.0	1.8	62.9	22.6	1529.4	437.8	36.0	Bearing failure at loading nose
		4.1	14.0	1.8	62.9	22.6	1901.0	515.2	35.0	Bearing failure at loading nose
LY556	M51	4.1	14.1	1.9	63.0	22.2	1954.6	520.4	38.0	Single point tensile failure on underside of specimen
		4.0	14.1	1.9	63.0	22.2	2290.2	653.6	26.0	Bearing failure at loading nose
		4.1	14.1	1.9	63.0	22.2	2079.0	567.3	34.0	Single point tensile failure on underside of specimen
		3.7	14.1	1.9	63.0	22.2	1953.2	642.0	38.0	Single point tensile failure on underside of specimen
		4.2	14.1	1.9	63.0	22.2	1808.9	470.1	36.0	Bearing failure at loading nose
		4.1	14.1	1.9	63.0	22.2	1834.5	479.0	34.0	Bearing failure at loading nose
		4.1	14.1	1.9	63.0	22.2	1846.5	494.0	35.0	Bearing failure at loading nose

NOTE: The shaded flexural strength results are erroneous due to the failure mode exhibited by the specimen upon loading. As a result, these results were not included in the result summary in Section 3.6.

Appendix G: Double cantilever Beam results

Table G-1 – Double Cantilever Beam (DCB) specimen test results

Resin	Copolymer	Specimen thickness	Specimen width	Specimen length	a_0	G_{IC}			Average NL G_{IC}	stdev NL G_{IC}	Average MAX G_{IC}	stdev MAX G_{IC}
		mm	*mm*	*mm*	*mm*	*J/m2*			*J/m²*	*J/m²*	*J/m²*	*J/m²*
						VIS	**NL**	**MAX**				
K3600	nil	4.4	21.9	136.3	45.8	266.95	652.12	1021.60	604.9	54.5	908.71	199.06
		4.2	21.7	136.1	45.7	602.04	641.02	949.01				
		3.9	22.2	136.3	47.0	524.20	532.40	598.64				
		3.7	22.2	136.4	46.9	671.38	638.49	853.58				
		4.7	22.6	136.1	45.6	595.58	560.54	1120.72				
K3600	E21	4.9	22.8	136.3	51.4	236.00	883.74	1362.31	1043.5	165.9	1462.97	340.19
		5.1	22.7	136.5	51.6	1249.86	1167.84	2055.10				
		5.1	22.9	136.7	51.1	637.16	1114.12	1238.45				
		5.1	22.8	136.5	50.6	598.14	847.57	1239.73				
		4.9	22.9	136.8	50.6	1125.23	1203.98	1419.25				
K3600	M51	4.5	22.7	136.2	43.3	323.65	837.81	1142.55	862.1	88.4	1172.71	178.82
		4.4	22.5	136.4	42.9	810.53	821.12	1427.11				
		4.3	22.6	135.9	44.0	1056.60	1018.73	1270.48				
		4.2	22.5	136.0	43.8	826.76	827.99	1032.77				
		4.0	22.4	136.1	43.9	853.39	804.60	990.66				

Table G-2 – Double Cantilever Beam (DCB) specimen test results (continued)

Resin	Copolymer	Specimen thickness	Specimen width	Specimen length	a_0	G_{IC}			Average NL G_{IC}	stdev NL G_{IC}	Average MAX G_{IC}	stdev MAX G_{IC}
		mm	*mm*	*mm*	*mm*	*J/m2*			*J/m²*	*J/m²*	*J/m²*	*J/m²*
						VIS	**NL**	**MAX**				
LY556	nil	4.1	24.6	130.1	42.6	246.00	435.85	802.65	459.3	111.7	862.52	103.19
		3.8	24.9	130.6	41.7	306.53	484.09	806.28				
		3.9	24.4	130.6	42.1	116.89	465.13	815.93				
		4.1	24.6	130.1	42.2	85.52	611.81	1044.97				
		4.2	24.9	130.5	42.7	116.82	299.84	842.77				
LY556	E21	4.8	24.7	130.2	42.2	905.78	905.78	1760.44	1033.1	244.6	1620.81	308.15
		4.5	24.4	130.0	41.7	797.35	797.35	1258.41				
		4.0	24.7	130.4	42.6	235.98	1043.80	1655.98				
		3.9	25.0	130.5	42.7	1340.56	1438.85	2038.76				
		4.5	25.0	130.7	39.6	104.40	979.66	1390.45				
LY556	M51	4.9	25.0	130.4	42.3	551.26	791.93	804.75	767.6	77.3	890.71	90.85
		4.5	24.9	130.4	42.8	829.85	829.85	829.85				
		4.0	24.7	130.4	42.6	192.98	794.08	926.09				
		4.4	24.7	130.5	43.1	107.57	1021.20	1021.20				
		4.7	24.6	130.3	42.4	654.65	654.65	1002.14				

NOTE: The shaded Mode I fracture toughness results for the LY556 + M51 specimen were not included in the specimens averaged results due as the pre-crack exceeded the length specified within the ASTM standard. The standard specifies a pre-crack length of between 3 – 5 mm, and due to unstable delamination growth, the pre-crack for this specimen was 12. 7 mm.

Appendix H: Long Crack Extension Testing

The Long Crack Extension (LCE) test is a Lockheed Martin standard derived from ASTM standard D3433 [42], D3762 [43] and Boeing specification BSS 7208 [44]. The specimen used for the test is shown in Figure H-1, with the required opening displacement achieved by screwing two bolts threaded into each half of the LCE adherends.

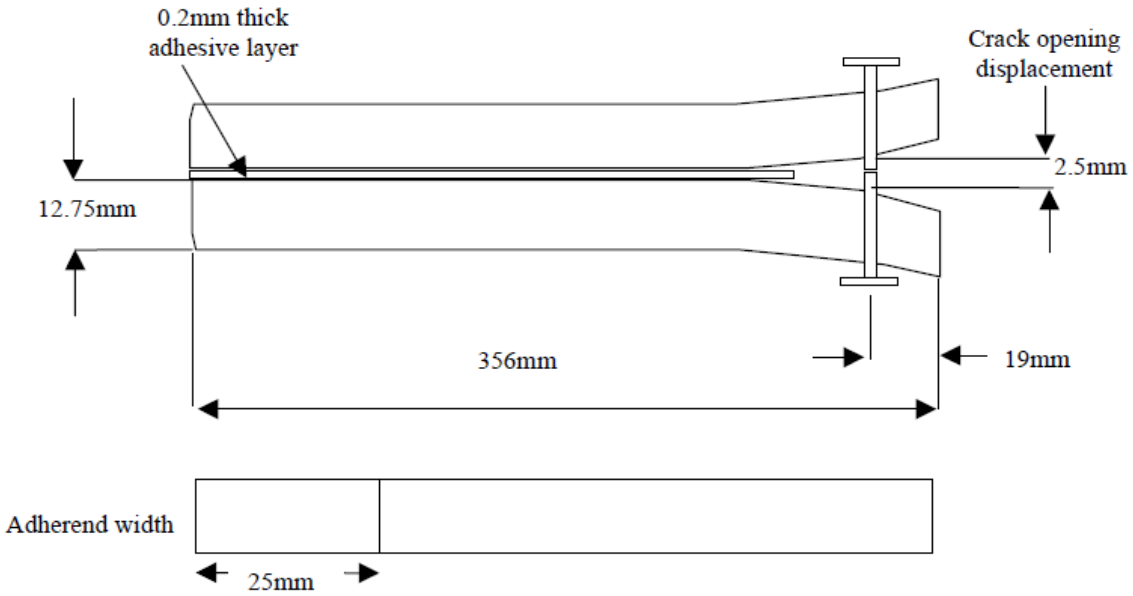

Figure H-1 – Long Crack Extension (LCE) specimen

Using this method, the mode I fracture toughness is calculated using Equation 14.

$$G_I = \frac{Y^2 E h^3 \left\{3\left[(a+0.6h)^2 + h^2\right]\right\}}{16\left[(a+0.6h)^3 + ah^2\right]^2} \qquad \textbf{(14)}$$

Where:

Y = crack opening displacement

h = adhered thickness

E = young's modulus of adherend

a = crack length

The crack length is measured through use of an optical travelling microscope, and the crack length monitored over time until a steady-state value is reached. The results for K3600 neat and K3600 toughened with 10% parts by weight E21 copolymer are shown in Tables H-1 and H-2 following.

Table H-1 – LCE results for Neat K3600 system.

		Crack length *m*				G_{IC} *J/m2*	
	Time (h)	0	25	49	0	25	49
Crack location	1	0.14	0.14	0.16	415.83	348.36	216.25
	2	0.13	0.13	0.13	500.46	433.67	433.67
	3	0.14	0.14	0.14	410.09	357.79	339.23
	Average G_{IC}				442.13	379.94	329.71
	Stdev G_{IC}				50.60	46.77	109.02

Table H-2 – LCE results for K3600 system toughened with 10% part by weight E21 copolymer.

		Crack length *M*				G_{IC} *J/m2*	
	Time (h)	0	25	49	0	25	49
Crack location	1	0.08	0.10	0.11	2562.09	1475.69	878.48
	2	n/a	n/a	n/a	n/a	n/a	n/a
	3	n/a	n/a	n/a	n/a	n/a	n/a
	Average G_{IC}				2562.09	1475.69	878.48
	Stdev G_{IC}				n/a	n/a	n/a

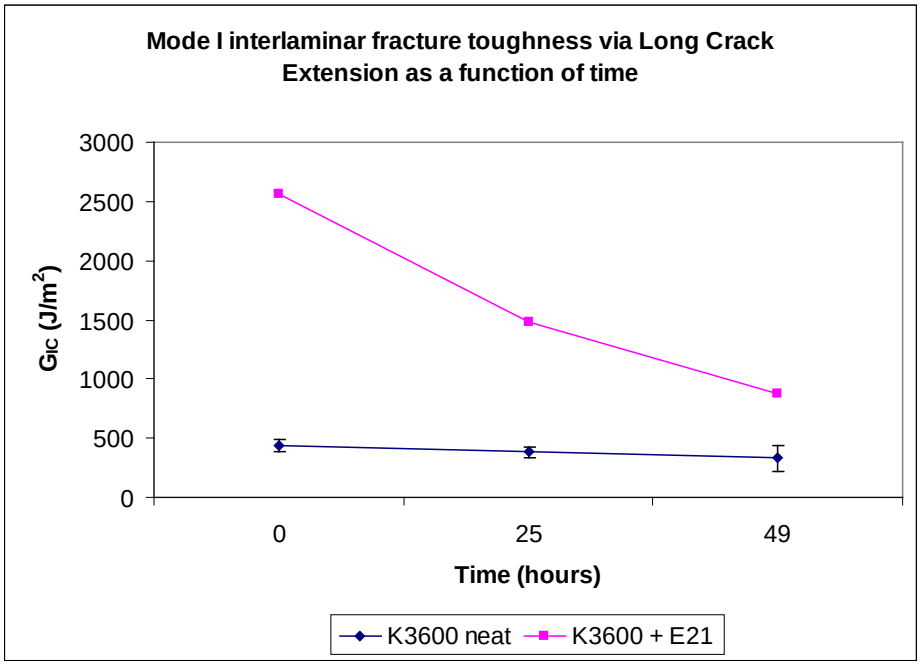

Figure H-2 – Mode I fracture toughness as a function of time for LCE test.

DEFENCE SCIENCE AND TECHNOLOGY GROUP DOCUMENT CONTROL DATA	1. DLM/CAVEAT (OF DOCUMENT)

2. TITLE	3. SECURITY CLASSIFICATION (FOR UNCLASSIFIED REPORTS THAT ARE LIMITED RELEASE USE (U/L) NEXT TO DOCUMENT CLASSIFICATION)
Copolymer Toughening of Epoxy Resin Systems for Low Temperature Cure Bonded Composite Repair	Document (U) Title (U) Abstract (U)
4. AUTHOR(S) Andrew D. M. Charles and Andrew Rider	5. CORPORATE AUTHOR Defence Science and Technology Group 506 Lorimer St Fishermans Bend Victoria 3207 Australia

6a. DST Group NUMBER	6b. AR NUMBER	6c. TYPE OF REPORT	7. DOCUMENT DATE
DST-Group-TR-3344	AR-016-808	Technical Report	February 2017

8. Objective ID	9. TASK NUMBER	10. TASK SPONSOR
AV14717336	SRI 07/292	Defence Science and Technology Group

13. DOWNGRADING/DELIMITING INSTRUCTIONS	14. RELEASE AUTHORITY
To be reviewed three years after date of publication	Chief, Aerospace Division

15. SECONDARY RELEASE STATEMENT OF THIS DOCUMENT

Approved for public release

OVERSEAS ENQUIRIES OUTSIDE STATED LIMITATIONS SHOULD BE REFERRED THROUGH DOCUMENT EXCHANGE, PO BOX 1500, EDINBURGH, SA 5111

16. DELIBERATE ANNOUNCEMENT
No Limitations

17. CITATION IN OTHER DOCUMENTS Yes

18. RESEARCH LIBRARY THESAURUS
Bonded composite repairs; Epoxy resins; Toughness

19. ABSTRACT
Epoxies are the most widely used resins for bonded composite repair; however they possess low fracture toughness, impact strength and peel strength due to high cross linking densities. Toughening agents can be added to epoxy resins to improve these qualities; however these typically lead to an increase in resin viscosity and undesirable changes in mechanical performance, which can in turn make the resin unsuitable for use in certain bonded composite repair applications. In this work, the impact of two commercially available tri-block copolymers on the mechanical performance of two different low temperature cure epoxy resin systems was evaluated. It was found that with the addition of the copolymers to these resins in a wet lay-up scenario (typical of bonded composite repair applications), the resin fracture toughness could be improved by as much as 125%, with negligible impact to resin interlaminar shear strength, flexural strength and glass transition temperature. Use of these resins will improve standard bonded composite repairs and support development of indigenous composite multi-functional structures for aerospace applications.